DISSERTATION FOR THE DEGREE OF DOCTOR OF PHILOSOPHY (PHD)

Identification and characterization of bacterial metabolites with antineoplastic activity in breast cancer

by Gyula Ujlaki

UNIVERSITY OF DEBRECEN
DOCTORAL SCHOOL OF MOLECULAR MEDICINE

DEBRECEN, 2024

DISSERTATION FOR THE DEGREE OF DOCTOR OF PHILOSOPHY (PHD)

Identification and characterization of bacterial metabolites with antineoplastic activity in breast cancer

by Gyula Ujlaki

Supervisor: Prof. Dr. Péter Bay

UNIVERSITY OF DEBRECEN

DOCTORAL SCHOOL OF MOLECULAR MEDICINE

DEBRECEN, 2024

Abbreviations

ACC	Acetyl-CoA carboxylase
ANOVA	Analysis of variance
AMPK	Adenosine-monophosphate-activated protein kinase
ASR	Age standardized rate
ATP5G1	**(**ATP5MC1) mitochondrial ATP synthase
bFGF	Basic fibroblast growth factor
BG	β-glucuronidase gene
BMI	Body mass index
BSA	Bovine serum albumin
BRCA1/2	Breast cancer type 1/2 susceptibility protein
CAEC	Cancer associated endothelial cells
CAF	Cancer-associated fibroblasts
CAR	Constitutive androstane receptor
CNN	Convolutional neural network
CPU	Central processing unit
CT	Computed tomography
CTL	Control
ECM	Extracellular matrix
FBS	Fetal bovine serum
FCN	Fully convolutional network
CP	CellProfiler
CSC	Cancer stem cell
CYP27A1	Cytochrome P450 family 27 subfamily A member 1 (sterol 27-hydroxylase)
CYP7A1	Cytochrome P450 family 7 subfamily A member 1 (cholesterol 7α hydroxylase)
CYP8B1	Cytochrome P450 family 8, subfamily B polypeptide 1 (sterol 12α-hydroxylase)
DAPI	4’6-diamidino-2-phenylindole
DCA	Deoxycholic acid

DHODH	Dihydroorotate dehydrogenase
DL	Deep learning
DMEM	Dublecco's modified eagle medium
ECAR	Extracellular acidification rate
ECIS	Electric cell-substrate impedance sensing
EGF	Epidermal growth factor
EGFR	Epidermal growth factor receptor
EMT	Epithelial-mesenchymal transition
ER	Estrogen receptor
EtOH	Ethanol
FBS	Fetal bovine serum
FGF	Fibroblast growth factor
FOXO1	Forkhead box O1
FXR	Farnesoid X receptor
GPT1	Alanine transaminase 1
gus	β-glucuronidase gene
GSK-3α/β	Glycogen synthase kinase-3 alpha/beta
HER2	Human epidermal growth factor receptor 2
HGF	Hepatocyte growth factor
HIF	Hypoxia-inducible factor
HRP	Horseradish peroxidase
HSD	Honestly significant difference
IC	Inflammatory cell
IGF	Insulin-like growth factor
LCA	Lithocholic acid
LPS	Lipopolysaccharide
LXR	Liver X receptor
MEM	Minimal essential medium
MET	Mesenchymal-epithelial transition
miRNA	MicroRNA
MMP	Matrix metalloproteinase

MRI	Magnetic resonance imaging
mtDNA	Mitochondrial DNA
mTOR	Mammalian target of rapamycin
NDUFB5	NADH:Ubiquinone oxidoreductase subunit B5
NF-κB	Nuclear factor kappa-light-chain-enhancer of activated B cells
NRF1/2	Nuclear respiratory factor 1/2
NST	Non-special type
OCR	Oxygen consumption rate
OXPHOS	Oxydative phosphorylation
PAGE	Polyacrylamide gel electrophoresis
PBS	Phosphate buffered saline
PDGF	Platelet-derived growth factor
PDH	Pyruvate dehydrogenase
PFA	Paraformaldehyde
PGC-1α/β	Peroxisome proliferator-activated receptor-gamma coactivator-1α/β
PI	Propidium iodide
PI3K	Phosphoinositide 3-kinase
POX	Proline oxidase
PR	Progesteron receptor
PSP	Pyramid scene parsing
Rb	Retinoblastoma
ROS	Reactive oxygen species
SCFA	Short-chain fatty acid
SDF-1	Stromal cell-derived factor 1
SD	Standard deviation
SDS	Sodium dodecyl sulfate
SNAI1	Snail family transcriptional repressor 1
SRB	Sulforhodamine-B
TCA	Trichloroacetic acid
TGF-β1	Transforming growth factor beta 1
TGR5/GPBAR1	G protein-coupled bile acid receptor 1

TIL	Tumor-infiltrating lymphocyte
TMA	Trimethylamine
TMAO	Trimethylamine N-oxide
TNM	Tumor, node, metastasis
TRIS	Trisaminomethane
TWIST1	Twist family bHLH transcription factor 1
UDCA	Ursodeoxycholic acid
VEGF	Vascular endothelial growth factor
VEH	Vehiculum
VGG-UNet	Visual geometry group UNet
WB	Western blot
WHO	World Health Organization
ZEB1	Zeb family zinc finger homeodomain transcription factor
ZO-1	Zonula occludens protein 1

1. Overview

The gut microbiome refers to the complex community of bacterial species, that reside in the digestive tract. It plays an important role in various aspects of human health, including immune function, metabolism and even the development of certain diseases, such as cardiovascular pathologies, diabetes, obesity, and certain types of cancer [1]. Although, the gut microbiome strongly correlates with intestinal diseases, recent studies showed that there are connections between the microbiome and remote parts of the body. This connection is maintained by microbial metabolites and immune modulation [2].

MiMeDB, a recently developed database of human microbial characteristics, contains data on 25 254 metabolites belonging to 72 different chemical classes. From this collection, 1 808 metabolites are microbial-only, and 14 210 are human-microbe co-metabolites. The remainder of 8236 are human-only metabolites where 1524 are exogeneous (drug, food, cosmetic, pollutant) compounds. A microbial-host co-metabolite is a result of the combination of human and microbial metabolism. In other words, for the microbial-host co-metabolite, there must be at least one microbial-specific reaction and at least one host-specific reaction during the synthesis of the metabolite [3]. In the diverse set of microbial metabolites, both adverse and advantageous compounds can be identified. For example, choline metabolites and lipopolysaccharide (LPS) were identified as adverse metabolites, due to their capacity to promote inflammation. Conversely, advantageous compounds include, among others, the bacterially synthesized members of the vitamin B group. Furthermore, there are also metabolites that have important physiological roles, but also involved in pathophysiological processes. Examples for such metabolites are tryptophan, tryptophan derivatives, and bile acids, with advantageous properties through influencing biofilm formation, virulence, intestinal barrier functions, gut hormone secretion, gut motility, lipid and vitamin absorption, gut microbiome composition, and intestinal immune processes. However, tryptophan, tryptophan derivatives, and bile acids play adverse roles in ulcerative colitis, irritable bowel syndrome, obesity, and nonalcoholic fatty liver disease. The multifaceted nature of these metabolites emphasizes the intricate nature of the impact of gut microbiome on human health and highlights the path for further investigation and exploration [4].

Dysbiosis is characterized by an abnormal shift in the host's microbial composition, and this shift is associated with breast cancer and other neoplastic diseases. In recent years, multiple bacterially synthesized cytostatic metabolites have been identified including cadaverine [5],

indole metabolites [6]-[7], or short-chain fatty acids (SCFAs) [8]-[9]. These metabolites, among others, modulate cell proliferation and epithelial-mesenchymal transition (EMT) [10]. The metabolic capacity of the microbiome is suppressed in patients with breast cancer, leading to a decrease in the production of the aforementioned antineoplastic metabolites [5], [7], [11]–[13].

2. Introduction

2.1. Breast cancer

2.1.1. Epidemiology of breast cancer

Malignant tumors are complex systemic diseases that result from multiple cellular and genomic alterations [14], posing an increasingly severe healthcare problem in Hungary. According to data from the Hungarian National Cancer Registry, in 2020, 7144 new patients were identified with malignant breast tumors [15].

Among US women, breast cancer is the second leading cause of cancer-related death [16]. Approximately one million cases are diagnosed each year, with an estimated annual mortality of 23.1 deaths per 100,000 persons in Europe [17]. According to the 2019 breast cancer report published by the American Cancer Society, the incidence of breast cancer increased by an average of 0.3% annually between 2012 and 2016. However, the mortality rate has significantly decreased in recent decades due to the widespread adoption of regular screening [18]. In the United States, there were approximately 287,850 newly diagnosed cases of invasive breast cancer and 51,400 newly diagnosed cases of *in situ* breast cancer in 2022. Based on statistical data, it is estimated that 43,250 women were expected to die from breast cancer in the United States in 2022 [19]. Breast cancer incidence shows significant geographic and economic disparities, with higher occurrence rates observed in developed countries [20] (**Figure 1**). Nevertheless, due to the promotion of screening programs and consequently early detection, the five-year survival rate for breast cancer is 99% for *in situ* breast cancer, 86% for breast cancer with regional lymph node metastasis, and 30% for breast cancer with distant metastasis according to the SEER database [21].

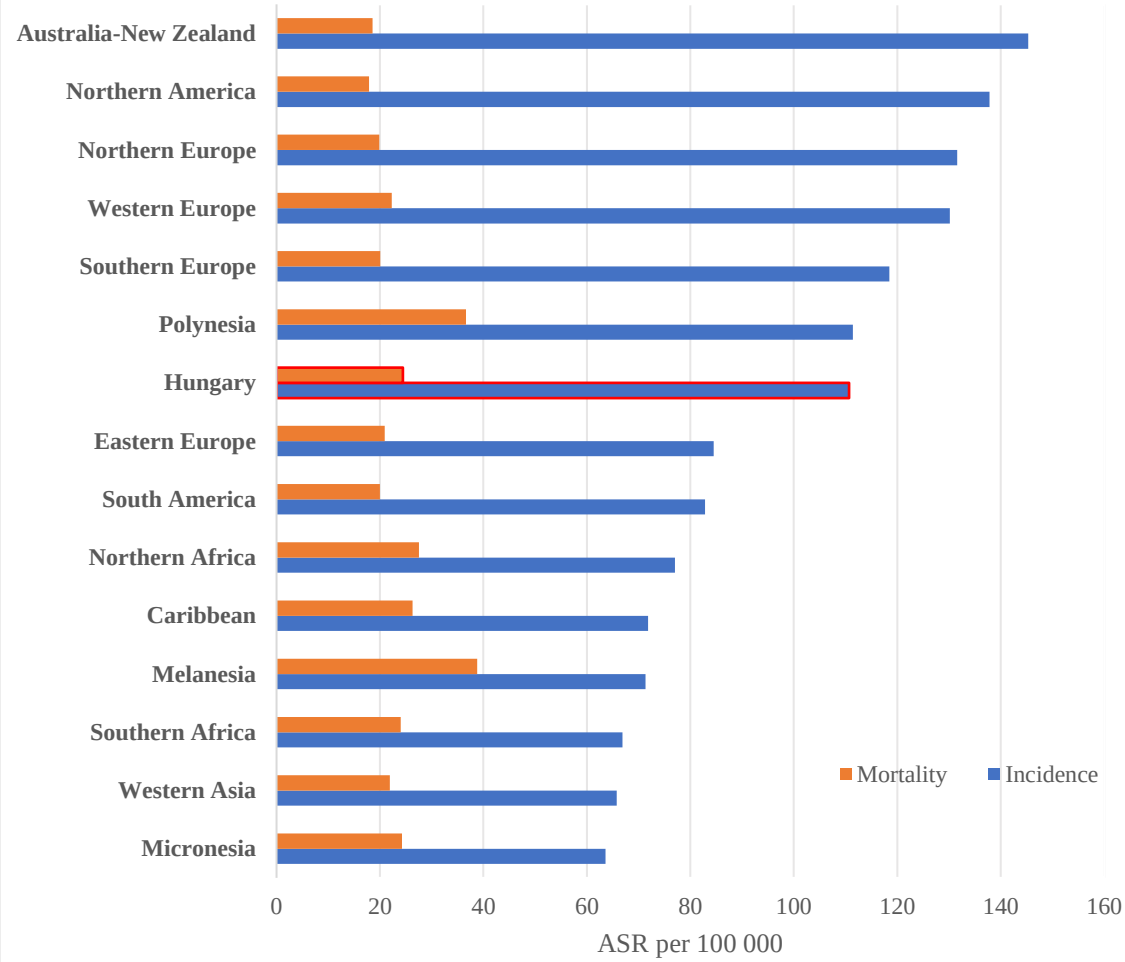

Figure 1: Breast cancer statistics in 2022.

Age Standardized Rate (ASR) of breast cancer incidence and mortality (per 100 000) among females from 15 to 85+ years old, according to the Global Cancer Observatory [22].

The risk factors for the development of breast cancer are:

- Gender and age [23],
- Genetic and epigenetic factors, including BRCA1 and BRCA2 gene mutations, high expression of epidermal growth factor receptor (EGFR) and human epidermal growth factor receptor (HER2) [24],
- Prolonged hormone exposure, such as the use of oral contraceptives, hormone replacement therapies, as well as early menarche or late menopause [23],

- Breast cancer or other neoplastic diseases in the medical history of the family [24],
- Obesity, regular smoking, and alcohol consumption [24],
- Dense breast tissue [17], [25].

In contrast, pregnancy, breastfeeding, regular physical activity, and healthy lifestyle free from harmful addictions can reduce susceptibility to breast cancer [26].

2.1.2. Breast cancer classification

Breast cancer is a highly heterogeneous disease. The application of effective classification systems, including histological type, Nottingham grade, TNM stage (tumor, node, metastasis), and receptor status determination is of high importance for determining appropriate therapy.

Malignant breast tumors can be classified into two main groups based on their cell origin, distinguishing between carcinoma of epithelial origin and sarcoma originating from the mesenchyme. Their histopathological classification is carried out according to the criteria set by the World Health Organization (WHO) [27]. Malignant breast lesions are primarily of epithelial origin, mostly presenting as *in situ* or invasive forms of ductal or lobular carcinoma. *In situ* carcinomas are characterized by malignant cells confined to the breast ducts without penetrating the basal membrane. In contrast, invasive tumors have the ability to breach the basal membrane, enter the lymphatic and blood circulation, and form distant metastases [28]. A significant portion of invasive breast tumors are ductal carcinomas, identified as non-special type (NST) according to the WHO classification [27]. The occurrence of breast sarcomas is less frequent [29].

Histological grade is a prognostic factor that characterizes the degree of differentiation of tumor cells. The Nottingham grade evaluates the tendency of tubule formation, takes into account nuclear pleomorphism (cell nucleus shape, size, number of nucleoli), mitotic activity (mitosis index), as well as lymphatic and vascular invasion. Based on these criteria, grade 1 tumors contain well-differentiated cancer cells, infiltrate the stroma to a small extent, and do not exhibit mitotic activity. Grade 2 tumors are moderately differentiated, with cancer cells present in the glandular tissue and characterized by moderate mitotic activity. Poorly differentiated tumors are classified into grade 3, where the tumor mass consists of amorphous neoplastic cells showing significant nuclear atypia and high mitotic rate and are associated with markedly poor prognosis [30].

For assessing the expected course of the disease, determining the TNM stage of the tumor is crucial, based on the size of the primary tumor, involvement of regional lymph nodes, and

presence of distant metastases [31]. Stage 0 indicates *in situ* carcinoma (ductal or lobular) or pre-cancerous condition, while stage 1-3 are determined by the size of the primary tumor and lymph node infiltration, without detectable metastases. Metastatic breast cancer is identified by stage 4, characterized by an unfavorable prognosis and survival rate [32].

The expression of hormone receptors such, as HER2 (EGFR2), estrogen (ER), and progesterone receptors (PR) on the surface of breast tumor cells provides therapeutic predictive information and defines the treatment plan. ER+ and PR+ tumors generally have more favorable outcome, whereas increased expression of the HER2 gene serves as a negative prognostic marker [17]. These receptors have been targeted for the development of the first targeted therapies in adjuvant breast cancer treatment [33]. On the other hand, triple-negative cases (ER-, PR-, HER2-) without targeted treatment modalities are associated with significantly worse prognosis [34]. Breast tumors can be classified into the following molecular subtypes based on their immunophenotype [35]:

- Luminal A: ER+, PR+, HER2-, low proliferative activity
- Luminal B (HER2-): ER+, PR-, HER2-, high proliferative activity
- Luminal B (HER2+): ER+, PR+, HER2+, low/high proliferative activity
- HER2+: ER- or PR-, HER2+
- Basal type (triple-negative): ER-, PR-, HER2-, frequent BRCA1 gene mutation

2.2. Hallmarks of cancer

Breast cancer is characterized by the acquisition of specific functional capabilities known as the “hallmarks of cancer”. Hallmarks of cancer was originally proposed as a comprehensive set of attributes acquired by human cells during their transformation from normal, terminally differentiated cells into a malignant tumor. There are eight hallmarks of cancer: avoiding immune destruction, reprogramming cellular metabolism, activating invasion and metastasis, inducing/accessing vasculature, enabling replicative immortality, resisting cell death, evading growth suppressors, sustaining proliferative signaling. While originally considered separate, deregulated cellular metabolism and immune destruction avoidance are now recognized as core hallmarks of cancer [36] (**Figure 2**).

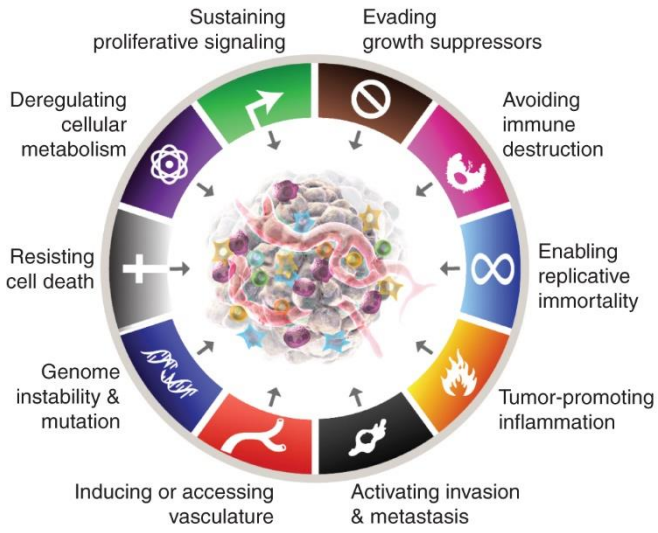

Figure 2:Hallmarks of Cancer.

The hallmarks of Cancer, as of 2022, encompass eight hallmark capabilities and two enabling characteristics. The hallmarks of cancer graphic has been adapted from Hanahan and Weinberg [36].

One of the most fundamental characteristics of (breast) cancer cells is their capability to maintain continuous proliferation. Unlike normal tissues, where the production and release of growth-promoting signals is tightly regulated to control cell cycle progression and maintain a balance of cell numbers, cancer cells exhibit dysregulated growth signals. This disruption can lead to uncontrolled cell division, jeopardizing the normal architecture and function of tissues [14]. In this study, we will specifically concentrate on the aspects of proliferation, invasion and metastasis, and the deregulation cellular metabolism.

2.2.1. Tumor microenvironment

Tumors consist of two interconnected compartments: the parenchyma, containing cancer cells and cancer stem cells (CSCs), and the stroma, induced by non-transformed parenchymal cells and housing them within its structure [37].

Cancer cells serve as the foundation of the disease, initiating and driving tumor progression, although tumors are heterogeneous cell populations. The precise mechanism underlying the development of heterogeneous tumor remains a topic of ongoing discussion, however simplest explanations to this heterogeneity often include CSCs in central role. For instance, in the CSC or hierarchy model, only stem cells harbor tumorigenic potential, while differentiated cells have

little or none. An alternative model suggests that mutations gather gradually in cells, and any cell may have tumorigenic potential. The plasticity model introduces another perspective, suggesting that differentiation could be a two-way street, allowing previously differentiated non-tumorigenic cancer cells to revert differentiation into CSCs once again [38]. CSCs have been found to be present in most tumors, and they have the ability to effectively seed new metastases. Additionally, CSCs are more resistant to various chemotherapeutic treatments [39]–[43]. It is important to note that cancer cells can transform into CSCs. In this process, epithelial-mesenchymal transition (EMT) transcription factors contribute to the acquisition of stem-like features. Classifying these cells into static classes, such as cancer cells or CSCs, could only represent their current state [44].

While transformed parenchyma cells actively proliferate and form tumors, non-transformed stromal cells, including cancer-associated fibroblasts (CAFs), pericytes, cancer-associated endothelial cells (CAECs), immune inflammatory cells (ICs) and stromal stem and progenitor cells, play a supporting role in facilitating cancer growth [14].

CAFs constitute majority of stromal cells in breast, prostate, and pancreatic cancer. In comparison to normal fibroblast cells, CAFs show increased rate of proliferation, promote sustained inflammation by secreting inflammatory cytokines and support angiogenesis [45]. CAFs, as normal fibroblasts during wound healing process, produce extracellular matrix (ECM) proteins in the tumor microenvironment. ECM proteins in breast cancer have shown to prompt immunosuppression by recruiting PD-1+ tumor associated macrophages [46]. CAFs also contribute to tumor progression and EMT through secretion of stromal cell-derived factor-1 (SDF-1) and transforming growth factor-beta (TGF-β) [47]. Tumor energy metabolism is also supported by CAFs via secretion of pyruvate, lactate, ketone bodies, and fatty acids generated during aerobic glycolysis. These molecules are then taken up by cancer cells and used to produce ATP, facilitating tumor growth and angiogenesis [48].

Upon TGF-β induction, normal endothelial cells undergo EMT, leading to the formation of CAECs with distinctive gene expression profiles, cell surface markers, and morphology. These cells constitute the inner layer of blood vessels in solid tumors and, hence play important role in tumor-associated angiogenesis and vascularization to developing tumor tissues [45]. The outer layer of blood vessels is formed by pericytes, a specialized mesenchymal cell type which participate in angiogenesis [49]. These cells are involved in the remodeling of the basement membrane [50] and regulation of immune cells [46].

Characterization of tumor immunoreactivity involves identifying infiltrating immune cells. Under the influence of chemokines and inflammatory mediators produced by the tumor or tumor-associated stroma, a large number of immune cells appear in the tumor microenvironment [51]. Immune cells can create a favorable environment for tumor cell proliferation, resistance to apoptosis, angiogenesis, and the development of metastases [52], [53]. Additionally, immune cells (especially tumor associated macrophages) can secrete matrix metalloproteinases (MMP), which supports the formation of metastases by malignant cells [54]. However, immune cells can also induce apoptosis through the production of reactive oxygen species (ROS), and ROS can activate cytotoxic T cells, natural killer cells, or B lymphocytes [55]. The ratio of tumor stromal-infiltrating lymphocytes (TILs) is a prognostic marker, determining the response to neoadjuvant treatment for breast cancer. A higher TIL ratio correlates with better therapeutic efficacy and indicates a more favorable prognosis mediated through tumor-specific immunity [55].

These stromal changes and the development of a reactive tumor-promoting microenvironment contribute to tumorigenesis by stimulating survival and anti-apoptotic signals and supporting angiogenesis, migration, and invasion, creating an optimal environment for tumor growth and metastasis. The metabolism of malignant cells is regulated by the tumor microenvironment. The microbiome is an essential part of the tumor microenvironment, influencing the metabolism of tumor cells through maintaining healthy barrier functions, inducing inflammation, and producing various genotoxins and bacterial metabolites [5].

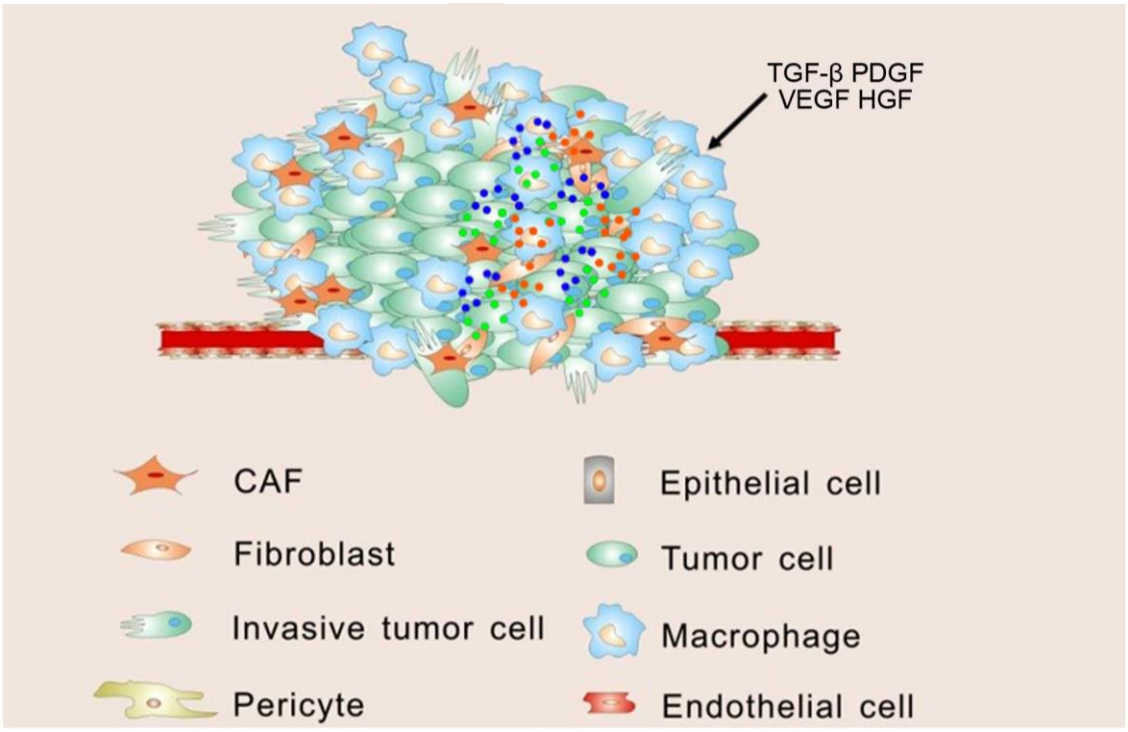

Figure 3:The tumor microenvironment

CAF, cancer associated fibroblast; Figure adapted from Yuan et al [56].

2.2.2. Sustained proliferation in breast cancer

In normal tissues, the expression of growth-promoting signals is tightly regulated to sustain tissue homeostasis, structure, and function. However, cancer cells acquire the capability to sustain proliferative signals and continuously proliferate beyond their normal lifespan, thereby disrupting the structure of the normal tissue.

Cancer cells can sustain their growth promoting signals through:

- overexpressing growth factor receptors [57],
- producing their own growth factors (autocrine signaling) [58],
- mutations in the growth factor signaling pathways [59].

Mutations in growth signaling pathways allow cancer cells to prevent apoptosis, compromise cell cycle exit, or drive cell cycle progression. Gene mutations in growth signaling are frequently

occurring in the members of MAPK [60], PI3K [61], Akt signaling [62], and mTOR signaling pathways [63]. These mutations also provide resistance against conventional therapeutic approaches [64].

Losing growth control mechanisms in neoplastic cells provide them the ability to avoid growth inhibition and elimination by tumor suppression proteins. These tumor suppressor proteins inhibit the proliferation of mutated cells by controlling cell cycle, induce senescence, quiescence or even apoptosis in critically damaged cells. Genetic mutations are not only affecting growth promoting signals, but also occur in tumor suppressor genes at approximately 70% of the cases [59], [65]. The two most important tumor suppressors are the Retinoblastoma protein (Rb) and tumor protein 53 (p53), which are mediating the G0/G1 phase checkpoints of the cell cycle [66].

The literature on sustained cellular proliferation is vast, therefore, we will focus on those pathways that are important for the interpretation of our results. In breast cancer cell proliferation and growth signaling, the Wnt/β-catenin pathway holds a central position. Mutations leading to the stabilization of β-catenin or β-catenin targets are frequently associated with increased tumor aggressiveness [67]. When the WNT pathway is downregulated, β-catenin is ubiquitinated and phosphorylated by GSK-3β on the destruction complex. This leads to the degradation of β-catenin. Alternatively, when the WNT pathway upregulated, the destruction complex is disrupted, GSK-3β does not phosphorylate the β-catenin. In this active state, β-catenin translocates to the nucleus, where it induces the expression of *CYCLIN D1*, *c-MYC*, *PDK*, *MTC-1*, *MMP7*, fibronectin, *COX2* and *AXIN-2* genes. Constitutive β-catenin signaling appears to support the survival and growth of stem cells during the early stages of tumor development. Constitutive activation of the β-catenin pathway is frequently associated with CTNNB1, APC, AXIN-1 and AXIN-2 gene mutations [67]. To assess β-catenin activity, the phosphorylation status of GSK-3α/β is usually assessed, as when GSK-3α/β is phosphorylated (deactivated), it cannot effectively phosphorylate β-catenin, which protects β-catenin from degradation [68].

2.2.3. EMT in breast cancer

Cells in carcinomas usually lose their epithelial morphology in a process, called epithelial-mesenchymal transition (EMT). EMT is a complex biological process through which epithelial cells undergo a series of molecular changes that result in a transition to a mesenchymal cell

phenotype (**Figure 4**). In general, mesenchymal cells lose their ability for focal adhesion and become mobile. Mobility enables the spreading of cancer and metastasis formation. This process plays a critical role during embryonic development, tissue repair and wound healing, as these cells have the ability to migrate. EMT has been implicated in various pathological conditions, including cancer progression and metastasis [69].

Epithelial cells undergo EMT in response to signals received from their (micro)environment, or in response to mutations in EMT signaling. Studying EMT is challenging, since cell morphology and molecular characteristics are usually not painting a binary picture, exclusively indicating either epithelial or mesenchymal state. Certain cytokines like transforming growth factor-β (TGF-β), fibroblast growth factor (FGF) family, epidermal growth factor (EGF), and hepatocyte growth factor (HGF) are known to induce or promote the EMT. These EMT-inducing signals up-regulate specific transcription factors, such as SNAI (Snail Family Transcriptional Repressor), TWIST (Twist Family BHLH Transcription Factor), ZEB (Zinc finger E-box binding homeobox) [70], and β-catenin [71]. EMT transcription factors often collaborate with miRNAs and various epigenetic and post-translational regulators to orchestrate EMT control. The miR-34 family is recognized for its role in regulating EMT and suppressing early phases of tumor metastasis. In particular, miR-34a prevents TGF-β induced EMT and regulates SNAI1 expression through its 3'-UTR. It also suppresses SLUG and ZEB1. Carcinoma cells typically exhibit a spectrum of epithelial-mesenchymal characteristics, among which E-cadherin, occludins, and cytokeratins are commonly used as epithelial markers, while N-cadherin and vimentin are applied as mesenchymal markers [70]. E-cadherin and occludins are located in tight junctions on the surface of epithelial cells, where their main role is to maintain cell-cell connections [72], while cytokeratins are members of cytoskeletal intermediate filaments and their composition is different when comparing normal and cancerous cells [73]. The mesenchymal marker N-cadherin also mediates cell-cell adhesion, but induce changes in cell behavior in favor of migratory phenotype in EMT [74]. Vimentin is an intermediate filament protein associated with EMT phenotype [75]. Recent research has shown that certain cancer cells express both epithelial and mesenchymal markers, as observed in breast, pancreatic, renal, lung, and colorectal cancers [70].

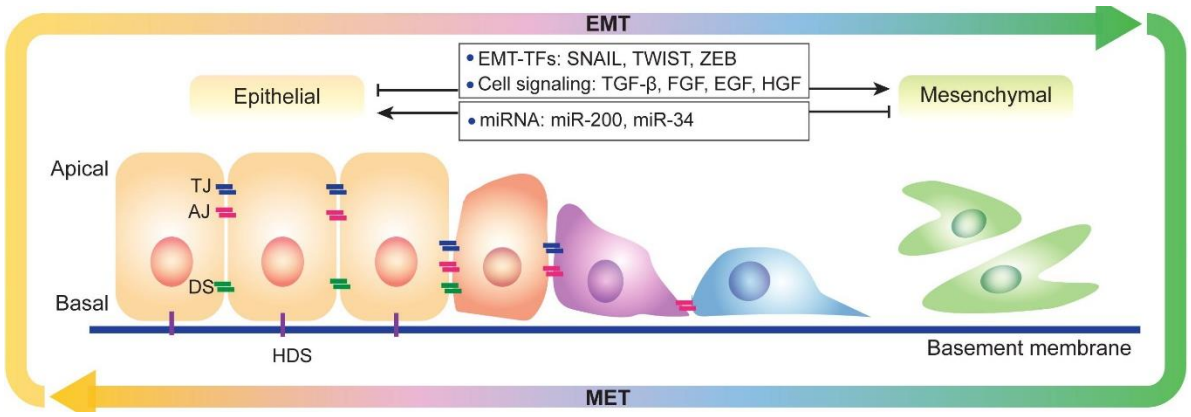

Figure 4: Epithelial-mesenchymal transition (EMT)

During EMT, cells lose their intercellular and basement membrane connections, change their characteristic epithelial morphology, and migrate to other parts of the body. Mesenchymal cells express higher levels of EMT transcription factors. TJ, tight junction; AJ, adherens junction; DS, desmosome; HDS, hemidesmosome. Adapted from Lai et al., 2020 [70].

Table 1. Cell culturing media mixtures.

EMT marker name	**Marker**
E-cadherin	Epithelial
N-cadherin	Mesenchymal
Vimentin	
β-catenin	
EMT transcription factors	**Marker**
Snail Family Transcriptional Repressor-1	(EMT inducing) Mesenchymal
Twist Family Transcription Factor-1	
Zinc Finger E-box binding homeobox-1	
Signaling pathways/receptor ligands	**Marker**
Transforming Growth Factor-β (TGF-β)	(EMT inducing) Mesenchymal
Wnt/β-catenin	
Fibroblast Growth Factor (FGF)	
Epidermal Growth factor (EGF)	
Hepatocyte Growth Factor (HGF)	

2.2.4. Angiogenesis in cancer

Angiogenesis, the process of forming new blood vessels, plays a crucial role in cancer development. Tumor growth beyond a certain size is dependent on the establishment of an adequate blood supply to provide nutrients and oxygen, as well as to remove waste products [76]. In cancer, angiogenesis is often dysregulated, resulting in an imbalance between pro-angiogenic and anti-angiogenic factors. Tumor cells can produce and release pro-angiogenic factors, such as vascular endothelial growth factor (VEGF), basic FGF, and platelet-derived growth factor (PDGF). These factors stimulate the proliferation and migration of endothelial cells, the building blocks of blood vessels leading to the formation of new blood vessels within the tumor microenvironment [77]. The vasculature formed in tumors is often abnormal and leaky. Angiogenesis also facilitates metastasis formation. Leaky vessels enable cancer cells to enter the bloodstream or lymphatic vessels and subsequently disseminate to distant organs. Once at a secondary site, the establishment of new blood vessels through angiogenesis supports the growth of metastatic tumors [78]. The abnormal tumor vasculature hinders the delivery of anti-cancer drugs and immune cells, therefore reducing the effectiveness of therapeutic interventions [79].

2.2.5. Tumor cell energy metabolism

The Warburg effect is a prominent metabolic hallmark of cancer and has significant implications for tumor development and progression. The Warburg effect, also known as aerobic glycolysis, is a metabolic phenomenon commonly observed in cancer cells. It refers to the preference of cancer cells to generate energy through glycolysis, a process that occurs in the cytoplasm, even in the presence of sufficient oxygen amounts (aerobic conditions). This metabolic shift is in contrast to normal cells, which primarily rely on oxidative phosphorylation in the mitochondria to produce energy (**Figure 5**) [80].

Cancer cells, undergoing Warburg-type metabolic transformation, exhibit enhanced glucose uptake and an increased rate of glycolysis, leading to the production of lactate as a byproduct. In addition, mitochondrial oxidative phosphorylation is inhibited, instead the mitochondria perform intermediary metabolic processes and biosynthesis. Despite the less efficient production of ATP in cancer cells with Warburg-type metabolism compared to oxidative phosphorylation in normal, differentiated cells, Warburg metabolism supports the survival of cancer cells [81]. The lower level of oxidative phosphorylation in cancer cells leads to the production of lactate. In the

extracellular environment, lactate may influence immune responses and facilitate tumor immune evasion [82]. However, the mitochondrial metabolism change is more extensive in cancer cells, than simply disrupting glycolysis and oxidative phosphorylation. The Warburg effect also promotes the mitochondrial biosynthesis of key metabolic intermediates that are utilized for the synthesis of nucleotides, lipids, and amino acids required for rapid cell division [83], [84].

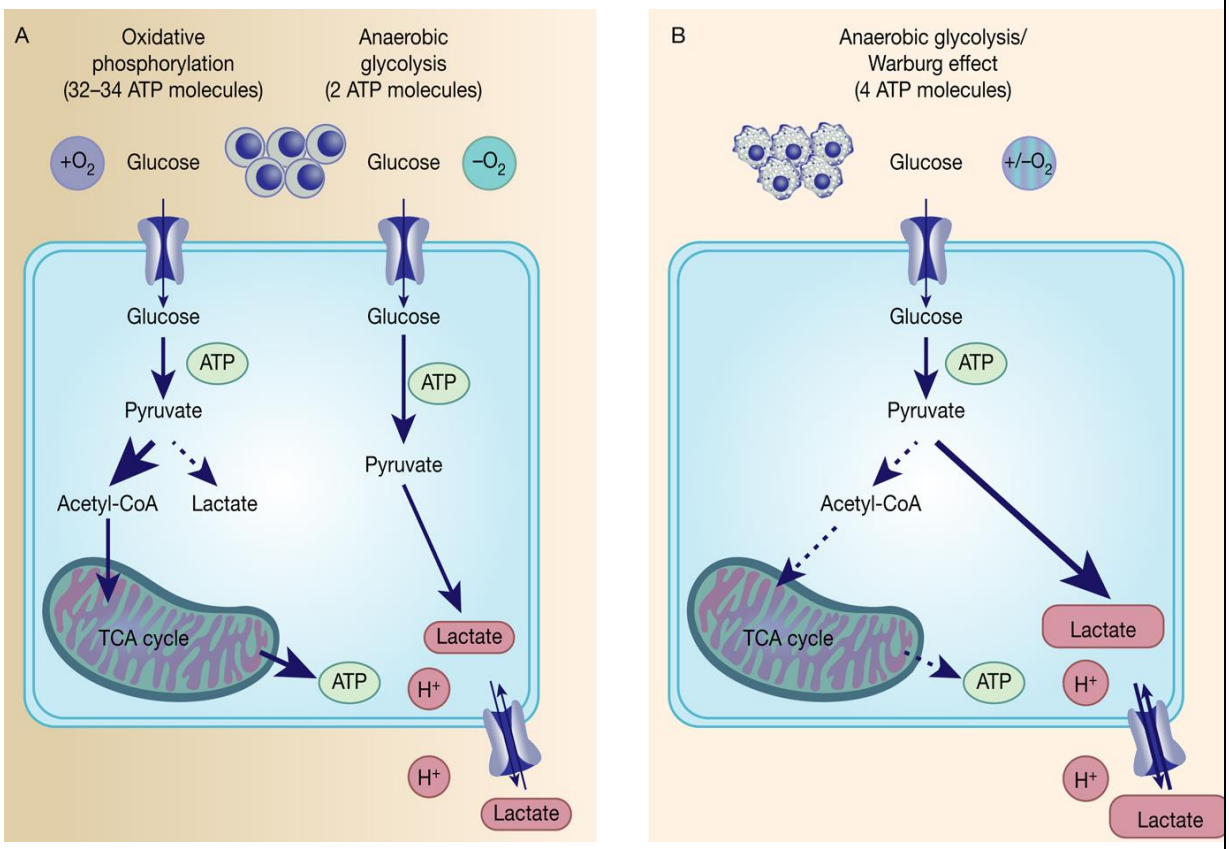

Figure 5: The Warburg effect

Cancer cells exhibit enhanced glucose uptake and increased rate of glycolysis, while ATP production through oxidative phosphorylation is inhibited. Figure adapted from Unterlass and Curtin [85]

The most prevalent course for pyruvate, the product of glycolysis, involves its conversion through the pyruvate dehydrogenase (PDH) complex into acetyl-coenzyme A. Acetyl-coenzyme A is subsequently transformed to citrate by condensing with oxaloacetate through the action of citrate synthase. Consequently, citrate can either be converted into isocitrate as part of the citric acid (or Krebs) cycle, or it can exit the mitochondria. When citrate leaves the mitochondria, it is metabolized by ATP citrate lyase to produce cytosolic acetyl-coenzyme A. That serves as a

substrate for processes, such as *de novo* lipogenesis and protein acetylation. The proper functioning of the pyruvate-citrate shuttle within mitochondria is thus crucial for the synthesis of fatty acids, cholesterol, and protein acylation. With some exceptions, such as in the cases of hypoxia, the primary source of lipogenic acetyl-coenzyme A for most cancer cells originates from glucose-derived pyruvate via the PDH pathway [84].

Apart from carbohydrates, amino acids play a vital role as substrates that fuel both mitochondrial metabolism and the creation of proteins, lipids, and various other molecules. Particularly in the context of cancer, specific mitochondrial enzymes involved in processing glutamine, proline, aspartate, and alanine are of significant interest. Among these, glutamine holds special importance as a nutrient crucial for cell proliferation. This is due to the fact that the amido nitrogen within this amino acid serves as an essential substrate for generating hexosamine and nucleotides in the cytosol. Moreover, glutamine may serve as an important anaplerotic substrate, contributing to the replenishment of intermediates within the TCA cycle's metabolic processes [86]. Carbon from glutamine can additionally contribute to the production of acetyl-coenzyme A, which is essential for synthesizing lipids. This process occurs when glutamine undergoes metabolic reactions facilitated by malic enzymes through either glutaminolysis or reductive carboxylation pathways. These malic enzymes are found both in the cytosol and within mitochondria. Tumor cells have the capacity to upregulate the expression of either one or both isoforms of malic enzymes [84].

The role of mitochondrial metabolism has a definitive role in the generation of numerous non-essential amino acids and their subsequent incorporation into biosynthetic pathways. Within this context, the *in vivo* detection of glutamine *de novo* synthesis in tumors has been detected administering infusions of [^{13}C]glucose into mice that carried orthotopic human glioblastoma tumors [87]. Moreover, certain breast epithelial cells exhibit the ability to achieve glutamine independence through the expression of glutamine synthetase [88].

The mitochondrial metabolism and synthesis of proline is of paramount importance for tumor cells, primarily because of the alterable chemical properties it imparts to protein synthesis. Proline synthesis stems from glutamine or ornithine derived from the urea cycle [84]. Downregulation of proline catabolism, observed frequently in various tumor types, complements its biosynthesis. The first stage of this process takes place within the mitochondria and is catalyzed by proline

oxidase (POX). Notably, the production of this enzyme is diminished in many cancer types when compared to healthy tissue from the same patient [89].

Aspartate can be produced from the oxaloacetate intermediate of the TCA cycle through the activity of glutamate-mediated transamination. Hence, the synthesis of aspartate and downstream metabolites is intricately linked to mitochondrial function [90].

Alanine, generated by alanine transaminases (GPT1 in the cytosol and GPT2 in the mitochondria), facilitates the transfer of an amino group between glutamine and pyruvate, yielding both alanine and α-ketoglutarate. This process not only provides alanine for protein synthesis but also supplies α-ketoglutarate for TCA cycle participation [91].

Lastly, the metabolism of branched-chain amino acids is also notably facilitated by transaminases, both in the cytosol (via BCAT1) and in the mitochondria (via BCAT2) [84].

Beyond the processes of amino acid and lipid synthesis, the creation of nucleotides is significantly reliant on mitochondrial metabolism and its related intermediary compounds. While the ribose portion of nucleotides is formed solely within the cytosol, a number of constituents crucial for building both pyrimidine and purine bases stem directly or indirectly from mitochondria. The formation of pyrimidine ring necessitates the presence of glutamine and aspartate, which can be sourced from mitochondrial pathways as previously mentioned. Additionally, the involvement of a mitochondrial enzyme called dihydroorotate dehydrogenase (DHODH) is crucial for pyrimidine synthesis [84]. In addition to its role as an enzyme, inhibiting DHODH also disrupts the proper functioning of complex III within the electron transport chain. This disruption leads to the accumulation of p53 and triggers apoptosis, establishing a stronger connection between mitochondrial respiration and the growth and survival of cancer cells [92].

For the synthesis of purine nucleotides, nitrogen sourced from aspartate and glutamate, along with glycine and formate for backbone construction, are necessary components. While the enzymes participating in glycine and formate synthesis are found in both the cytosol and mitochondria, mounting evidence suggests that the primary source of formate (and possibly glycine) for this pathway predominantly originates from mitochondrial metabolic processes [84].

The metabolic changes are associated, with the complex reprogramming of the cellular energy sensor system. Among others, this web of sensors encompass mTOR [93], forkhead box O1 (FOXO1) [94], adenosine monophosphate-activated protein kinase (AMPK) [95], as well as peroxisome proliferator-activated receptor gamma coactivator-1α and β (PGC-1α and PGC-1β).

The induction of mTOR complexes (mTORC1 and mTORC2) enhances the expression and activity of genes involved in the Warburg effect and glutaminolysis. Meanwhile, the FOXO1 transcription factor primarily triggers cell cycle arrest or decreased cell proliferation capacity through the inhibition of mTORC1 leading to tumor suppression [96], [97]. In patients with breast cancer, lower activity of the serine/threonine kinase, AMPK was observed. Low AMPK activity is associated with aerobic glycolysis (Warburg effect) and enhanced tumor growth [95], [98]. The antitumor effect of AMPK plays a crucial role in maintaining energy homeostasis and stimulates mitochondrial biogenesis through the regulation of PGC-1α and PGC-1β [99], [100]. In human breast cancer, the activity of nuclear respiratory factor 1 (NRF1) is upregulated. NRF1 and NRF2 play essential roles in regulating the expression of electron transfer chain subunits encoded by the nuclear genome and in binding to the promoters of genes involved in mitochondrial DNA (mtDNA) transcription. These transcription factors are influenced by transcription coactivators, predominantly by PGC-1α [101]. In breast cancer, therapeutic approaches targeting Warburg-type metabolic rearrangements can reduce the proliferation of cancer cells holding a promise for identifying druggable signaling pathways (e.g. [102]).

2.2.6. MCF7 human breast cancer cell line

The MCF7 breast cancer cell line was created in 1973 by the Michigan Cancer Foundation. These cells were derived from the pleural effusion of a 69-year-old woman with metastatic breast cancer. The patient had undergone mastectomies of her right and left breasts 7 and 3 years before the establishment of the cell line, respectively. After the mastectomies, local recurrences were managed for an additional 3 years using radiotherapy and hormone therapy, but widespread nodular recurrences later appeared in the left anterior chest. Two months after the nodules were removed, the patient developed a pleural effusion. Sample from the pleural effusion was collected and later identified as MCF7 cells [103].

The MCF7 cells belong to the Luminal A tumor type [104]. Luminal A tumors are defined by the presence of ER and/or PR and the absence of HER2. Clinically, these tumors are low grade, slow-growing, and have the best prognosis, with a lower incidence of relapse and a high survival rate. They typically respond well to hormone therapy, such as tamoxifen or aromatase inhibitors, and are less responsive to chemotherapy [105].

The MCF7 cell line exhibits a wide range of aneuploidy, with chromosome numbers varying from 60 to 140 depending on the specific variant. Additionally, MCF7 cells contain a subset of stem cells capable of generating clonal variability, which may explain the heterogeneity observed in this cell line [104].

The cell line show differentiated mammary epithelium characteristics, and express epithelial markers such as: E-cadherin, β-catenin, cytokeratin 18, claudins, zonula occludens protein 1 (ZO-1). The cells are negative to mesenchymal markers. Parental MCF7 cells proliferate and form compact colonies with a typical epithelial polygonal shape, maintaining close contact with each other [104]. The doubling time of the cell line is 24 hours [106].

The MCF7 cell line is commonly used in experiments involving ER-positive breast cancer. Numerous subclones have been developed to represent different classes of ER-positive tumors, with varying levels of nuclear receptor expression [107].

2.2.7. 4T1 mouse breast cancer cell line

The 4T1 cells were isolated from a mouse mammary tumor virus receptor positive ($MMTV^+$) BALB/c mouse, nursed by a C3H mother in 1978. These cells exhibit high tumorigenicity, invasiveness, and the ability to spontaneously metastasize from the primary mammary gland tumor to various distant sites, including lymph nodes, liver, lungs, brain, and bone [108].

The 4T1 cell line lacks expression of ER, PR, and HER2 and is used for researching triple-negative breast cancer (TNBC) [109]. Due to its invasive characteristics, the 4T1 cell line is widely used to model Stage IV triple negative breast cancer [110].

Genomic analysis revealed that the 4T1 breast cancer cell line's median gene copy number is four, suggesting a tetraploid genome in most cells. Components of the Wnt pathway is upregulated in 4T1 cells. In line with the cell line's metastatic phenotype, the mesothelin (MSLN), epithelial cell transforming protein 2 (ECT2), and polo like kinase (PLK1) genes are upregulated [109].

Morphologically, the 4T1 mammary carcinoma displays malignant epithelial growth arranged in a solid arrangement, marked by the proliferation of pleomorphic cells [111]. The mean doubling time of the 4T1 cells in cell culture is 13.6 hours [112].

2.3. The gut microbiome

The microbiome refers to the assembly of microbial species of a compartment identified through next generation sequencing and subsequent sequence alignment. The microbiome is characterized by the number and the abundance of the species in a compartment [113]. Diversity of the microbiome also extends beyond individual species. It encompasses the genetic diversity within each microbial species, allowing functional versatility and adaptation to changing environments This genetic diversity enables the microbiome to produce a wide range of bioactive compounds, including enzymes and vitamins too, which can have profound effects on human health [114]. Disruptions or imbalances in microbiome composition, known as dysbiosis, is associated with various diseases and conditions [115].

The diversity of the microbiome is shaped by various factors, such as the individual's age, ethnicity, hormonal levels, and lifestyle choices as diet, prebiotics, probiotics, stress, hygiene, alcohol consumption, smoking habits, antibiotic use, or iatrogenic factors as chemotherapy and radiation [116]. The composition of the microbiome varies significantly from person to person, giving rise to a unique microbial fingerprint for each individual.

2.3.1. Dysbiosis of the gut microbiome in breast cancer

Dysbiosis denotes an abnormal shift in the microbiome, marked by an atypical microbial composition and function [117]. In breast cancer, oncobiotic changes in various microbial compartments occur, including breast tissue, milk ducts, the intrinsic microbiome of breast carcinoma, the distal gut, and the urinary microbiome [10]. However, no differences were observed in the microbiome of the nipple [106]-[107] when comparing healthy individuals and patients with breast cancer. Moreover, breast cancer tissue have been found to contain viruses (parapoxviruses, human papillomavirus, Herpesviridae, Retroviridae, Parapoxviridae, Polyomaviridae, Papillomaviridae), fungi, and parasites [10], though these markers are not consistently found in all individuals. Microbiome signatures within the oncobiome are associated with survival in breast cancer, highlighting the importance of oncobiotic changes [120]. Microbiome is now recognized as a constituent of the tumor microenvironment [121]. Breast cancer risk factors are linked to reduced diversity, high-density breast tissue [122], early menarche, low physical activity [123], and increased body mass index (BMI) [111]-[112].

Additionally, excessive use of antibiotics, which decreases diversity, may increase the risk of breast cancer, whereas probiotics that enhance diversity may have a protective effect [10].

Distinctive shifts in the gut microbiome were detected among different clinical stages and grades, receptors status, MIB positivity, and proliferative capacity. Notable alterations in taxa between patients and cohorts include *Clostridiales*, *Blautia*, and *Akkermansia muciniphila*. Collection of the identified changes in microbiome further detailed in article titled: *"The involvement of oncobiosis and bacterial metabolite signaling in metastasis formation in breast cancer"*[10].

The gut microbiome and the breast tumor are separated, therefore signaling pathways are required to establish connections between these distant compartments. Numerous pathways facilitate cross-connections between the microbiome and the tumor tissue. Intestinal bacteria that express β-galactosidases (gus and BG genes [125]–[127]) can deconjugete excreted conjugated estrogens. The gus gene is widespread among bacteria, whereas alterations in BG involve *Bacteroidetes* and *Firmicutes* [126]. Several bacteria, including *Collinsella, Edwardsiella, Alistipes, Bacteroides, Bifidobacterium, Citrobacter, Clostridium, Dermabacter, Escherichia, Faecalibacterium, Lactobacillus, Marvinbryantia, Propionibacterium, Roseburia*, and *Tannerella* have been found to express β-glucuronidases [128]. The oncobiome exhibits an increased capacity to reactivate estrogens [10], enabling their reuptake and promotion of the development of estrogen-dependent breast tumors that express the estrogen receptor (ER+). It is noteworthy that the ability to reactivate estrogen was discovered through analyzing the pathways within the microbiomes of the breast and nipple aspirates [118].

Metabolites with bioactive properties, produced by either the microbiome or the oncobiome, can act similarly to hormones and establish a link between the microbiome and cancer cells in remote locations [10]. Considering the gut microbiome harbors the largest number of bacteria in the body, its metabolic capacity is significant. However, the biosynthetic capacity of the microbiome is suppressed relative to the eubiome [11], [13]. Several bioactive bacterial metabolites have been discovered that can influence the behavior of breast cancer cells. These metabolites include cadaverine [5], secondary bile acids [129], indole metabolites [6]-[7], and short-chain fatty acids (SCFAs) [8]-[9]. Notably, these metabolites modulate different processes in carcinogenesis, such as cell proliferation, EMT and oxidative stress [6], [7], [10]. Studies have also revealed that the metabolic capacity of the gut microbiome is suppressed in breast cancer,

resulting in a reduction in the production of well-known antineoplastic metabolites [5], [7], [11]–[13].

In addition to the already characterized metabolites, mentioned before, there are likely other, yet undiscovered bacterial metabolites bioactive in breast cancer. In MiMeDB, a database of human microbial characteristics, 1808 metabolites are listed as microbial only metabolites, 14210 as human-microbe co-metabolites, 8236 human-only. A microbial-host co-metabolite is a result of the combination of human and microbial metabolism. In the human-only metabolite group, 1524 compounds are of exogeneous origin. These are drugs, food supplements, cosmetics, and pollutants [3], which can also influence gut microbiome composition. For example, increased exposure to antibiotics increases the risk of antibiotic-associated dysbiosis [130]. A recent study from a large cohort of individuals also identified 726 metabolites associated with diet, and 208 were associated with the microbiome. These metabolites belong to various chemical classes: lipid-like compounds, organic acids and derivatives, organoheterocyclic compounds, phenylpropanoids, polyketides, benzoids, organic oxygen compounds, and 12 other smaller molecule groups [131].

Dysbiosis can also lead to a shift in microbial metabolite production and can potentially result in altered stool redox potential. For example, a decrease in beneficial bacteria that produce SCFAs, such as butyrate, may impact the antioxidant capacity of the stool. Additionally, dysbiosis can lead to an overgrowth of certain pathogenic or opportunistic microorganisms, which might produce pro-oxidant compounds that contribute to an imbalance in stool redox potential [132], [133]. The relationship between stool redox potential and microbial dysbiosis is currently a subject of active investigation, but our comprehension of this field is still limited.

2.3.2. Secondary bile acid biosynthesis and reabsorption

Bile acids are important molecules involved in the digestion and dietary fat absorption. The liver synthesizes around 200-600 mg of primary bile acid daily from cholesterol. These primary bile acids are the cholic acid and chenodeoxycholic acid. About 5% of the total bile acid pool is eliminated through stool each day, while the rest is reabsorbed at the terminal ileum and enters the enterohepatic circulation. The total bile acid quantity is approximately 3 g. The synthesis of primary bile acids from cholesterol involves the activity of 17 different enzymes located in different cellular compartments, including the cytoplasm, endoplasmic reticulum, mitochondria,

and peroxisomes. The key initial reaction in the classic transformation is catalyzed by cholesterol 7α-hydroxylase (CYP7A1), which is the rate-limiting step in bile acid synthesis. The presence of sterol 12α-hydroxylase (CYP8B1) during the synthesis results in the end product cholic acid, while its absence leads to the formation of chenodeoxycholic acid. On the alternate pathway, sterol 27-hydroxylase (CYP27A1), a mitochondrial cytochrome P450 enzyme expressed in various tissues, catalyzes the first reaction. However, in the liver, only 9% of the synthesized bile acids are formed via this alternative pathway. After synthesis, the carboxyl group of most bile acids is conjugated with either glycine or taurine. In the distal ileum, conjugated cholic and chenodeoxycholic acids undergo deconjugation, and bacterial 7α-hydroxylases transform them into secondary bile acids, as deoxycholic acid (DCA) and lithocholic (LCA) respectively. Furthermore, bacterial epimerases facilitate the conversion of chenodeoxycholic acid's 7α-hydroxy group to a 7β-hydroxyl group, yielding ursodeoxycholic acid (UDCA). Bacterial enzymes involved in secondary bile acid production are assembled in the bile acid inducible (bai) operon. Transformations of bile acids result in the hydrophobic nature of secondary bile acids, causing them to lose their capability to function as detergents or toxins against bacteria [129]. Subsequently, bile acids are reabsorbed at the terminal ileum and enter the enterohepatic circulation, where they recirculate to the liver. However, a small portion of bile acids bypasses the liver and remains in the systemic circulation, allowing them to reach distant parts of the body through the bloodstream [134] (**Figure 6**).

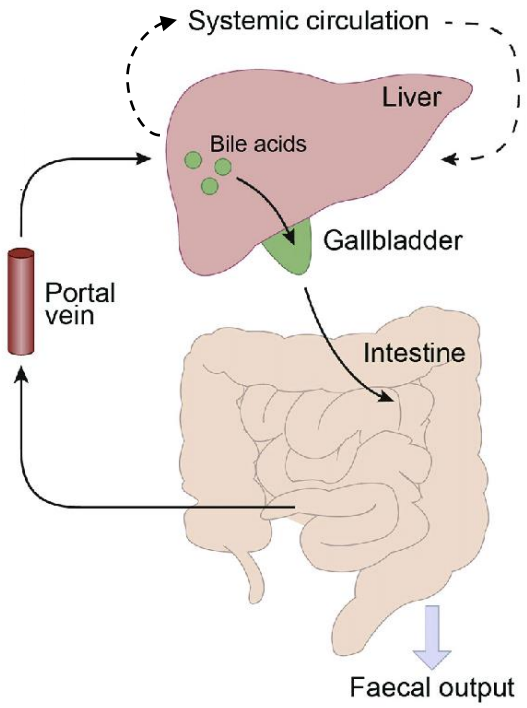

Figure 6: The enterohepatic circulation of bile acids

Primary bile acids, secreted by the liver, enter the ileum where microbiome transforms a part of the pool to secondary bile acids. Secondary bile acids are reabsorbed with the primary bile acids at the terminal ileum and enter the enterohepatic circulation. Modified scheme based on Mertens et al., 2017.

Dysregulation in bile acid metabolism and signaling is implicated in various types of cancer. Certain bile acids, particularly secondary bile acids, can have tumor-promoting effects. They can activate signaling pathways involved in cell proliferation, survival, and inflammation. Bile acids can also promote DNA damage and genomic instability, contributing to the initiation and progression of cancer [129]. Bile acids can also interact with specific receptors, such as farnesoid X receptor (FXR) and the G-protein-coupled bile acid receptor 1 (TGR5), which are expressed in various tissues including the liver, intestine and colon. Activation of these receptors by bile acids can modulate gene expression and cellular responses that influence cancer development [136]. On the other hand, some studies suggest that certain bile acids may have anti-cancer properties. For example, UDCA has been investigated for its potential to inhibit cell proliferation and induce apoptosis in liver cancer cells [137].

The gut microbiome also plays a role in bile acid metabolism, and alterations in the gut microbial composition can impact bile acid profiles. The relation between bile acids and microbial composition is not unidirectional; bile acids also influence the composition of the gut microbiome [138]. The impact of bile acids on the gut microbiome is likely the result of altering the quorum sensing system in bacteria. Quorum sensing is a mechanism that controls the activation of genes in response to changes in the number of cells within a population. Bacteria are engaged in the quorum sensing produce and release chemical signal molecules known as autoinducers, which accumulate as the cell population grows. When the concentration of these autoinducers reaches a specific threshold, it triggers changes in gene expression. Both Gram-positive and Gram-negative bacteria employ quorum sensing communication systems to regulate wide range of biological processes, including virulence, competence, conjugation, antibiotic synthesis, movement, sporulation, and formation of biofilms [139]. In this regard, bile acids may be implicated in quorum sensing, as they influence the composition of the gut microbiome.

The intestinal microbiome plays a crucial role in the conversion of primary bile acids into secondary bile acids [140]. As a result, the changes caused by secondary bile acids directly implicate the involvement of the intestinal microbiome. In our investigation, we focused on three major secondary bile acids – LCA, DCA, and UDCA. During our experiments, we used secondary bile acids in a specific concentration range representing the secondary bile acids in the serum (LCA: 31 nM, DCA: 701 nM, UDCA: 147 nM) [129], [141], [142], and in breast cyst fluid (LCA: 9-23 μM, DCA: 17-160 μM) [129].

2.4. Convolutional neural networks (CNNs) in image analysis

Detecting objects – like the detection of nuclei in a large set of images – with conventional segmentation methods requires readjustment of segmentation parameters between datasets. This could lead to analysis errors between datasets – e.g., wrongly adjusted detection parameters lead to detection of staining artefacts, while leaving faint but valid signals undetected. In the last decade, convolutional neural networks (CNNs) solved this problem in image analysis and by using semantic segmentation models, segmentation of high throughput microscopy images can be standardized between individual datasets as well.

CNNs have been used for computer vision tasks for many years [143]–[145]. However, their true potential was not fully realized until the ImageNet competition in 2012, where their

efficiency was showcased by harnessing the power of graphics processing units (GPUs), rectified linear unit activation, dropout regularization, and effective data augmentation [145]. CNNs have gained popularity not only among computer vision experts, but also in various applications such as processing natural language, analysis of hyperspectral images, and medical image analysis. The primary strength of CNNs lies in their deep architecture [146]–[149], enabling the extraction of distinctive features at multiple levels of abstraction. Nevertheless, the full training of a deep CNN from scratch presents challenges [150]. Firstly, CNNs demand a substantial amount of labeled training data, which is a challenge often encountered in the medical field, where obtaining expert annotations can be costly. Secondly, deep CNN training requires considerable computational and memory resources; otherwise, the process becomes excessively time-consuming. Thirdly, overfitting and convergence issues often complicate the training of a deep CNN, necessitating iterative adjustments in the network's architecture or learning parameters to guarantee uniform learning across all layers. As a result, deep learning from scratch can be laborious, time-consuming, and demands considerable expertise and patience. An encouraging option besides training a CNN from the ground up is fine-tuning a pre-trained CNN that has been trained on a large, labeled dataset from a different application. Pre-trained models have been successfully applied in various computer vision tasks as feature generators or as baselines for transfer learning [151]–[153].

An essential characteristic of CNNs lies in the “transferability” of knowledge embedded within pre-trained CNNs. Research indicates that the effectiveness of knowledge transfer relies on the gap or dissimilarity between the dataset used for training a CNN and the target database for knowledge transfer [151]. Although natural image databases and medical imaging databases differ considerably, recent research shows promising potential for knowledge transfer to the medical imaging domain. An application method of transfer learning involves using a pre-trained CNN as a feature generator [154]–[156]. In this approach, the pre-trained CNN is utilized on an input image, and the CNN generates (extracts) features from a particular layer of the network. These extracted features are then used to train a new pattern classifier, also known as the output layer of a CNN [143]-[144].

Certain visual tasks, especially in biomedical image processing (e.g., nuclei segmentation), the desired output should involve localization, meaning that a class label needs to be assigned to each pixel in the image. Moreover, obtaining thousands of training images is often challenging in

biomedical tasks. To address these issues, a sliding-window setup is adopted to train a network, where the goal was to predict the class label of each pixel by providing a local region (patch) around that pixel as input [157]. This approach has two advantages. Firstly, the network can achieve localization. Secondly, the training data in the form of patches is significantly larger than the number of training images [157]. However, this strategy has two drawbacks as well. It is relatively slow since the network needs to be run separately for each patch, and there is redundancy due to overlapping patches. Then, there is a trade-off between localization accuracy and the use of context. Larger patches allow for more context information but may reduce localization accuracy due to additional max-pooling layers. Conversely, smaller patches enable better localization accuracy but provide limited context information. More recent approaches have proposed classifier outputs that consider features from multiple layers, enabling good localization while using context effectively [158], [159]. This method of classifying each pixel on an image is called semantic segmentation.

In biomedical image analysis, semantic segmentation with CNNs have found applications beyond computer-aided detection systems. Recent uses include carotid intima-media thickness measurement in ultrasound images [160], pancreas segmentation in CT images [161], brain tumor segmentation in MRI scans [162], multimodality isointense infant brain image segmentation [163], knee cartilage segmentation in MRI scans [164], and many applications beyond the scope of this short overview. During the past decade, several popular semantic segmentation models have emerged in the field of biomedical image segmentation:

- UNet stands out as one of the pioneers in biomedical image segmentation, and the model encompasses a symmetric encoder-decoder structure with skip connections [165].
- DeepLab is utilizing “atrous” convolutions for multi-scale contextual information [166].
- Mask R-CNN was initially designed for instance segmentation but it’s adaptation to semantic segmentation is also widely applied [167].
- PSPNet: Pyramid Scene Parsing Network was introduced in 2016, designed to capture multi-scale contextual information in an efficient manner [168].
- FCN: Fully Convolutional Network is based on an encoder-decoder structure, and widely adopted and adapted for different applications, including biomedical image segmentation [169].

- LinkNet: It is a lightweight architecture designed for semantic segmentation tasks, and it has gained popularity due to its computational efficiency and effectiveness [170].

3. The aims of the study

The dysbiosis of the gastrointestinal microbiome can be associated with various diseases, including the development of breast tumors [5]–[7]. We set out to identify and characterize bacterial metabolites, synthesized by the gut microbiome that can reach breast tumor cells through the bloodstream and alter the signaling pathways of the tumor cells to modulate cell proliferation and EMT. According to this, our aims were the following:

1. To assess the cytostatic effects of LCA.
2. To assess the effects of LCA on EMT.
3. To assess the effects of LCA on cellular energy metabolism.
4. To determine the receptor responsible for the effects of LCA.
5. To construct a library of bacterial metabolites with possible antineoplastic effects.
6. To establish high content screening-based methods for the assessment of cell proliferation and EMT.
7. To identify cytostatic bacterial metabolites using the metabolite library.
8. To identify bacterial metabolites affecting EMT.

4. Materials and Methods

4.1. Cell culture

Cell lines were maintained at 37 °C with 5% CO_2. The study employed various cell lines as representative models, including 4T1 murine breast cancer, MCF7 human breast cancer, SKBR3 human breast cancer, A2780 human ovarian cancer, and Capan2 human pancreatic adenocarcinoma cell lines, and also primary fibroblast cells. Exact composition of culture media is specified in **Table 2**.

Table 2. Cell culturing media mixtures.

Cell line	Medium	Reference number	FBS	Penicillin-Streptomycin, (v/v%)	L-glutamine	HEPES	Pyruvate (v/v%)
4T1	RPMI-1640	Sigma R5886	10 %	1 % (P: 100 000U/L, S: 10 mg/l)	2 mM	-	1 % (1 mM)
A2780	RPMI-1640	Sigma R5886	10 %	1 % (P: 100 000U/L, S: 10 mg/l	2 mM	-	-
MCF7	MEM	Sigma M8042	10 %	1 % (P: 100 000U/L, S: 10 mg/l	2 mM	-	-
Capan2	MEM	Sigma M8042	10 %	1 % (P: 100 000U/L, S: 10 mg/l	2 mM	-	-
SKBR3	MEM	Sigma D6429	10 %	1 % (P: 100 000U/L, S: 10 mg/l	2 mM	10 mM	-
Primary fibroblasts	DMEM low glucose	Sigma D5546	20%	1 % (P: 100 000U/L, S: 10 mg/l	2 mM	10 mM	-

4.2. Chemicals

Cambridge Isotope Laboratories (Andover, MA, USA) provided the ^{13}C labeled substrates used in the pulse-chase metabolomics experiment. The inhibitors and antagonists used in the TGR5 experiments (U73343 (phospholipase C inhibitor), NF449 (Gsα-selective antagonist), CINPA1 (CAR antagonist), DY268 (FXR antagonist), GSK2033 (LXR antagonist) were obtained from Tocris Bioscience and were applied at a concentration of 5 µM, with the exception of U73343, which was used at a final concentration of 1 µM.

4.3. Sulphorhodamine B (SRB) cell proliferation assay

4.3.1. SRB proliferation assay for measuring effects of secondary bile acids

For the assessment of cell proliferation, we used the SRB assay. Cells were seeded on 96-well plates (3000-5000 cells/well). Cells were treated with secondary bile acids for 48 hours. Then cells were fixed with 10% trichloroacetic acid (TCA) and stained with SRB solution (0.4% in 1% acetic acid). Unbound dye was removed by washing with 1% acetic acid. Bound dye was solubilized with 10 mM TRIS base. Absorbance was read on an automated plate reader (Thermo Labsystems Multiskan MS, Thermo Fisher Scientific, Waltham, MA, USA) at 540 nm.

4.3.2. SRB proliferation assay for validating image analysis-based cell proliferation assay

Cells were seeded on 96-well tissue culture test plates and fixed after 8 hours. In parallel to this, cells were also seeded on 96-well high content imaging microplates in the same manner. Cells on tissue culture test plates were fixed with 10% TCA and stained with SRB solution. Unbound dye was removed by washing with 1% acetic acid. Bound dye was solubilized with 10 mM TRIS base. Absorbance was read on an automated plate reader (Thermo Labsystems Multiskan MS) at 540 nm.

Cells on high content imaging microplates were fixed with 4% paraformaldehyde (PFA), then permeabilized with 1% Triton-X 100/PBS solution, unspecific binding sites were blocked with 1% BSA/PBS solution. Nuclei were stained with 4’6-diamidino-2-phenylindole (DAPI). Imaging was made with PerkinElmer Opera Phenix High Content Screening System.

4.4. Colony forming assay

In the colony formation assays, a total of 500 cells were initially seeded in each well of a 6-well plate, containing complete growth medium. These cells were then cultured for 7 days in the presence of varying concentrations of LCA, as indicated. After the assay period, the plates were washed twice with PBS. Next, the colonies were fixed in methanol for 15 minutes, followed by drying and staining with May-Grünwald-Giemsa stain for another 15 minutes. Subsequently, the plate was washed with water, and the colonies were quantified using ImageJ software.

4.5. DNA and mRNA preparation and quantitation

Total RNA from cells and tumor samples were prepared using TRIzol reagent (Invitrogen Corporation, Carlsbad, CA, USA). For the assessment of the expression of individual genes, two micrograms of RNA were reverse transcribed using High Capacity cDNA Reverse Transcription Kit (Applied Biosystems, Foster City, CA, USA). The qPCR reactions were performed with qPCRBIO SyGreen Lo-ROX Supermix (PCR Biosystems Ltd., London, UK) on Light-Cycler 480 Detection System (Roche Applied Science). Geometric mean of 36B4 and cyclophylin was used for normalization. Primers are listed in **Table 3**.

Table 3. Primers used in the RT-qPCR reactions**.**

Gene symbol	Murine forward and reverse primer (5′-3′)	Human forward and reverse primer (5′-3′)
Atp5g1	GCTGCTTGAGAGATGGGTTC AGTTGGTGTGGCTGGATCA	CTAAACAGCCTTCCTACAGCAACTT TGAACCAGCCACACCAACTGT
Ndufb5	CTTCGAACTTCCTGCTCCTT GGCCCTGAAAAGAACTACG	GTATTCATTGGTCAAGCTGAACTAG CAGCTCCTTTACCCGTAATTCAGC
Cytc	TCCATCAGGGTATCCTCTCC GGAGGCAAGCATAAGACTGG	TAAGAACAAAGGCATCATCTGG AGGCAGTGGCCAATTATTACTC
36b4	AGATTCGGGATATGCTGTTGG AAAGCCTGGAAGAAGGAGGTC	CCATTGAAATCCTGAGTGATGTG GTCGAACACCTGCTGGATGAC
Cyclophilin	TGGAGAGCACCAAGACAGACA TGCCGGAGTCGACAATGAT	GTCTCCTTTGAGCTGTTTGCAGAC CTTGCCACCAGTGCCATTATG

4.6. SDS-PAGE and western blotting

Cells were lysed in RIPA buffer (50 mM Tris, 150 mM NaCl, 0.1% SDS, 1% Nonidet P-40, 1 mM Na_3VO_4, 1 mM NaF, 0.5% sodium deoxycholate, 1 mM phenylmethylsulfonyl fluoride, protease inhibitor mixture, pH 8.0), then boiled with 50 mM Tris, 2% (w/v) SDS, 3.34% (v/v) glycerol, 16,67 mM β-mercaptoethanol. Protein lysates were separated by SDS-PAGE on 10% acrylamide gels and transferred onto a nitrocellulose membrane (Bio-Rad Laboratories, Supported, Hercules, CA, USA). Antibodies were diluted in 5% BSA solution and are shown in **Table 5**. The secondary antibody was anti-rabbit IgG HRP-linked Antibody (Cell Signaling Technology, Danvers, MA, USA). Labelled proteins were detected by a Chemidoc Touch Imaging System using Supersignal West Pico and Supersignal West Femto ECL Kit (Thermo Fisher Scientific). Blots were quantified by densitometry using Image Lab (Bio-Rad) software.

Table 4. Antibodies used in the study

Antibody/dye	Concentration	Vendor
Phospho-ACC (Ser79)	1:1000	Cell Signaling Technology (#3661)
Phospho-AMPKα (Thr172)	1:1000	Cell Signaling Technology (#2531)
NRF1	1:1000 (WB) 1:100 (immunocytochemistry)	Abcam (ab175932)
PGC1β	1:1000	Abcam (ab176328)
FOXO1	1:1000	Cell Signaling Technology (#9454)
Phospho-GSK-3α/β (Ser21/9) (D17D2)	1:2000	Cell Signaling Technology (#8566)
GSK-3α/β (D75D3)	1:2000	Cell Signaling Technology (#5676)
β-Catenin	1:1000	Sigma (C7082)
TGR5/GPBAR1	1:1000	NOVUS (NBP2–23669)
TexasRed-X Phalloidin	1:150	Life Technologies (T7471)
SnaiI	1:1000	Cell Signaling Technology (3879S)
Vimentin	1:1000	Cell Signaling Technology (5741S)
β-actin	1:20 000	Sigma (A3854)

4.7. Detection of cell death

The assessment of LCA-induced cytotoxicity was conducted using propidium iodide (PI) uptake as an indicator. For the experiment, cells were seeded in 6-well plates (MCF7 – 200 000 cells/well; 4T1 – 75 000 cells/well) and treated with LCA for two days. Subsequently, the cells were stained with 100 µg/mL of propidium iodide (PI) for 30 minutes at 37 °C, washed once with PBS and analyzed using flow cytometry (FACS Calibur, BD Biosciences, San Jose, CA, USA).

4.8. Electric cell-substrate impedance sensing (ECIS)

The electric cell-substrate impedance sensing (ECIS) model Zθ by Applied BioPhysics Inc. (Troy, NY, USA) was utilized to monitor the transcellular electric resistance of MCF7 and 4T1

cells, which were seeded (MCF7 – 40 000 cells/well; 4T1 – 20 000 cells/well) on type 8W10E arrays. After 20 hours, the cells were treated with either vehicle or 0.3 µM LCA, and total impedance values were subsequently measured for an additional 48 hours. Multifrequency measurements were taken at 62.5, 125, 250, 500, 1 000, 2 000, 4 000, 8 000, 16 000, 32 000, and 64 000 Hz. The ECIS modeling tool was employed to assess the barrier resistance values of each well at fixed 180s intervals. The reference well was designated as a no-cell control with complete medium.

4.9. Metabolomics, pulse-chase metabolomics

Cells treated with LCA were collected after 48 hours of treatment. Following rapid freezing in liquid nitrogen, the labeled cells (cultured in D5030 medium with 10 mM [U-^{13}C]-glucose or [2-^{13}C]-acetate (Cambridge Isotope Laboratories, Andover, MA, USA) and unlabeled cells were extracted using a methanol-chloroform-H_2O solution at 4 °C. The resulting supernatant was separated through centrifugation (15 000g for 10 minutes at 4 °C) and stored at -80 °C for later analysis. The samples were then dried and sonicated in a solution of 3-nitrobenzyl alcohol-trimethyl-chlorosilane, followed by incubation at 80 °C. The reaction was halted by adding ammonium bicarbonate. Subsequently, the samples were diluted with an acetonitrile-water solution, and the derivative metabolites were separated using reversed-phase chromatography in Waters Acquity LC system. To conduct measurements, a Waters Micromass Quattro Micro triple quadrupole mass spectrometer (Waters Corporation, Milford, MA, USA) was employed, operated with an electrospray source in positive ion mode.

4.10. Cytochemistry

4.10.1. Immunocytochemistry in secondary bile acid experiments

Cells were grown on coverslips, which were subsequently washed with PBS. The cells were then fixed using 4% PFA for 15 minutes and permeabilized with 1% Triton-X-100 for 5 minutes. Following this, the samples were blocked with 1% BSA for 1 hour and incubated with TexasRed-X Phalloidin (Invitrogen, Oregon, USA) for 45 minutes to analyze cellular morphology. For the cellular localization of the NRF1 protein, the samples were incubated overnight with the NRF1 primary antibody at 4 °C. After washing, the samples were exposed to the secondary antibody

(1:600, anti-rabbit Alexa 488, Life Technologies) for 1 hour at room temperature. TO-PRO-3 iodide (1:1000, Life Technologies) was used to visualize nuclei. The coverslips were rinsed and mounted in Mowiol/Dabco solution. Confocal images were acquired using a Leica SP8 confocal microscopa and LAS AF v3.1.3. software.

4.10.2. Cytochemistry for bacterial metabolite library screening experiments

96-well high content imaging microplates were used for culturing the cells until they reached 70% confluency. The samples were fixed with 4% PFA for 15 minutes, permeabilized using 1% Triton-X 100, and then blocked with 1% BSA/PBS solution. DAPI (Thermo, Cat. No. R3706) was applied to label the nuclei for 5 minutes, while TexasRed-X Phalloidin (Thermo, T7471) was used to label actin filaments for 1 hour. Fluorescent images of the nuclei were captured at 1080x1080 image resolution, using a 10x objective (N.A. 0.3, 1.196 µm/px). DAPI signals (excitation/emission λ: 405/456) were detected across the entire well, encompassing 21 fields. Morphology images (fluorescent pictures of phalloidin-stained cells) were acquired at 2160x2160 pixel image resolution, with a 20x objective (N.A. 0.4, 0.299 µm/px). DAPI and TexasRed-X Phalloidin signals (excitation/emission λ: 561/599) were detected, covering 25 fields in each well. Both sets of images were acquired using the PerkinElmer Opera Phenix High Content Screening System.

4.11. Image analysis in metabolite library screening

4.11.1. Deep learning training dataset – nuclei segmentation

A training dataset was generated from a database of DAPI-stained images of A2780 human ovarian cancer cell line, 4T1 mouse breast cancer cell line, Capan2 human pancreatic cancer cell line, and MCF7 human breast cancer cell line. From our image database, 82 images were selected and used as a training dataset. The selection of these images aimed to provide the highest possible variation both within a single image and between images. Criteria for selecting good examples included images with 1) relatively high or low fluorescent signals, 2) staining errors or artefacts, or 3) overconfluent nuclei with mixed nuclear morphology that covered part of the well edge. First, nuclei were segmented using CellProfiler (Broad Institute, Cambridge, MA, USA) and subsequently, manual corrections were applied. The original dataset underwent augmentation

using the Albumentations (Python3) library, incorporating rotation by 90°, cropping, and brightness changes. As a result, 277 pairs of gray-scale images and the corresponding segmented images were obtained. The order of images in the augmented dataset was randomized, and the dataset was divided into training, test, and validation sets in a 80:10:10 ratio. Training and analysis was done on an 4 core 8 thread, 4.5 GHz processor.

4.11.2. Training parameters for deep learning

On the prepared DAPI dataset, a VGG-UNet semantic segmentation model was trained. The model's architecture was extracted from Keras-segmentation 0.3.0 library (Python3). The model was trained on central processing unit (CPU) for 2 epochs, 8 images per batch through 33 steps. The model used for evaluating the model experimental data, had a loss value of 0.0512 and an accuracy value of 0.9874 on the validation dataset.

4.11.3. Nuclei counting proliferation assay

CellProfiler's integrated object segmentation method (adaptive Otsu method with three classes – middle class assigned to background) was employed to segment the nuclei (https://cellprofiler.org/, version 3.1.8.). Subsequently, the object number on each image was counted. In parallel, the trained semantic segmentation model was applied to replace CellProfiler's segmentation method, and then the objects were counted using CellProfiler.

4.11.4. Cell Morphology analysis

The acquired morphology images were segmented and analyzed using Harmony 4.8 software. First, nuclei and cytoplasms were segmented, and then properties of texture, signal intensity, and position of the segmented objects were calculated. Subsequently, a linear regression model was trained with the calculated morphological properties of TGF-β treated, SB-431542 treated, and control cells to classify the cells into either epithelial or mesenchymal morphology groups.

4.12. Animal experiments, infiltration score, and TIL calculation

All animal experiments were authorized by the local and national ethical board (reg. 1/2015/DEMÁB) and were performed to conform the relevant EU and US guidelines.

Experimental animals were female BALB/c mice between 8 and 10 weeks of age (20-25g). Animals were bred in the "specific pathogen free" zone of the Animal Facility at the University of Debrecen, and kept in the "minimal disease" zone during the experiment. Animal studies are reported in compliance with the ARRIVE guidelines.

4T1 cells were suspended (2×10^6/mL) in ice cold PBS-matrigel (1:1, Sigma-Aldrich) at 1:1 ratio. From this suspension female BALB/c mice received 50 µL injections to their 2nd inguinal fat pads on both sides (10^5 cells/injection). Tumor growth and animal wellbeing was monitored daily.

Tumor infiltrating lymphocyte (TIL) content was counted in sections of HE-stained, formalin-fixed, paraffin embedded tumor tissues as the number of TILs per 100 tumor cells.

4.13. Bacterial metabolite screening library

TGF-β1 was acquired from Thermo Scientific (Ref.: #100.21), SB-431542 was acquired from Sigma (St. Louise, MO, USA, Ref.: S4317). Source, applied concentrations, and reference serum concentration of each metabolite is provided in **Table 6**.

Table 5. Specifications of the bacterial metabolites

Metabolite name	Solvent	Reference number	Serum reference concentrations (µM)	Applied concentrations (µM)
1-Butanol	PBS	Sigma B7906-500ML	0 - 0.27 [171]	0.005 , 0.015 , 0.044 , 0.13 , 0.4
1-Propanol	PBS	Sigma 96566-5ML-F	0 - 0.8 [171]	0.05 , 0.1 , 0.2 , 0.4, 0.8
2,3 butanediol	PBS	Sigma B84904	0.5 - 0.9 [172]	0.48, 0.56, 0.66, 0.77, 0.9
3,4-dihydroxyphenyl acetic acid	PBS	Sigma 850217-14	0.0102 - 0.104 [173], [174]	0.01, 0.018, 0.032, 0.058, 0.104
3-Hydroxyphenylacetic acid	PBS	Sigma H49901	0.11 - 0.174 [173]	0.106, 0.120, 0.136, 0.154, 0.174
3-Hydroxypropionic acid	PBS	Sigma 792659-1G	3, 6, 8 (individual values) [175]	0.5 , 1 , 2 , 4 , 8

Metabolite name	Solvent	Reference number	Serum reference concentrations (µM)	Applied concentrations (µM)
4-aminobenzoic acid	EtOH	Sigma A9878-5G	5.01 - 32.0 [176]	0.3, 1.2, 3.6, 10.8, 32.4
4-hydroxybenzoic acid	PBS	Sigma 8218140250	0.019 - 0.035 [173]	0.019, 0.022, 0.026, 0.03, 0.035
4-Hydroxyphenylacetic acid	PBS	Sigma H50004-54	0.283 - 0.61 [173]	0.28, 0.36, 0.41, 0.5, 0.61
Acetic acid	PBS	VWR UN2789	23 - 254.4 [171], [177]–[180]	15, 30, 60, 120, 240
Allantoin	DMSO	Sigma 05670	1.0 - 24.0 [181]–[183]	0.99, 2.2, 4.9, 10.8, 24
Butyric acid	PBS	Sigma B103500-5ML	1.39 - 14.15 [177], [178], [180]	1, 2, 4, 8, 16
D-alanine	PBS	Sigma A7377-5G	0 - 0.77 [184]	0.048, 0.96, 0.193, 0.385, 0.77
D-glutamic acid	PBS	Sigma G1001-1G	7.42 - 14.6 [184]	7.28, 8.66, 10.31, 12.27, 14.6
D-mannitol	PBS	Sigma M4125-10MG	no report, same concentrations as for D-mannose	6.25, 12.5, 25, 50, 100
D-mannose	DMSO	no data	13 - 73.87 [185]–[187]	6.25, 12.5, 25, 50, 100
Ethylene glycol	PBS	no data	no data, toxic (1.56 mg/kg)	1, 3, 9,27, 81
Formic acid	PBS	Sigma F0507-500ml	11.84 - 224.5 [188]	10, 30, 90, 270, 810
Glycolic acid	PBS	Sigma 124737	6.1 – 69 [175], [189]	1, 3, 9,27, 81
Hippuric acid	PBS	Sigma 112003	1.5 - 21.2 [173], [190]	0.024, 0.12, 0.6, 3, 15
Hydrocinnamic acid	EtOH	Sigma 135232-5G	0.131 - 0.354 [191]	0.128, 0.165, 0.213, 0.274, 0.354
Isobutyric acid	PBS	Sigma I1754-100ML	1.02 - 14.15 [177], [180]	1.02, 1.97, 3.80, 7.33, 14.15
L-pipecolic acid	PBS	Sigma P2519	1.2 - 3.72 [192]	0.25, 0.5, 1, 2, 4

Metabolite name	Solvent	Reference number	Serum reference concentrations (µM)	Applied concentrations (µM)
Oxalic acid	PBS	Sigma 75688	6.5 - 35.5 [193], [194]	6.5, 9.9, 15.2, 23.2, 35.5
Propionic acid	PBS	Sigma P1386-1L	4.86 - 15.33 [177], [178], [180]	1.25, 2.5, 5, 10, 20
Shikimic acid	DMSO	Sigma S5375-10MG	0.03 - 0.23 [195]	0.01, 0.03, 0.09, 0.27, 0.81
Trans-ferulic acid	DMSO	Sigma 52229	0.04 - 15.7 [173], [190]	0.016, 0.08, 0.4, 2, 10
Trimethylamine (TMA)	PBS	Sigma 92260	0.3 -14.44 [196], [197]	0.3, 0.79, 2.1, 5.4, 14.35
Trimethylamine-N-oxide (TMAO)	PBS	Sigma 317594	1.21 - 21.1 [198]–[200]	1.22, 2.48, 5.065, 10.33, 21.1
Vanillic acid	PBS	Sigma H36001	0.01 - 0.338 [173], [190]	0.01, 0.024, 0.058, 0.140,0.338

4.14. Statistical analysis

Unless stated otherwise, the comparison of two groups was conducted using a two-tailed Student's t-test. To achieve normal distribution in the LCA experiments, the fold data were $\log_2$ transformed. For multiple comparisons, a one-way analysis of variance test (ANOVA) was employed, followed by Tukey's honestly significant difference (HSD) post-hoc test. The data is presented as average ± SD unless stated otherwise. Outliers for LCA experiments were identified using Thomson tau-test, while outliers in other cases were identified using the Z-score test. The statistical analysis was performed using GraphPad Prism v8.0.

5. Results

5.1. Lithocholic acid attenuates aggressivity of breast cancer

5.1.1. Lithocholic acid inhibits cell proliferation.

In the first phase of our study, we performed short-term proliferation assays to assess the impact of secondary bile acids on cell proliferation. LCA reduced cellular proliferation in MCF7, SKBR3 and 4T1 breast cancer cells within the concentration range of 10 nM to 10 μM (**Figure 7, Table 6**) that encompassed the reference concentration range of LCA in serum (31 nM [129], [141], [142]) and breast cyst fluid (9-23 uM, [129]). This effect was specific to cancer cells, as primary fibroblasts showed no response to LCA at the same concentrations (**Figure 7, Table 6**).

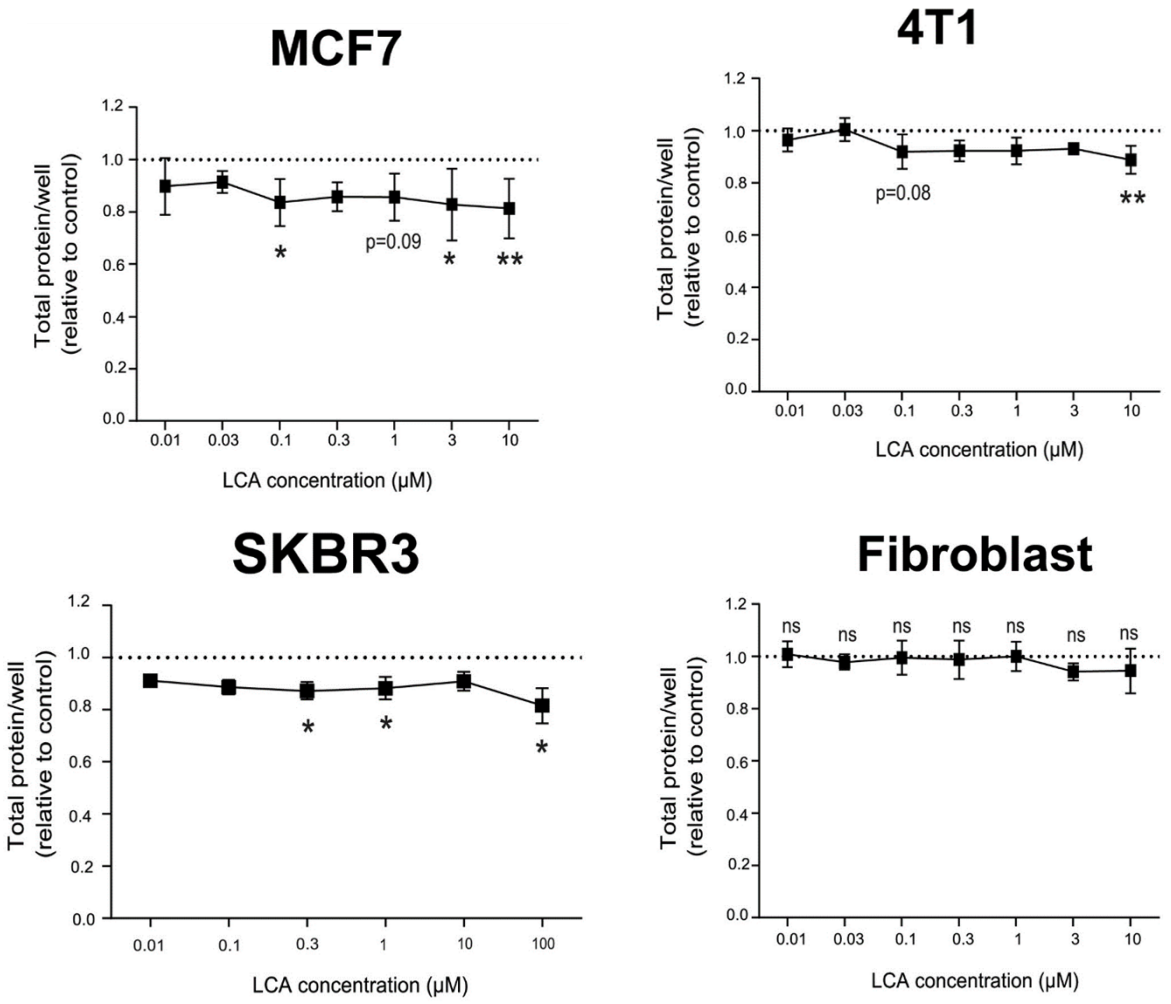

Figure 7: LCA inhibits cell proliferation in MCF7, 4T1 and SKBR3 cell cultures, while no significant cell proliferation changes in fibroblast cells.

MCF7, 4T1, SKBR3, and fibroblast cells were treated with LCA for 48 hours, then total protein content was measured with SRB assay (MCF7: n=8; 4T1: n=6; SKBR3: n=3; fibroblasts: n=5). The protein content values are represented as fold changes, where a value of 1 corresponds to the protein content in control cells. Data is presented as average±SD. * and ** indicate statistically significant difference between vehicle and treated groups at $p<0.05$ or $p<0.01$, respectively.

Table 6. Primary data expressed as percent change for **Figure 7.**

	CTL		LCA 0.1 µM		LCA 0.3 µM		LCA 1 µM	
	AVG	**SD**	**AVG**	**SD**	**AVG**	**SD**	**AVG**	**SD**
MCF7	100.00	0.00	83.52	8.95	85.81	5.57	85.68	8.87
4T1	100.00	0.00	91.88	6.67	92.25	3.99	92.24	5.16
SKBR	100.00	0.00	88.59	2.73	87.20	3.32	88.14	4.32

Conversely, other secondary bile acids, namely DCA and UDCA, did not exhibit any significant effect on the proliferation of MCF7 and 4T1 breast cancer cells (**Figure 8, Table 7).** These findings suggest that the impact of secondary bile acids on breast cancer cell proliferation is not uniform among different types of secondary bile acids.

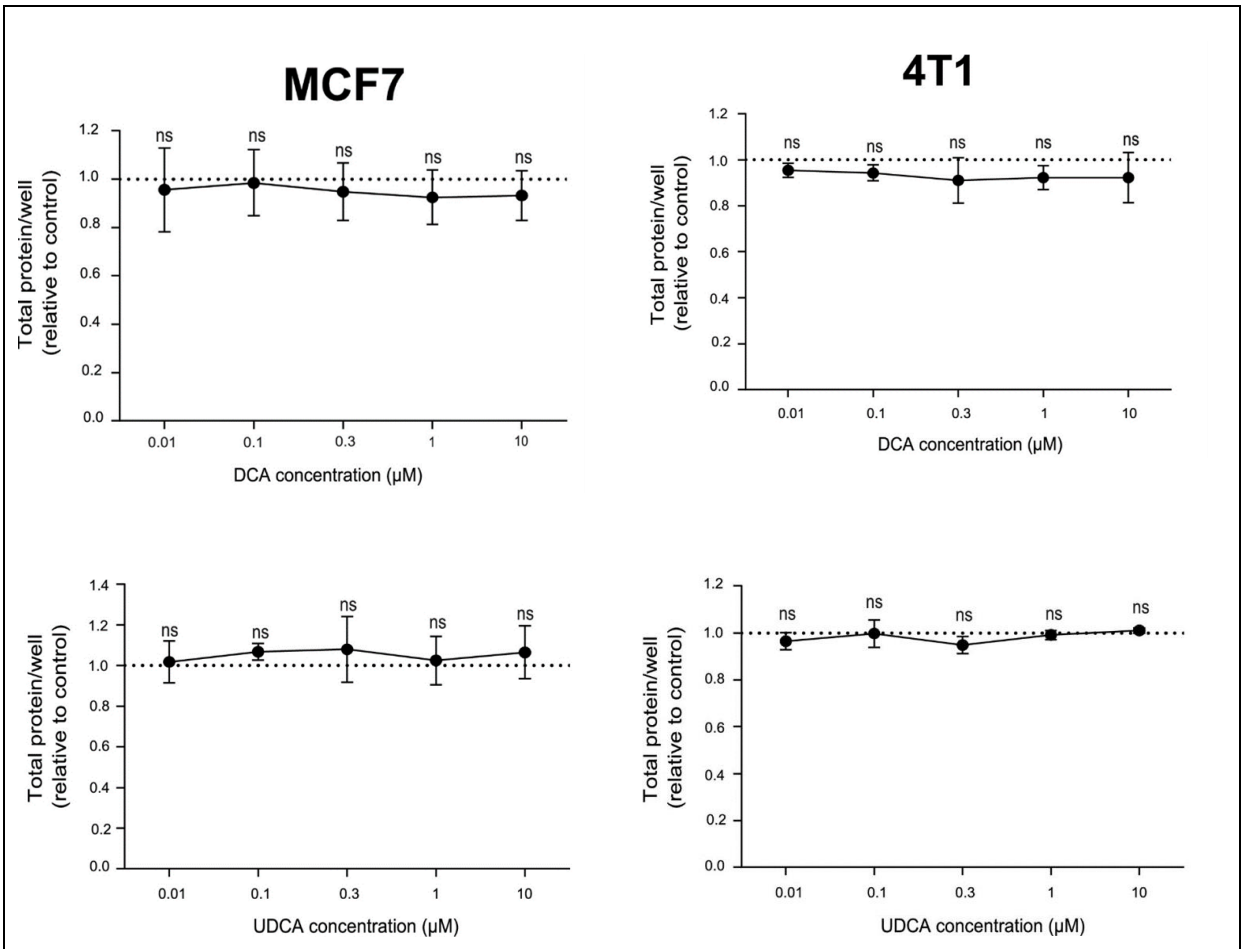

Figure 8: DCA and UDCA treatment has no significant effect on MCF7 and 4T1 cell proliferation.

MCF7 and 4T1 cells were treated with DCA and UDCA for 48 hours, then total protein content was measured with SRB assay (MCF7: n=4; 4T1: n=3). The protein content values are represented as fold changes, where a value of 1 corresponds to the protein content in control cells. Data is presented as average±SD. * and ** indicate statisticall significant difference between vehicle and treated groups at $p<0.05$ or $p<0.01$, respectively.

Table 7. Primary data expressed as percent change for **Figure 8.**

	CTL		0.01 µM		0.1 µM		0.3 µM		1 µM		10 µM	
	AV	**SD**	**AV**	**SD**	**AV**	**SD**	**AV**	**SD**	**AV**	**SD**	**AV**	**SD**
MCF7/DCA	1.00	0.00	0.96	0.17	0.99	0.14	0.95	0.12	0.93	0.11	0.93	0.10
MCF7/UDCA	1.00	0.00	1.02	0.11	1.07	0.04	1.08	0.16	1.03	0.12	1.06	0.13
4T1/DCA	1.00	0.00	0.95	0.03	0.94	0.03	0.91	0.10	0.92	0.05	0.92	0.11
4T1/UDCA	1.00	0.00	0.97	0.04	1.00	0.06	0.95	0.04	0.99	0.02	1.01	0.01

The cytostatic effect of LCA was validated in colony forming assays (**Figure 9, Table 8**). While our investigation revealed a notable reduction in cell proliferation in response to LCA treatment, it was also possible that this decline could be influenced by cell death. To assess this aspect, we performed a propidium iodide assay, which allowed us to examine cell death. The results of this assay demonstrated that the number of propidium iodide positive cells did not exhibit any significant increase upon exposure to LCA. This outcome was consistently observed across both the 4T1 and MCF7 cell lines (**Figure 10, Table 9**).

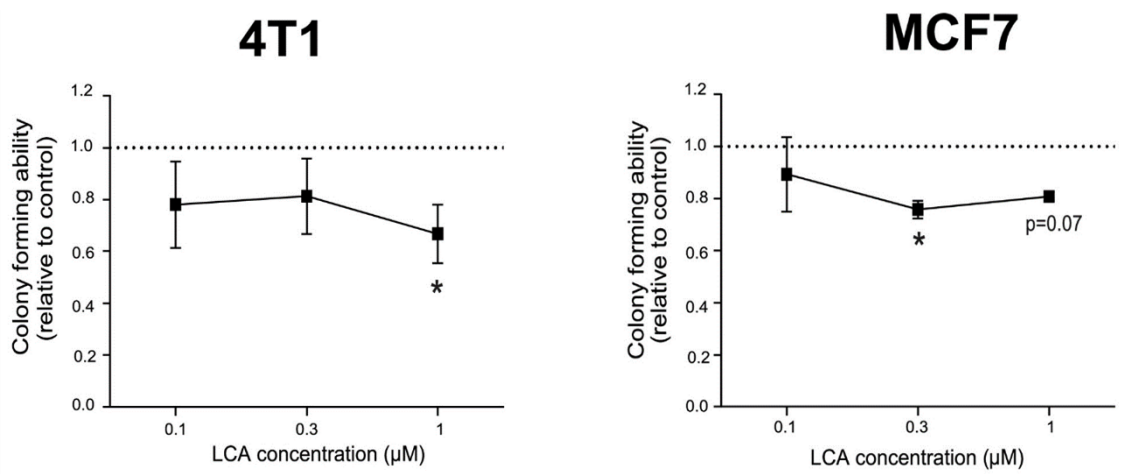

Figure 9: Cytostatic effect of LCA verified in longer colony forming assays on 4T1 and MCF7 cell line.

MCF7 and 4T1 cells were treated with LCA for 7 days, and colonies were stained with May-Grünwald-Giemsa. Images were counted using ImageJ software (MCF7: n=3; 4T1: n=4). Values represented as fold changes, where a value of 1 corresponds to colony count in control treatment. Data is presented as average±SD. * and ** indicate statisticall significant difference between vehicle and treated groups at $p<0.05$ or $p<0.01$, respectively.

Table 8. Primary data expressed as percent change for **Figure 9.**

	CTL		**LCA 0.1 μM**		**LCA 0.3 μM**		**LCA 1 μM**	
	AVG	**SD**	**AVG**	**SD**	**AVG**	**SD**	**AVG**	**SD**
MCF7	100.00	0.00	89.22	14.31	75.72	3.40	80.75	1.65
4T1	100.00	0.00	74.15	18.04	81.25	14.51	63.85	11.99

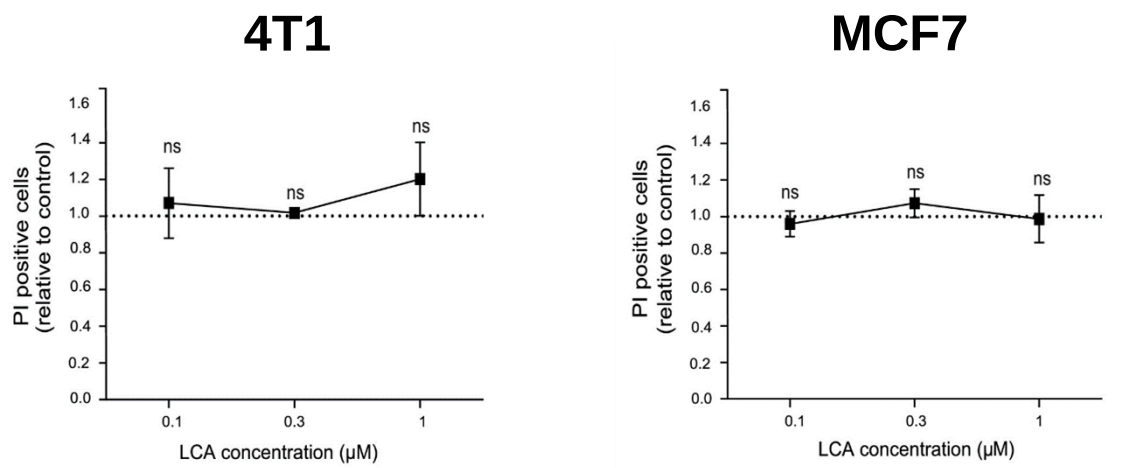

Figure 10: The number of propidium iodide positive cells remained unchanged after LCA treatment, indicating that LCA did not cause cell death.

MCF7 and 4T1 cells were treated with LCA for 48 hours, then dead cells were stained with propidium iodide (PI) and analyzed by flow cytometry (MCF7: n=3; 4T1: n=3). Values represented as fold changes, where a value of 1 corresponds to PI positive cell count in control treatment. Data is presented as average±SD. * and ** indicate statisticall significant difference between vehicle and treated groups at $p<0.05$ or $p<0.01$, respectively.

Table 9. Primary data expressed as percent change for **Figure 10.**

	CTL		**LCA 0.1 μM**		**LCA 0.3 μM**		**LCA 1 μM**	
	AVG	**SD**	**AVG**	**SD**	**AVG**	**SD**	**AVG**	**SD**
MCF7	1.00	0.00	0.96	0.07	1.07	0.08	0.99	0.13
4T1	1.00	0.00	1.07	0.19	1.02	0.03	1.20	0.20

5.1.2. LCA impact on EMT and metastasis

Next, we investigated the potential of LCA to modulate epithelial-mesenchymal transition (EMT). LCA treatment shifted cellular morphology towards an epithelial-like phenotype. This phenomenon was consistently present both in MCF7 and 4T1 cell lines (**Figure 11A**). ECIS measurements showed increased total impedance (**Figure 11C, Table 10**), providing functional evidence of improved cell-to surface and cell-to-cell adhesion. Upon LCA treatment in scratch

assay experiments, a notable reduction in migration speed towards the void area was evident in case of 4T1 cell line (**Figure 11B**).

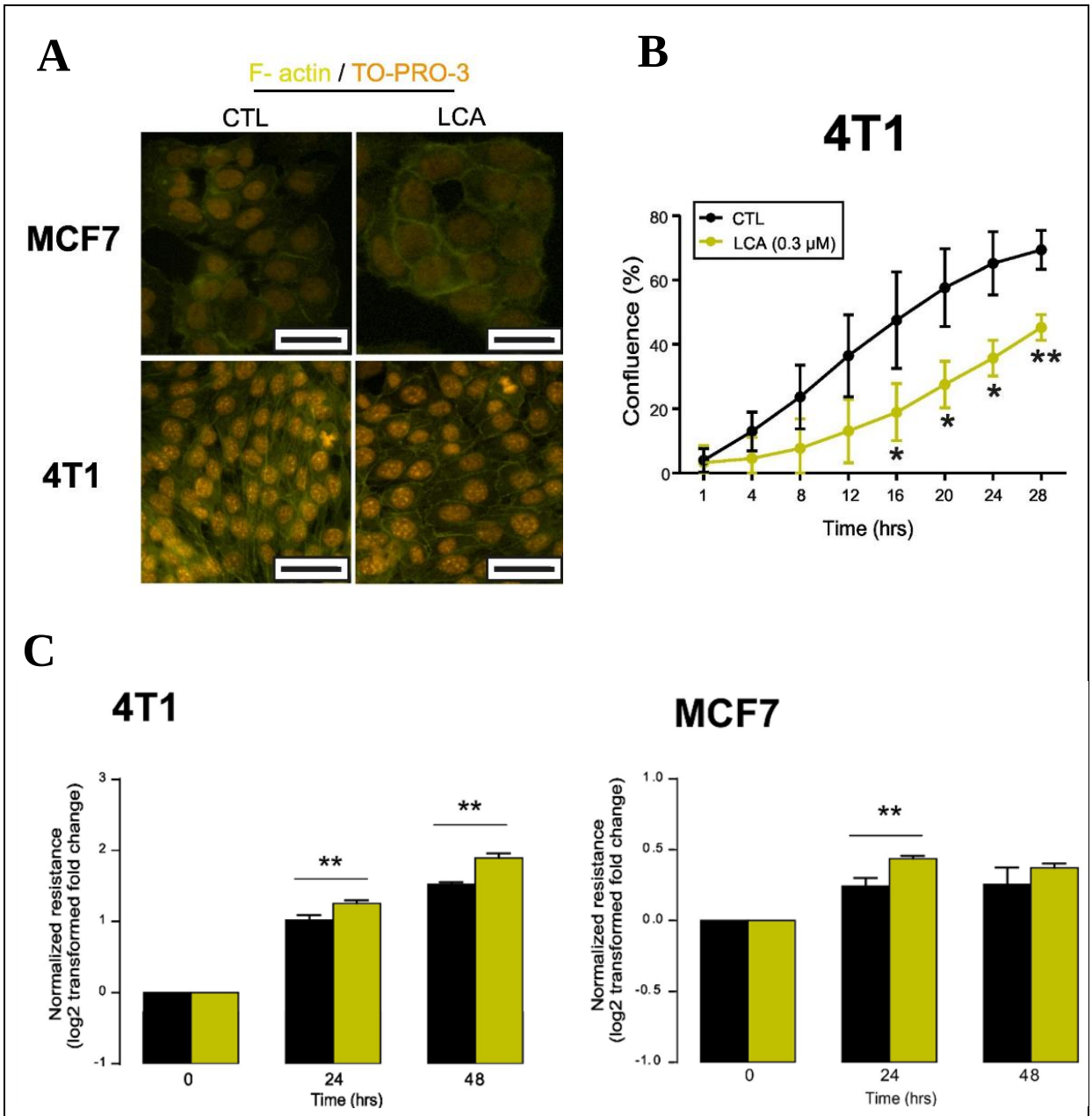

Figure 11: LCA reverses EMT

Cellular morphology was evaluated in MCF7 and 4T1 cells treated with LCA or VEH. This assessment was performed using TexasRed-X Phalloidin and To-Pro-3 staining, as depicted in a representative figure. Scale bar is 10 µm (**A**, n=3). Additionally, scratch assays were performed (**B**, n=3) and total resistance was measured in ECIS experiments (**C**, n=3). Data is presented as average±SD. * and ** indicate statisticall significant difference between vehicle and treated groups at $p<0.05$ or $p<0.01$, respectively.

Table 10. Primary data expressed as percent change for **Figure 11C**

	CTL						LCA 0.3 µM					
	0 h		24 h		48 h		0 h		24 h		48 h	
	AVG	SD	AVG	SD	AVG	SD	AVG	SD	AVG	SD	AVG	SD
MCF7	100.00	0.00	118.38	4.83	119.46	10.16	100.00	0.00	135.35	2.00	129.44	2.81
4T1	100.00	0.00	202.94	10.14	287.53	6.32	100.00	0.00	238.75	6.99	371.71	16.82

Additionally, LCA treatment hindered β-catenin signaling, evidenced by decreased phosphorylation of GSK-3α and GSK-3β, as well as reduced β-catenin protein content in both cell lines and *in vivo* (**Figure 12, Figure 13**).

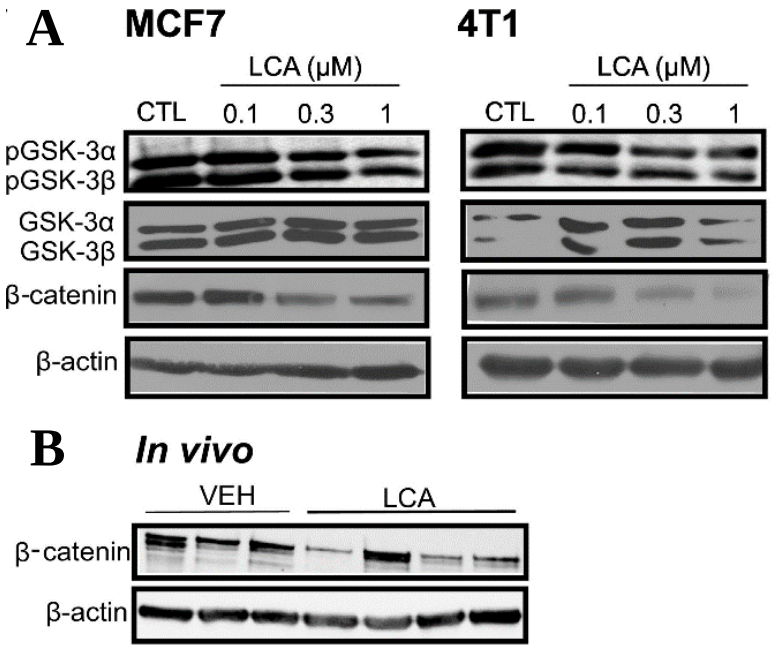

Figure 12: LCA treatment affects Wnt pathway by inhibiting β-catenin signaling

The expression of the indicated proteins was examined by Western blotting in LCA-treated 4T1 and MCF7 cells,. Western blot analysis was performed in triplicate (n=3) in the *in vitro* experiments (**A**). Female Balb/c mice were grafted with 4T1 cells and were treated with 15 nmol LCA or vehicle, daily, by mouth. Representative figure, VEH=vehicle control (**B**).

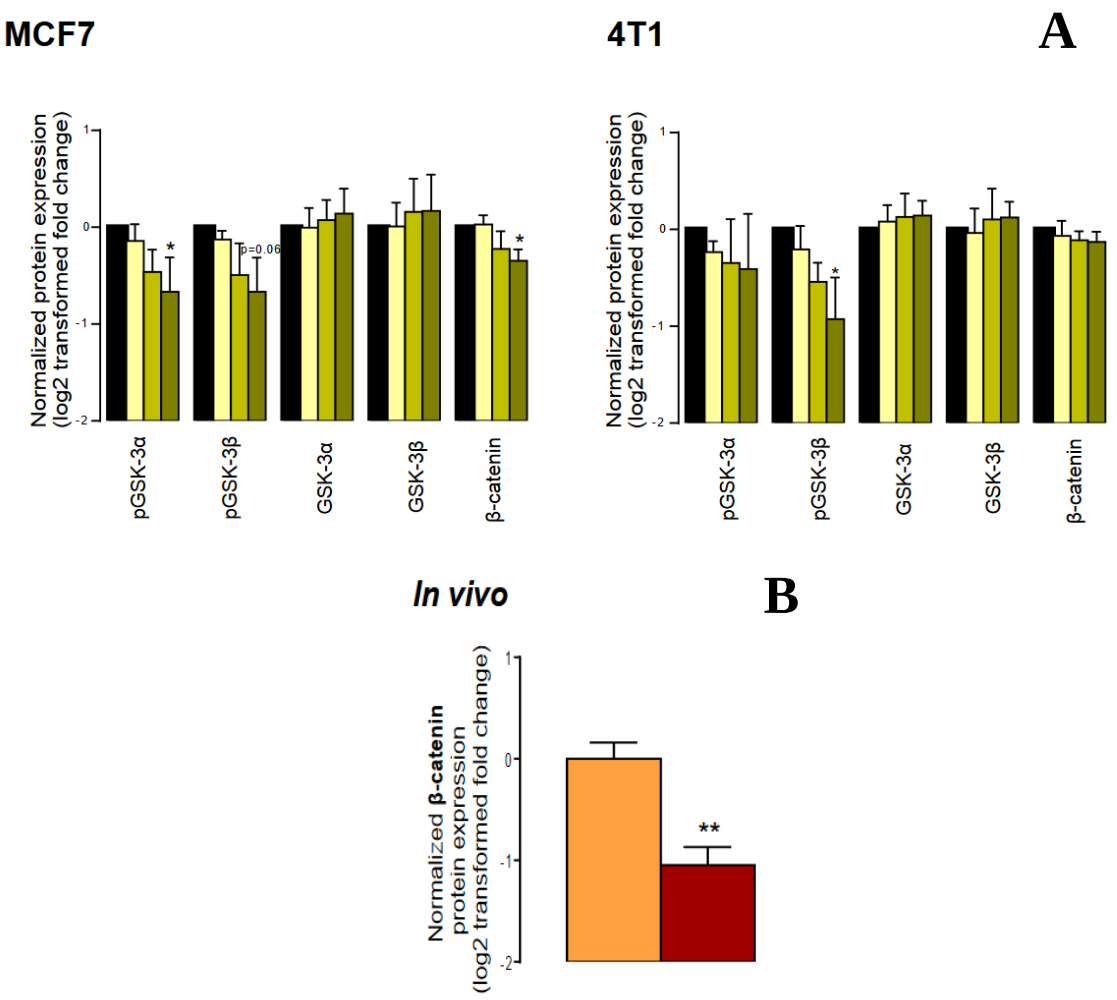

Figure 13: LCA treatment affects Wnt pathway by inhibiting β-catenin signaling - densitometric analysis for Figure 12

The expression of the indicated proteins was examined by Western blotting in LCA-treated 4T1 and MCF7 cells,. Western blot analysis was performed in triplicate (n=3) in the *in vitro* experiments (**A**). Female Balb/c mice were grafted with 4T1 cells and were treated with 15 nmol LCA or vehicle, daily, by mouth. Representative figure, VEH=vehicle control (**B**). * and ** indicate statisticall significant difference between vehicle and treated groups at $p<0.05$ or $p<0.01$, respectively.

LCA treatment also resulted in lower VEGF mRNA expression (**Figure 14A, Table 11**) and a higher number of tumor-infiltrating lymphocytes (TILs) in mice treated with LCA compared to vehicle-treated mice (**Figure 14B**).

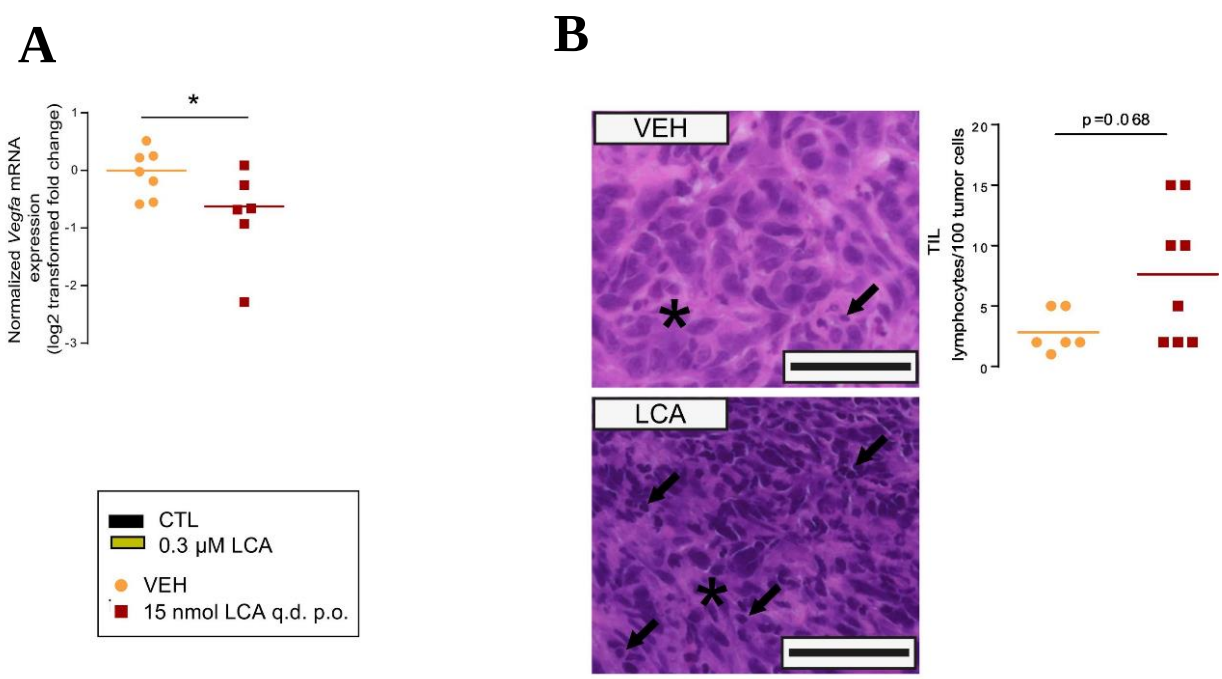

Figure 14: LCA treatment modulates VEGF expression and enhances tumor infiltrating lymphocytes in mice

Female Balb/c mice were grafted with 4T1 cells and were treated with LCA or vehicle for 18 days. Tumor samples were collected upon autopsy. *Vegfa* mRNA expression in tumors was quantified using RT-qPCR, with the mean expression indicated by a line (**A**). The morphology of LCA or VEH-treated tumors was evaluated by examining hematoxylin-eosin stained 4 µm thick histological sections. Additionally, the number of tumor infiltrating lymphocytes (TILs) was determined, and the mean count was indicated by a line. The relative number of TILs were calculated based on a recent diagnostic procedure, which involved counting both the tumor cells and intratumor lyphocytes within the same representative areas of the hematoxylin-eosin stained slides. TIL counts were reported as a percentage relative to the tumor cell count. In the histological sections, typical tumor cells are denoted by stars, while TILs are marked by arrows(**B**). Scale bar is 50 µm. q.d., *quaque die* (once a day); p.o., *per os* (by mouth).

Table 11. Primary data expressed as percent change for **Figure 14A**

	CTL		**LCA**	
	AVG	**SD**	**AVG**	**SD**
***in vivo*/tumor**	100,00	26,14	63,91	28,58

5.1.3. LCA affects energy metabolism

Warburg metabolism, a hallmark of cancer, has emerged as a prominent metabolic alteration in breast cancer. In this context, breast cancer cells generally display a characteristic shift towards a glycolytic phenotype, wherein they preferentially rely on glycolysis to produce energy under aerobic conditions [201]. Thus, we examined the impact of LCA on cellular metabolism. Treatment with LCA led to an increase in glycolysis (extracellular acidification rate -ECAR) and mitochondrial respiration (oxygen consumption rate – OCR) levels (MCF7 - **Figure 15A;** 4T1 – **Figure 16A**). Consistently, intracellular lactate and citrate levels, along with the citrate/lactate ratio, were elevated upon LCA treatment (MCF7 - **Figure 15B**; 4T1 – **Figure 16B**).

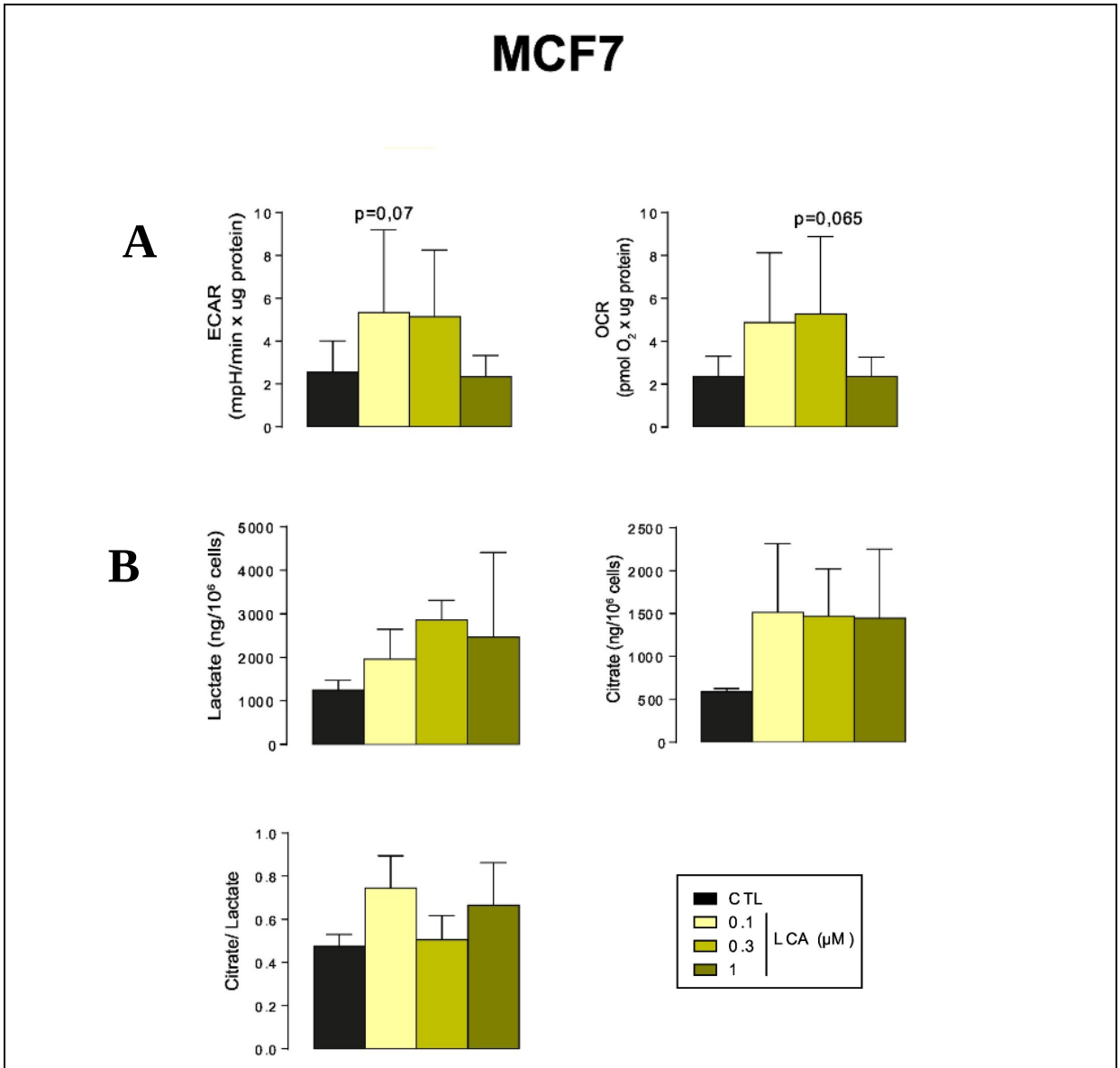

Figure 15: LCA treatment induces glycolysis and oxygen consumption in MCF7 breast cancer cells.

MCF7 cells were exposed to varying concentrations of LCA for 48 hours, followed by the execution of the specified measurements. The extracellular acidification rate (ECAR) and oxygen consumption rate (OCR) were determined and representative data is plotted (n=2, **A**). Intracellular lactate and citrate levels were assessed and plotted (n=2, **B**). Data is presented as average±SD.

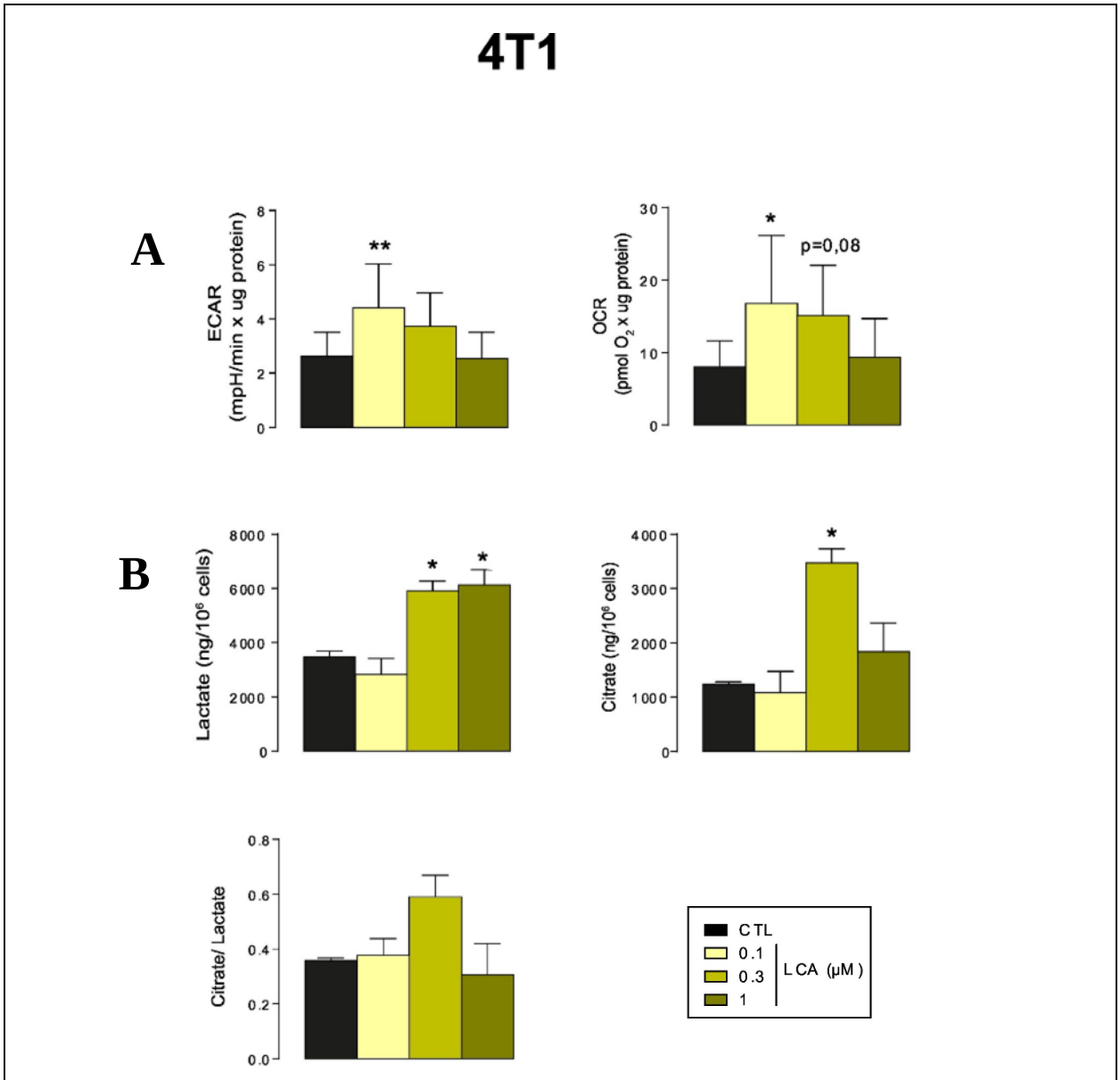

Figure 16: LCA treatment induces glycolysis and oxygen consumption in 4T1 breast cancer cells.

4T1 cells were exposed to varying concentrations of LCA for 48 hours, followed by the execution of the specified measurements. The extracellular acidification rate (ECAR) and oxygen consumption rate (OCR) were determined and representative data is plotted (n=2, **A**). Intracellular lactate and citrate levels were assessed and plotted (n=2, **B**). Data is presented as average±SD.

Moreover, LCA treatment induced the expression of a specific set of OXPHOS genes in both 4T1 and MCF7 cells (MCF7 **- Figure 17A;** 4T1 **– Figure 18A**, **Table 12**), aligning with these observations. Next, we conducted pulse-chase metabolomics experiments on MCF7 and 4T1 cells treated with 300 nM LCA. Upon loading the cells with ^{13}C-acetate, a metabolite that can fuel the TCA cycle, LCA treatment resulted in an augmented incorporation of ^{13}C into succinate and malate (MCF7 **- Figure 17B;** 4T1 **– Figure 18B**), indicating an increased flux through the TCA cycle. Additionally, when cells were supplied with ^{13}C-glucose, where ^{13}C atoms enter glycolysis and subsequently fuel the TCA cycle or form lactate, LCA treatment enhanced the levels of ^{13}C-labeled citrate and lactate in MCF7 cells and ^{13}C-labeled succinate and lactate in 4T1 cells (MCF7 **- Figure 17C;** 4T1 **– Figure 18C**). Consistently, the ratio between ^{13}C-citrate and ^{13}C-lactate or between ^{13}C-succinate and ^{13}C-lactate increased, providing further evidence of the mitochondrial dominance in the LCA-induced metabolic switching (MCF7 **- Figure 17C;** 4T1 **– Figure 18C**). We further examined the distribution of 13C-labeled carbons in citrate of MCF7 cells treated with vehicle or LCA. Collectively, these findings indicate that LCA treatment induces activation of the TCA cycle and oxidative phosphorylation (OXPHOS) in breast cancer cells.

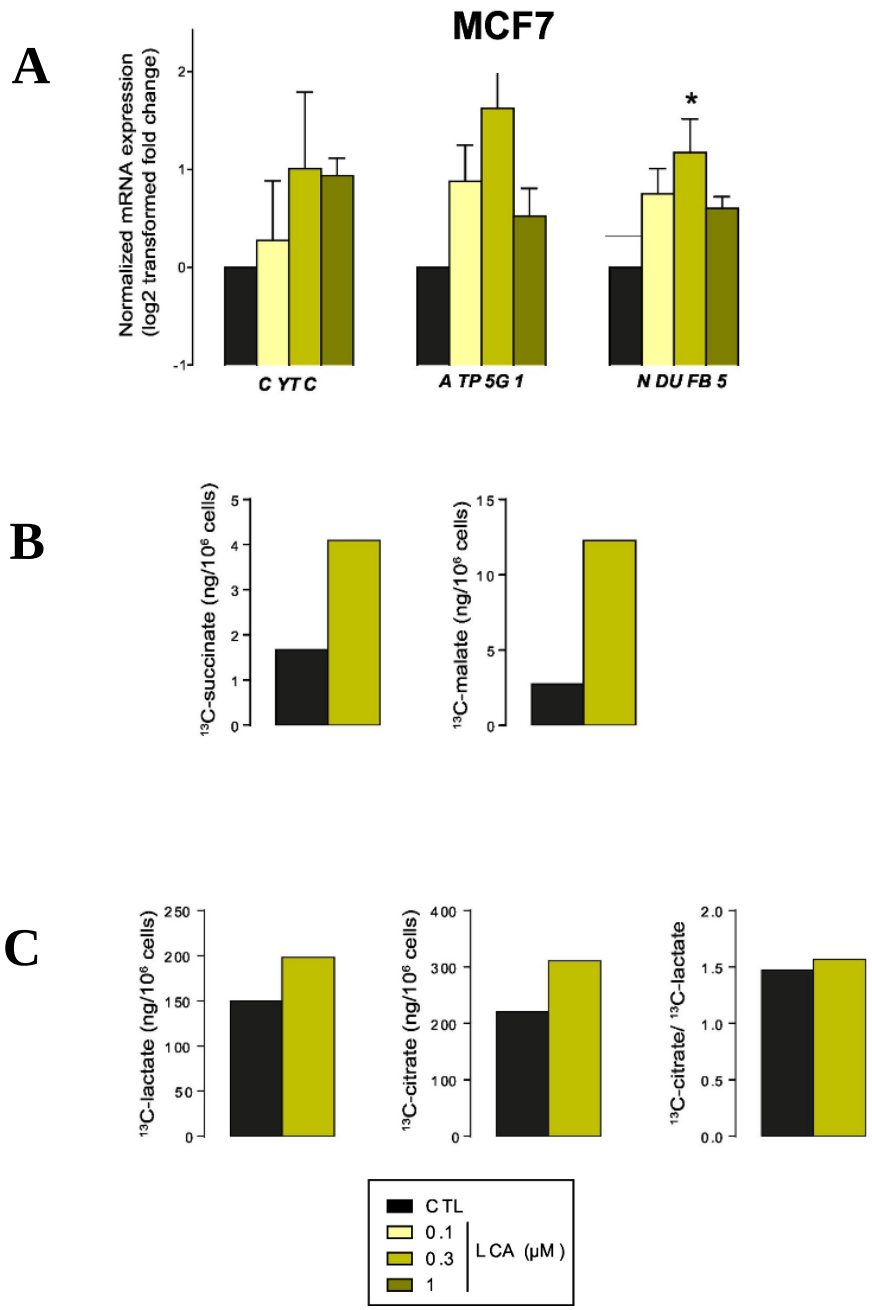

Figure 17: LCA treatment modulates OXPHOS gene expression and metabolic profile.

The expression of a set of genes were assessed using RT-qPCR reactions (**A**, n=3 for MCF7), with the error depicted as the standard error of the mean (SEM). MCF7 were treated with LCA at the indicated concentrations for 48 hours. Subsequently the cells were loaded with 10 mM 13C-acetate for 1 hour, and the measurement of the indicated metabolites was performed (**B**). Cells were treated with LCA and loaded with 10 mM 13C-glucose for 1 hour, then the indicated metabolites were measured (**C**). * and ** indicate statisticall significant difference between vehicle and treated groups at $p<0.05$ or $p<0.01$, respectively.

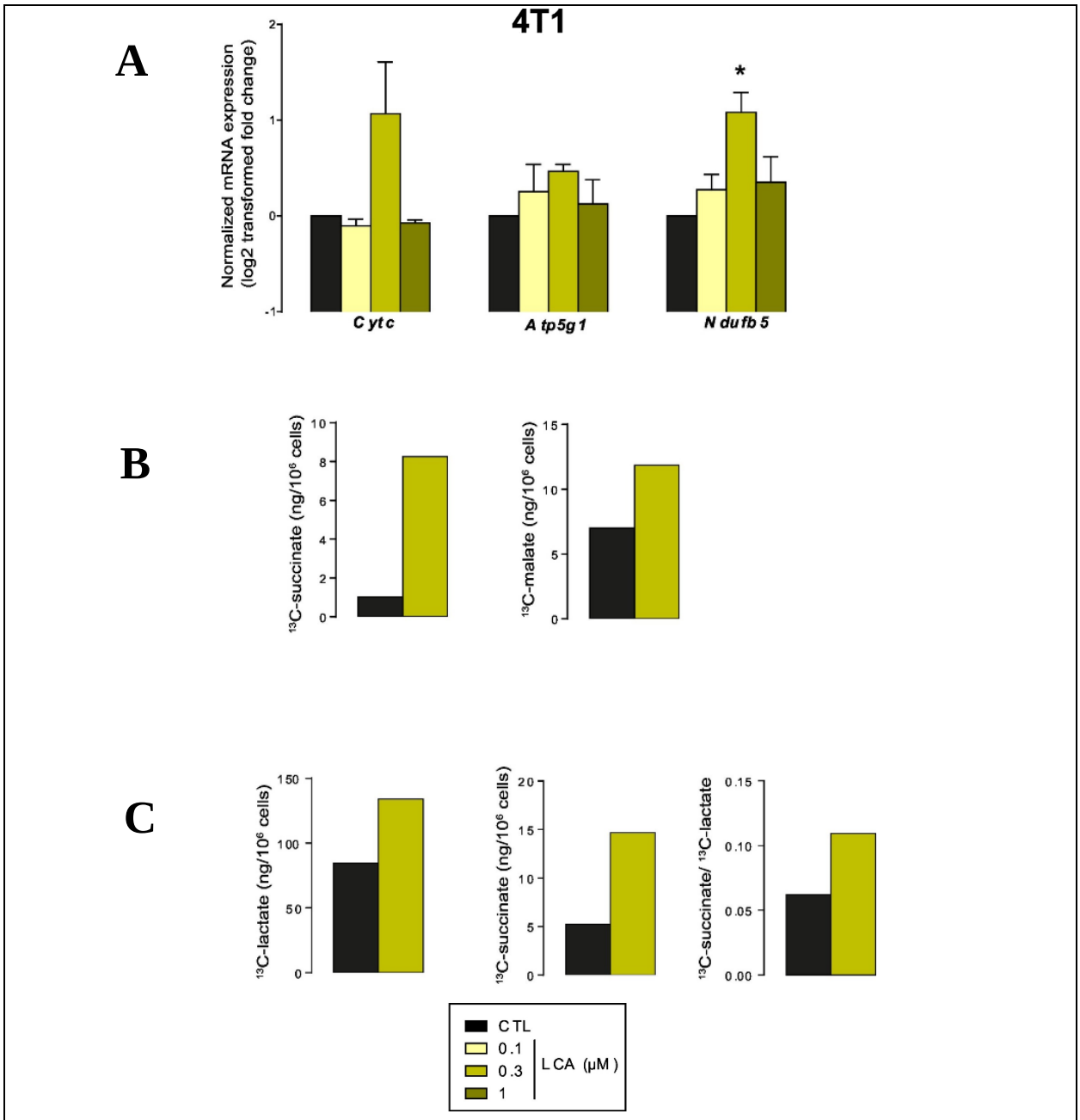

Figure 18: LCA treatment modulates OXPHOS gene expression and metabolic profile.

The expression of a set of genes were assessed using RT-qPCR reactions (**A**, n=2 for 4T1), with the error depicted as the standard error of the mean (SEM). 4T1 were treated with LCA at the indicated concentrations for 48 hours. Subsequently the cells were loaded with 10 mM 13C-acetate for 1 hour, and the measurement of the indicated metabolites was performed (**B**). Cells were treated with LCA and loaded with 10 mM 13C-glucose for 1 hour, then the indicated metabolites were measured (**C**). * and ** indicate statisticall significant difference between vehicle and treated groups at $p<0.05$ or $p<0.01$, respectively.

Table 12. Primary data expressed as percent change for **Figure 17A** and **Figure 18A.**

	CTL		**LCA 0.1 µM**		**LCA 0.3 µM**		**LCA 1 µM**	
	AVG	**SD**	**AVG**	**SD**	**AVG**	**SD**	**AVG**	**SD**
MCF7/CYTC	100.00	0.00	121.00	63.57	201.00	145.33	191.67	25.37
MCF7/ATP5G1	100.00	0.00	184.00	53.84	308.50	182.50	143.67	31.32
MCF7/NDUFB5	100.00	0.00	168.33	32.94	225.25	61.17	151.75	13.04
4T1/CYTC	100.00	0.00	93.00	4.51	209.33	95.25	95.00	2.00
4T1/ATP5G1	100.00	0.00	119.00	26.00	138.00	7.00	109.00	21.00
4T1/NDUFB5	100.00	0.00	120.67	14.24	211.67	32.67	127.33	26.03

To investigate the underlying mechanisms behind the observed metabolic changes, we examined various components of the cellular energy sensor network and mitochondrial transcriptional regulators. Notably, LCA treatment resulted in increased expression and activation of positive regulators of mitochondrial oxidative phosphorylation, including FOXO1, PGC-1β, and nuclear respirator factor-1 (NRF1) (**Figure 19A, Figure 20A**). Furthermore, LCA not only elevated their expression but also enhanced their activation, as evidenced by the augmented nuclear translocation of NRF1 (**Figure 21**) and increased phosphorylation of ACC (**Figure 19A, Figure 20 A**). In our *in vivo* experiments, we also observed that LCA treatment induced AMPK activity, as indicated by elevated levels of phospho-ACC and phospho-AMPK. Additionally, we observed an enhanced expression of FOXO1. However, LCA did not induce the expression of NRF1 or PGC-1β in the *in vivo* setting (**Figure 19B, Figure 20 B**).

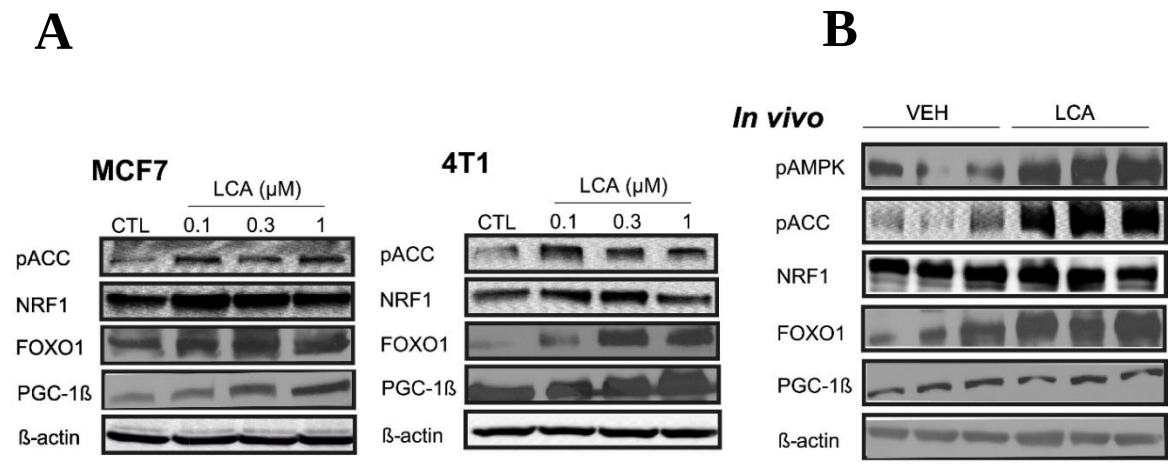

Figure 19: LCA treatment alters energy stress sensor protein expression.

Following a 48-hour treatment with LCA at the specified concentrations, MCF7 and 4T1 cells were subjected to protein extraction. The protein extracts were then separated using PAGE, transferred onto nitrocellulose membranes, and subsequently probed with the specified antibodies (n=3 for MCF7 and 4T1, **A**). Female Balb/c mice bearing 4T1 cell grafts were administered LCA (15 nmol q.d. p.o.) or vehicle (VEH) for a duration of 18 days. Protein extracts were obtained from the primary tumors, separated by PAGE, transferred onto nitrocellulose membranes, and probed with the indicated antibodies (**B**).

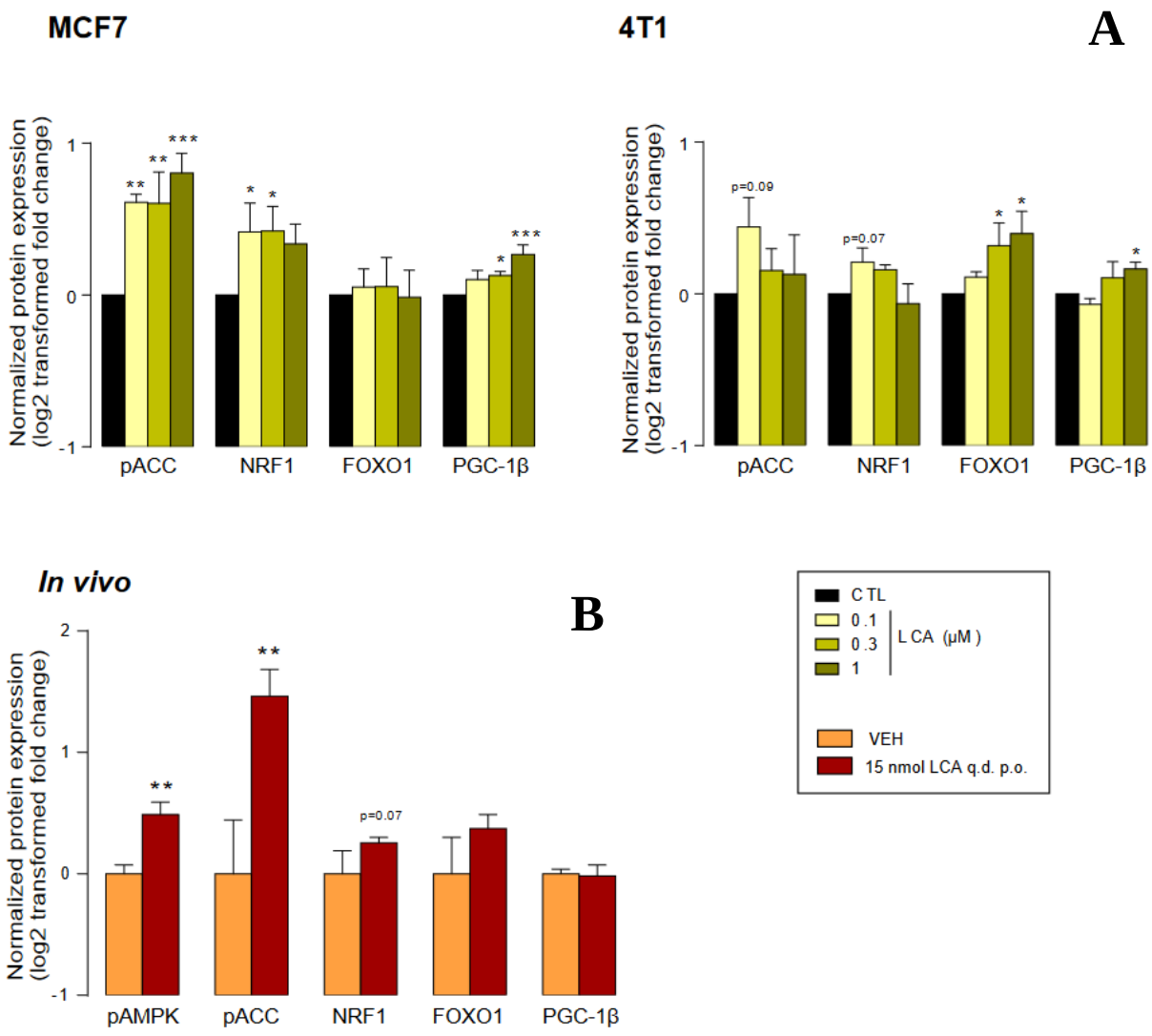

Figure 20: LCA treatment alters energy stress sensor protein expression - densitometric analysis for Figure 19

Following a 48-hour treatment with LCA at the specified concentrations, MCF7 and 4T1 cells were subjected to protein extraction. The protein extracts were then separated using PAGE, transferred onto nitrocellulose membranes, and subsequently probed with the specified antibodies (n=3 for MCF7 and 4T1, **A**). Female Balb/c mice bearing 4T1 cell grafts were administered LCA (15 nmol q.d. p.o.) or vehicle (VEH) for a duration of 18 days. Protein extracts were obtained from the primary tumors, separated by PAGE, transferred onto nitrocellulose membranes, and probed with the indicated antibodies (**B**). *, **, and *** indicate statisticall significant difference between vehicle and treated groups at $p<0.05$, $p<0.01$, or $p<0.001$ respectively.

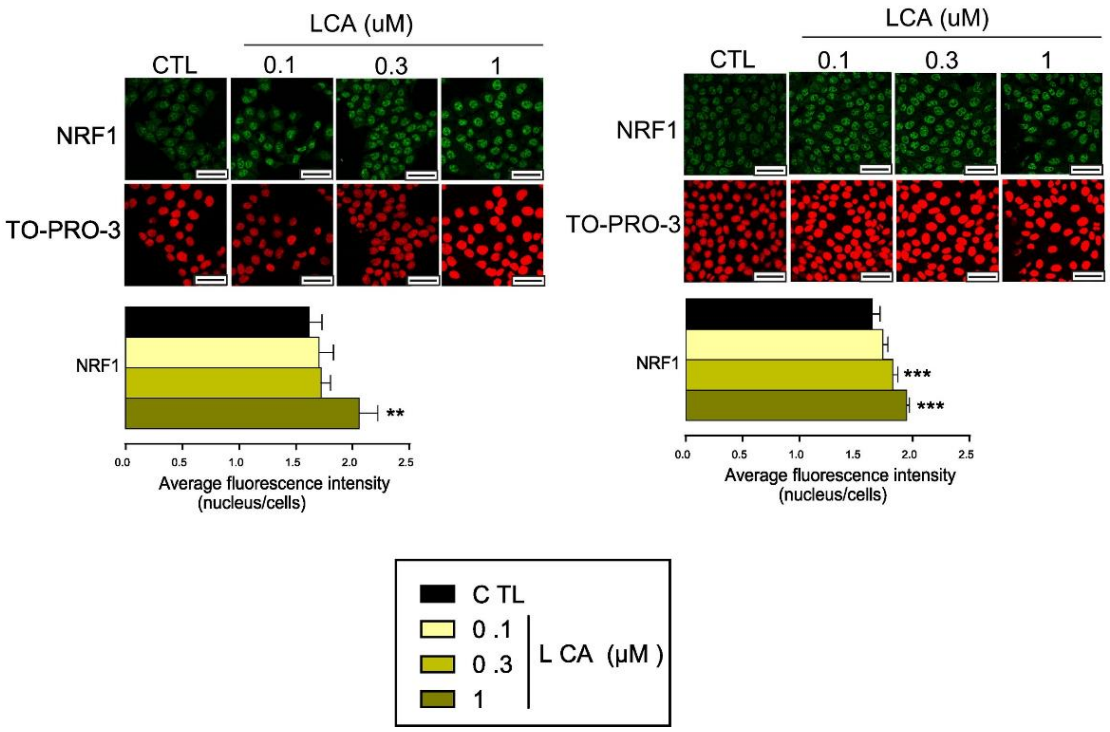

Figure 21: LCA treatment induces NRF1 expression.

Immunofluorescence and image analysis were employed to evaluate the localization of NRF1. The scale bar in the images represent a length of 50 μm. *, **, and *** indicate statisticall significant difference between vehicle and treated groups at $p<0.05$, $p<0.01$, or $p<0.001$ respectively

We subsequently investigated the potential (patho)physiological relevance of the induced metabolic regulators (NRF1, AMPK, PGCs) in humans. Previous studies have highlighted the antitumor activity of AMPK and FOXO1 in human subjects [102], [202], [203]. Utilizing the kmplot.com database, we discovered that high expression of NRF1 in breast cancer tissue is associated with improved survival following diagnosis (**Figure 22**). Collectively, these findings suggest that the modulation of AMPK, FOXO1, PGC-1β, or NRF1 may hold (patho)physiological relevance in influencing the effects triggered by LCA in humans.

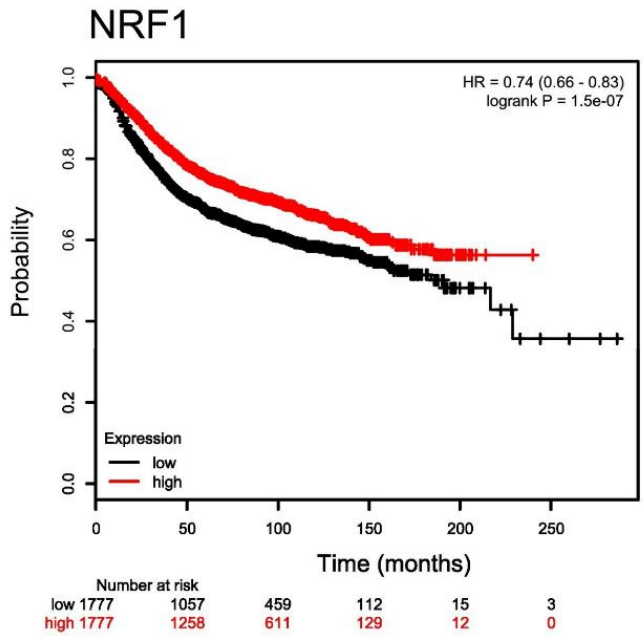

Figure 22: NRF1 expression impact survival in breast cancer.

The influence of NRF1 expression on survival in breast cancer was analyzed by examining the kmplot.com database (accessed in 2018).

5.1.4. Identification of LCA receptors

Our next objective was to determine the specific receptor(s) responsible for mediating the effects induced by LCA. To achieve this, we employed pharmacological inhibitors targeting different LCA receptors to assess their involvement in the LCA-induced effects. MCF7 cells were treated with LCA in combination with either vehicle or pharmacological agents that block potential LCA receptors. We observed that CINPA1 (CAR antagonist), NF449 (Gsα-selective antagonist), and U73343 (phospholipase C inhibitor) effectively blocked the LCA-mediated reduction in cell proliferation, while other inhibitors showed no significant effect (**Figure 23A, Table 13**). NF449 and U73343 effectively blocked inhibitory effect of LCA on cell proliferation and EMT, whereas CINPA1 did not exhibit the same efficacy (**Figure 23A-B**).

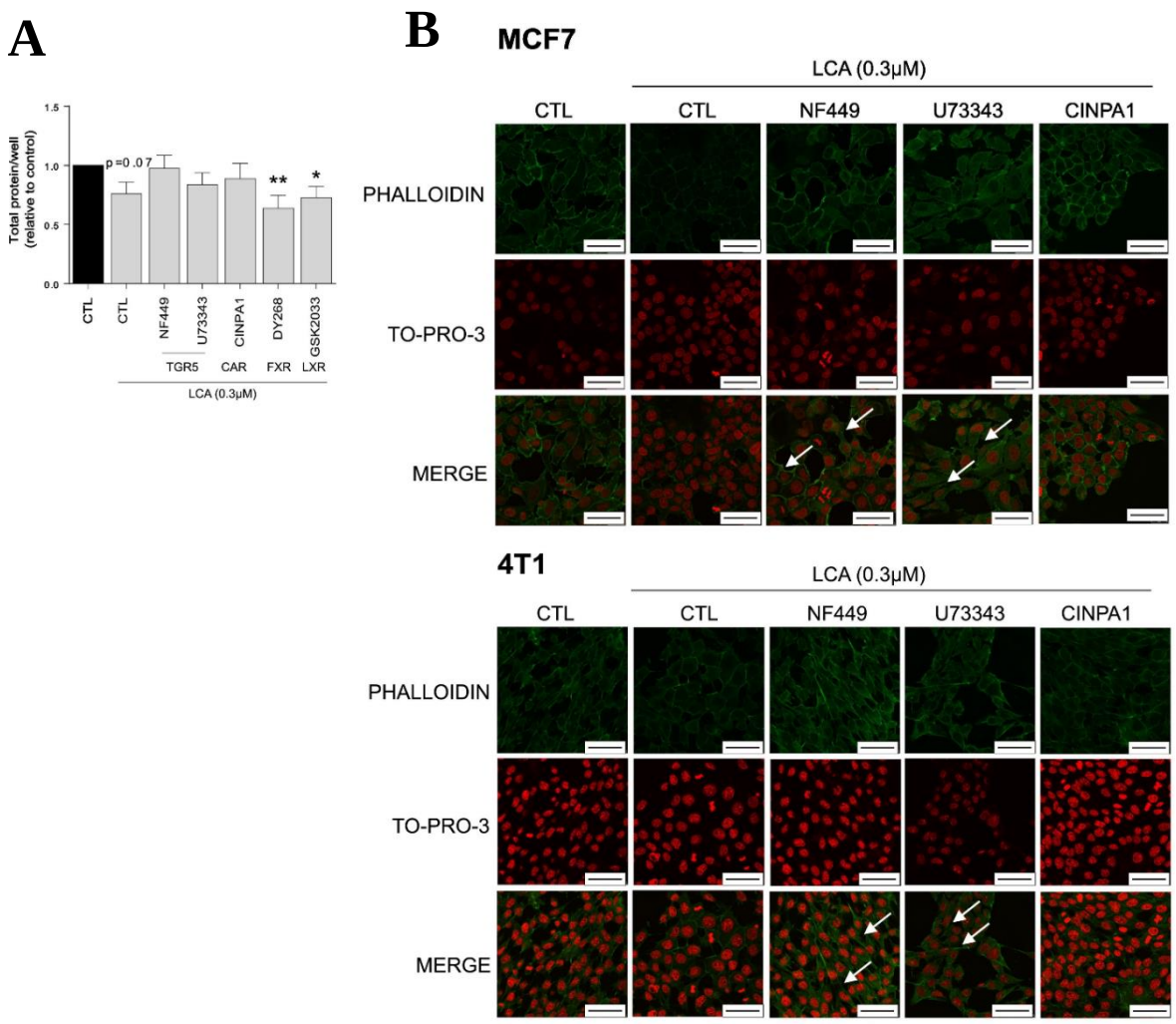

Figure 23: Specific receptor inhibitors revert LCA effects

MCF7 cells were subjected to treatment with 0.3 µM LCA along with the following agents: 5 µM NF449, 1 µM U73343, 5 µM CINPA1, 5 µM DY268, and 5 µM GSK2033 for a duration of 48 hours. Subsequently, cellular proliferation was assessed (n=3, **A**). Furthermore, MCF7 and 4T1 cells were treated with 0.3 µM LCA and one of the following agents: 5 µM NF449, 1 µM U73343, and 5 µM CINPA1 for 48 hours. Actin staining was performed using TexasRed-X-phalloidin, arrows marking the void areas and lost focal adhesion sites (n=3, **B**). The scale bar in the images corresponds to a length of 25 µm. * and ** indicate statistically significant difference between vehicle and treated groups at $p<0.05$ or $p<0.01$, respectively.

Table 13. Primary data expressed as percent change for **Figure 23A.**

	CTL		LCA		NF449 + LCA		U73343 + LCA		CINPA1 + LCA		DY268 + LCA		GSK2033 + LCA	
	AVG	**SD**	**AVG**	**SD**	**AVG**	**SD**	**AVG**	**SD**	**AVG**	**SD**	**AVG**	**SD**	**AVG**	**SD**
MCF7	100.00	0.00	75.99	9.95	97.44	11.18	83.69	10.15	88.83	12.92	63.86	10.88	72.75	9.74

To provide direct evidence for the involvement of TGR5, since NF449 and U73343 are not TGR5-specific inhibitors but can block TGR5 signaling by inhibiting Gsα and phospholipase C, we transiently silenced TGR5 in MCF7 cells (**Figure 24 B, Table 14**). Silencing TGR5 efficiently blocked the LCA-induced morphological changes of MCF7 cells (**Figure 24A**) and prevented the upregulation of mRNA expression of mitochondrial markers including CYTOCHROME C, ATP5G1, and NDUFB5 (**Figure 24C, Table 15**), as well as markers of AMPK activation (**Figure 24C**). Additionally, it is worth noting that in the concentrations of LCA used in this study, the dynamical properties and microdomain organization of biomembranes remained unaltered. This was demonstrated by the observation that neither the diffusion constant (D) nor the confinement time (tD) of LCA was affected, even upon treatment with 100 μM LCA (**Figure 25**).

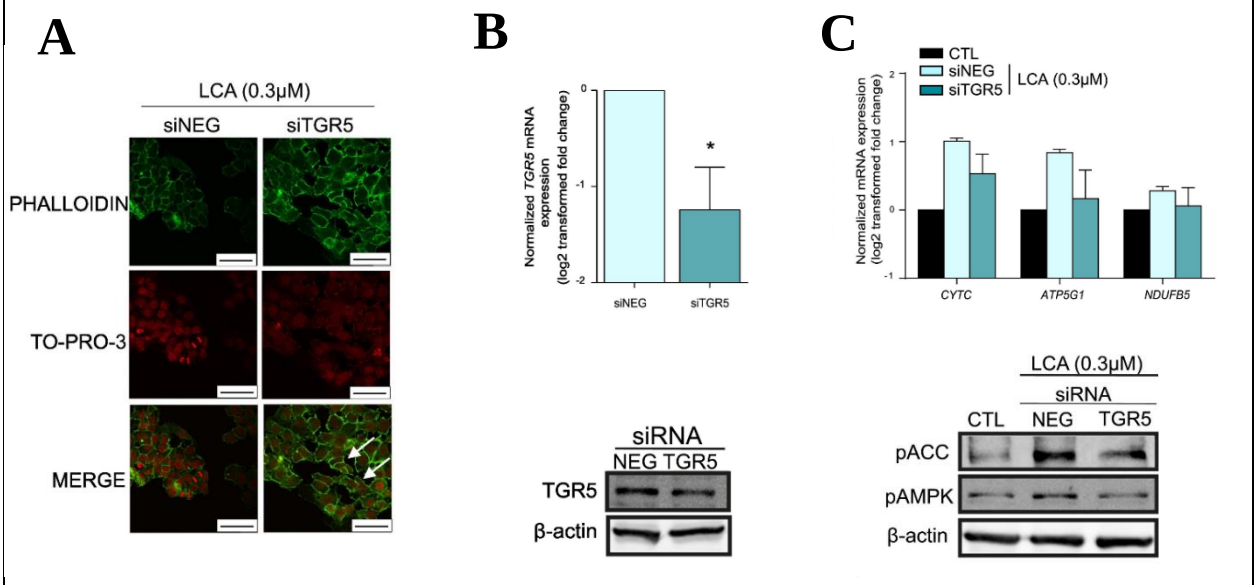

Figure 24: LCA effects are partly facilitated by TGR5

To investigate the role of TGR5, transient transfection of MCF7 cells was performed using siRNA specific to TGR5, or non-specific siRNA, for 48 hours. Cells were stained with TexasRed-X-Phalloidin, arrows marking the void areas and lost focal adhesion sites. The scale bar in the images represents a length of 25 μm (**A**). mRNA expression and protein level expression of *TGR5* was measured in siTGR5 and siNEG cells (n=3, **B**). TGR5-depleted MCF7 cells and negative control-transfected cells were subjected to a 48-hour treatment with 0.3 μM LCA. The mRNA expression levels of the indicated genes were determined by RT-qPCR, while the expression levels of the indicated proteins were assessed through western blotting (**C**). * indicate statistically significant difference between siNEG and siTGR5 groups at $p<0.05$.

Table 14. Primary data expressed as percent change for **Figure 24B/mRNA expression.**

	siNEG		**siTGR5**	
	AVG	SD	AVG	SD
MCF7	**100.00**	0.00	**42.06**	14.86

Table 15. Primary data expressed as percent change for **Figure 24C.**

	CTL		siNEG + LCA		siTGR5 + LCA	
	AVG	SD	AVG	SD	AVG	SD
MCF7/CYTC	100.00	0.00	200.96	9.11	144.49	44.62
MCF7/ATP5G1	100.00	0.00	178.93	8.26	112.18	53.39
MCF7/NDUFB5	100.00	0.00	121.49	7.58	104.11	30.04

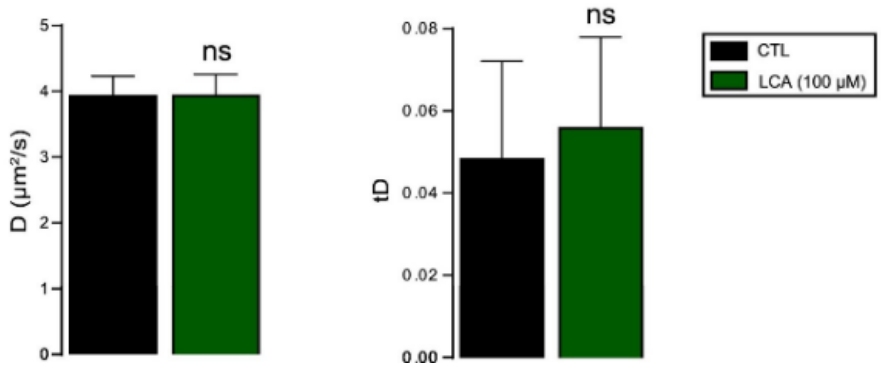

Figure 25: LCA is not affecting integrity of biomembranes

A supported bilayer consisting of a ternary lipid composition of DOPC/SM/cholesterol in a 1/1/1 ratio was treated with 100 µM LCA for 20 minutes. The diffusion coefficients of the STAR 488 PEG-cholesterol probe in both control and treated membranes, as well as the confinement times of the probe were measured (**D**). The error bars represent the standard deviations (n=6). It is important to note that the LCA concentration used in this experiment was 33 times higher than the highest concentration employed in *in vitro* experiments.

5.2. Identification of breast cancer cell modulating bacterial metabolites

5.2.1. Metabolite library construction

Bacterial metabolites affecting human metabolism were identified through an extensive literature search. To ensure accuracy, the identified metabolites were carefully curated to exclude any falsely identified compounds that are not produced by bacteria. The reference concentrations of these metabolites in serum were established by literature searches. A recent study [133] revealed that the presence of a tumor influences gut motility by modulating beta-adrenerg receptors. Altered passage speed within the gastrointestinal (GI) tract is likely to affect the redox environment [204], suggesting potential changes in the redox state of redox-labile metabolites in breast cancer patients. Therefore, the redox partners of each metabolite (mannose – D-mannitol, TMA – TMAO, 1-butanol – butyric acid, ethylene glycol – glycolic acid, oxalic acid) were incorporated into the metabolite library, and their serum reference concentrations were established through a comprehensive literature search. However, no specific literature data was available for ethylene glycol, so the same concentrations as the known redox pairs were utilized as reference. For a comprehensive overview of the metabolites, their serum reference concentrations, treatment concentrations, and corresponding literature sources, please refer to **Table 6**.

5.2.2. Developing high throughput techniques to assess cell proliferation

In our previous investigations, we identified and characterized a group of bacterial metabolites exhibiting cytostatic activity [5]–[7]. However, the antiproliferative effects of these metabolites were limited, and the SRB proliferation assay did not prove highly precise data within that concentration range. To address this limitation, we evaluated two alternative methods for nucleus counting, based on image analysis. One method involved image segmentation and nucleus counting using CellProfiler, while the other utilized a deep learning (DL)-based method developed specifically for this project for segmentation, with nucleus counting performed using CellProfiler. The SRB assay provided unreliable at low cell densities in a range of 100-300 cells per well. Additionally, the inherent limitations of photometry rendered values above an absorbance of 1.0 unreliable, restricting the maximum number of cells measurable at the end of an assay to 10 000 – 30 000 (**Figure 26A**). Values exceeding absorbance of 1.0 could be measured

following dilution, introducing the possibility of dilution errors. In contrast, the image analysis-based assays exhibited a wider dynamic range compared to the SRB assay. Both analysis-based methods provided reliable results even at low cell numbers (**Figure 26A**). Moreover, these assays were capable of detecting cell numbers up to 100 000 cells per well, with the DL-based method demonstrating superiority over CellProfiler's built-in method (**Figure 26A**). Furthermore, the trained semantic segmentation models used in the DL-based method did not require parameter adjustment for every run, unlike conventional methods, offering an additional simplicity and increased accuracy between experiments for this segmentation approach. It is worth noting that the image analysis-based assays consistently yielded lower cell counts than the initially plated numbers when the cell densities ranged from 1 000 to 10 000. Upon visual inspection of these wells, it became apparent that cells adhered less to the plates at these densities, resulting in reduced cell numbers in the wells. This decrease in cell count observed in the culture plates confirmed the precision of the image analysis-based assays (**Figure 26B**). Based on these findings, in subsequent experiments, we exclusively employed the image analysis-based methods.

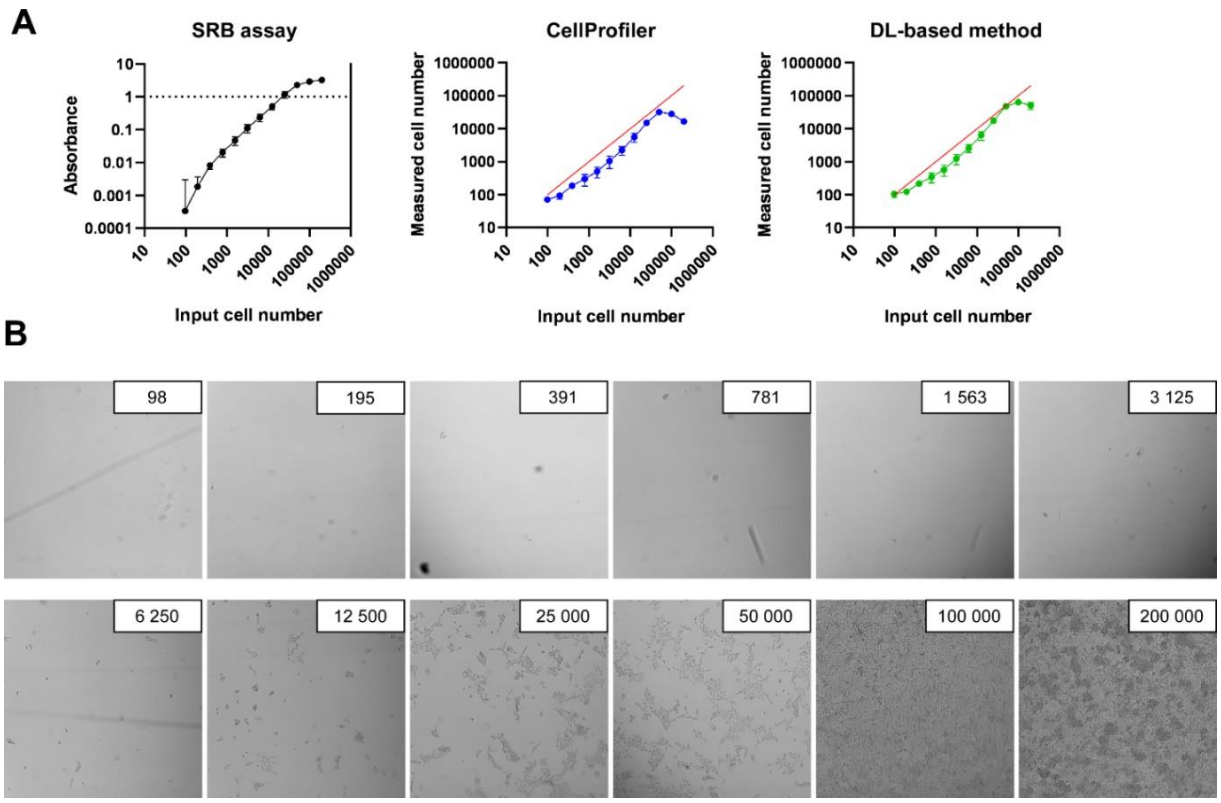

Figure 26: Validation of the image analysis-based proliferation assay

The specified number of 4T1 cells was seeded onto 96-well plates for the SRB assay and in parallel onto 96-well high content imaging microplates for the two high-content screening methods. The following day, an SRB assay was performed as previously described, or for the high-content screening methods, the nuclei were stained with DAPI. Next, the images were segmented using CellProfiler or the deep learning-based method, and the nuclei numbers were quantified using CellProfiler. In the graphs, the red line represents a 45°line, indicating the expected number of cells seeded. Representative phase-contrast images of the well containing the designated number of cells were also captured (n=3). Abbreviations: DL – deep learning.

5.2.3. Identifying microbial metabolites with pro- or antiproliferative properties

We evaluated the impact of the bacterial metabolites in our library on cell proliferation in 4T1 breast cancer cells. Cells were exposed to five different concentrations of each metabolite, covering the range of reference concentrations provided in **Table 5**. Statistical analysis was conducted independently for each metabolite's dose-response curve. Our findings revealed eight

bioactive metabolites changing cell proliferation: butyric acid, glycolic acid, D-mannitol, 2,3-butanediol, trans-ferulic acid, 4-hydroxybenzoic acid, vanillic acid, and 3-hydroxyphenylacetic acid (**Figure 27** and **Figure 28**). Notably, formic acid exhibited antiproliferative properties at the highest concentration tested; however, we considered this observation cautiously as the highest concentration significantly exceeded the upper limit of the reference range (as indicated by the bracket in **Figure 27**). Butyric acid, glycolic acid, D-mannitol, 2,3-butanediol, and trans-ferulic acid demonstrated antiproliferative effects at the highest concentration employed, while 4-hydroxybenzoic acid, vanillic acid, and 3-hydroxyphenylacetic acid exhibited supportive effects on proliferation at specific concentrations (**Figure 28**).

metabolite	CP	DL	concentration 1		concentration 2		concentration 3		concentration 4		concentration 5	
			CP	DL	CP	DL	CP	DL	CP	DL	CP	DL
butyric acid	*	**	1.01	0.98	1.00	0.94	0.97	0.93	0.93	0.90	0.84	0.81
glycolic acid	*	*	1.06	1.08	0.97	0.99	1.04	1.06	0.90	0.91	0.74	0.76
D-mannitol	*	*	0.92	0.92	0.97	0.97	0.92	0.92	0.93	0.93	0.85	0.85
2,3-butanediol		*	0.99	0.98	0.98	0.97	0.97	0.96	0.98	0.97	0.88	0.88
trans-ferulic acid	*	*	0.95	0.96	0.99	0.99	0.96	0.97	0.93	0.93	0.84	0.84
formic acid	(*)		1.03	1.02	1.01	1.01	1.00	1.00	0.98	0.97	0.90	0.90
L-pipecolic acid			0.98	0.99	0.96	0.96	0.96	0.96	0.91	0.91	0.87	0.87
trimethylamine-N-oxide			0.97	0.95	0.98	0.95	0.95	0.94	0.96	0.94	0.97	0.94
3-hydroxypropionic acid			0.99	0.97	0.95	0.93	0.93	0.92	0.97	0.95	0.88	0.88
oxalic acid			1.01	1.01	0.97	0.96	1.00	0.99	0.98	0.97	0.96	0.95
trimethylamine			0.99	0.98	1.02	1.01	1.01	1.00	0.97	0.96	0.96	0.97
1-butanol			1.01	1.01	0.96	0.96	0.97	0.97	0.90	0.90	0.96	0.96
D-glutamic acid			0.97	0.98	0.94	0.92	0.95	0.94	0.98	0.99	0.98	0.97
allantoin			0.97	0.99	1.01	1.00	1.01	1.00	0.98	0.96	1.00	0.97
propionic acid			1.04	1.12	1.00	1.07	0.92	1.00	0.88	0.99	0.88	0.95
4-aminobenzoic acid			1.03	1.03	1.03	1.04	1.02	1.02	0.93	0.93	0.97	0.97
shikimic acid			1.05	1.04	1.00	1.00	1.03	1.03	0.97	0.97	0.96	0.96
acetic acid			1.07	1.07	1.04	1.05	1.02	1.01	0.98	0.98	0.94	0.93
4-hydroxyphenylacetic acid			0.99	0.99	1.03	1.03	1.04	1.04	0.98	0.98	0.97	0.98
hippuric acid			1.04	1.04	1.02	1.02	1.02	1.03	1.02	1.03	0.89	0.90
isobutyric acid			1.05	1.04	1.01	1.01	1.03	1.03	0.98	0.99	1.01	1.02
D-alanine			1.03	1.02	0.98	0.98	1.06	1.05	1.01	1.01	0.99	0.99
hydrocinnamic acid			1.03	1.03	1.05	1.05	1.04	1.03	1.07	1.07	1.02	1.02
1-propanol			1.10	1.10	1.07	1.07	0.99	0.99	1.08	1.08	1.04	1.04
D-mannose			1.07	1.08	1.08	1.07	1.10	1.11	1.09	1.10	1.07	1.07
3,4-dihydroxyphenylacetic acid			1.05	1.05	1.04	1.03	1.06	1.06	1.07	1.06	1.07	1.06
ethylene glycol			1.05	1.08	1.03	1.04	1.11	1.14	1.08	1.09	1.03	1.05
4-hydroxybenzoic acid		*	1.04	1.04	1.08	1.07	1.04	1.04	1.07	1.09	1.05	1.05
vanillic acid		*	1.06	1.09	1.04	1.06	1.04	1.06	1.09	1.12	1.02	1.05
3-hydroxyphenylacetic acid	*	**	1.07	1.06	1.08	1.07	0.98	0.97	1.12	1.12	1.01	1.01

Figure 27: Identification of bacterial metabolites with cytostatic effects on 4T1 breast cancer cells.

96-well high content imaging microplates were utilized to seed 800 4T1 cells per well. The cells were subsequently treated with specific metabolites at the concentrations indicated in the figure or **Table 5** for a duration of 48 hours. The measurements were performed in a minimum of 3 independent experiments with 4 technical replicates each. Images of the cells were captured with PerkinElmer Opera Phenix High Content Screening System and segmented using either CellProfiler or deep convolutional neural network. Nuclei were counted with with CellProfiler. The data is presented as the mean ± SD from the biological replicates. Values were normalized to the vehicle-treated group, and fold change was calculated. Each metabolite was evaluated separately during the statistical analysis. A heatmap illustrating the impact of the metabolites on the proliferation of 4T1 cells, presented as fold change. * and ** indicate statistically significant difference between vehicle and treated groups at $p<0.05$ or $p<0.01$, respectively.

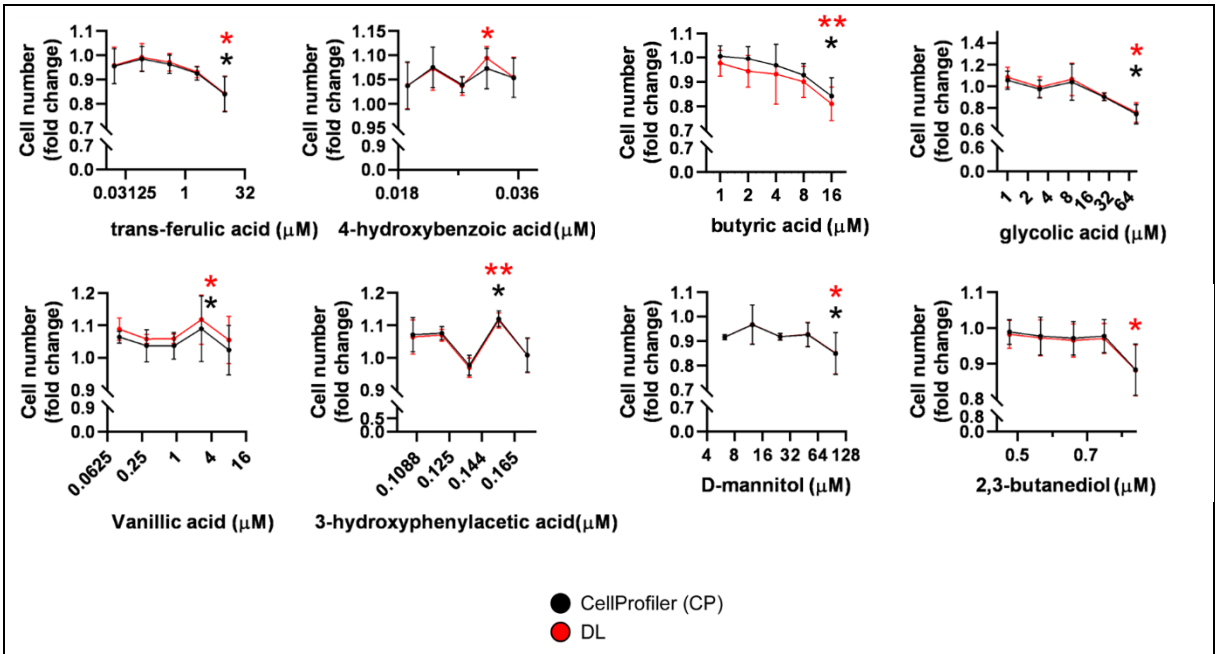

Figure 28: Identificationof bacterial metabolites with cytostatic effects on 4T1 breast cancer cells.

The impact of the metabolites on the proliferation of 4T1 cells, with metabolite concentrations displayed on logarithmic axes. Abbreviations: DL – deep learning segmentation, CP – CellProfiler's built-in method segmentation. * and ** indicate statistically significant difference between vehicle and treated groups at $p<0.05$ or $p<0.01$, respectively.

5.2.4. Development of a high-throughput approach for evaluating EMT.

The bacterial metabolites previously identified in breast cancer, such as lithocholic acid, cadaverine, indole-derivatives, and short chain fatty acids [10], we found to impact epithelial-mesenchymal transition (EMT). To explore the potential modulation of EMT by the metabolite library, we employed a high-content image analysis methodology based on the observation that EMT alters cellular morphology in breast cancer [205]–[207]. Additionally, we validated the results by assessing the protein-level expression of a set of EMT markers, such as vimentin and Snail. To establish positive and negative controls for EMT induction and inhibition, respectively, we applied transforming growth factor β 1 (TGF-β1) at a final concentration of 10 ng/mL [208], and SB-431542 at a final concentration of 2 μM [209], which is an inhibitor of TGF-β superfamily type I activin receptor-like kinases. The cells were treated with these compounds for 48 hours.

Protein markers associated with mesenchymal transition, such as Zinc finger protein SNAI1 (Snail) and vimentin, were found to increase upon TGF-β1 induction, while vimentin, but not Snail was suppressed upon SB-431542 treatment in 4T1 cells (**Figure 29A**). Furthermore, visual inspection of the cells confirmed the TGF-β-induced mesenchymal transition and the SB-431542 mediated epithelial transition (**Figure 29B**). Consistent with these observations, high-content screening-based cell classification method indicated an increase in proportions of mesenchymal cells upon TGF-β1 induction, and a decrease in the proportions of mesenchymal cells following treatment with SB-431542. Based on these findings, we concluded that the high-content screening-based methods are reliable for determining the proportions of epithelial and mesenchymal cells under these experimental conditions (**Figure 29B**).

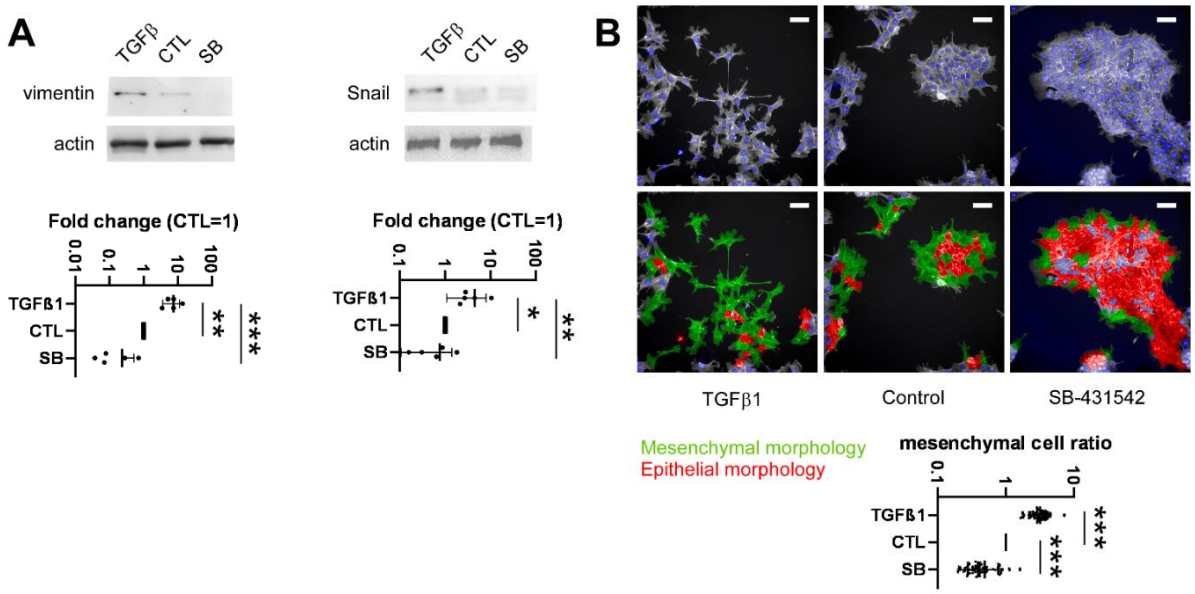

Figure 29: High content screening can identify cells undergoing epithelial-mesenchymal transition

A total of $1.5x10^6$ cells were seeded onto Petri dishes ant treated with either TGF-β1 or SB-431542 for a duration of 48 hours. The cellular proteins were analyzed using SDS-PAGE followed by Western blotting with specific antibodies. Sample blots were captured and their densitometric evaluation was performed, displaying individual observations along with the mean ± SD. The protein values were normalized to the control (vehicle-treated) cells, where the density of the control cells was set as 1 (**A**). In addition, 800 4T1 cells were seeded on 96-well high content imaging microplates and treated with TGF-β1 and/or SB431542 for 48 hours. Nuclei were stained with DAPI, and cellular visualization was achieved using Texas-Red-X-Phalloidin. The acquired images were processed using the Harmony software (PerkinElmer) to identify cells exhibiting either epihtelial or mesenchymal morphology. The proportions of mesenchymal cells were normalized with respect to the total cell number within each sample, as well as accounting for any inter-sample cell number differences. Normality was assessed, and statistical significance was determined as described in the Methods section. Representative fluorescence microscopy images and their algorithmically analyzed representations are provided. Cells classified to the mesenchymal morphology group are highlighted with green, and cells classified to the epithelial morphology group are hihglighted with red. Scale bar indicating a length of 10 µm (**B**). *, **, and *** indicate statisticall significant difference between vehicle and treated groups at $p<0.05$ or $p<0.01$, and $p<0.001$ respectively. Abbreviations: CTL (control), SB (SB-431542), TGF-β1 (transforming growth factor β).

5.2.5. Identifying bacterial metabolites affecting EMT

Following the validation of the developed method, we conducted an assessment of the metabolite library to determine their impact on EMT utilizing high-content screening. In this analysis, we identified 3-hydroxyphenylacetic acid, hydrocinnamic acid, 2,3-butanediol, and 4-hydroxybenzoic acid as compounds of interest (**Figure 30**). Notably, we observed a distinct V-

shaped curve where an optimal concentration of each compound significantly reduced the proportion of mesenchymal cells, while lower and higher concentrations were ineffective (**Figure 31A**). To validate these findings, we performed Western blot analysis. 4T1 cells were treated with the effective concentrations of the metabolites for 48 hours, and protein extracts were probed with anti-Snail and vimentin antibodies. With the exception of 2,3-butanediol, all metabolites exhibited a reduction in the expression of at least one mesenchymal marker, confirming the results obtained from the high-content screening method (**Figure 31B**). In the case of 2,3-butanediol, a decrease in the expression of EMT markers was observed but statistical tests did not reveal significant difference (**Figure 31B**).

metabolite		CC 1	CC 2	CC 3	CC 4	CC 5
4-hydroxybenzoic acid	**	−0.10	−0.48	−0.25	−0.03	−0.02
2,3-butanediol	**	−0.01	−0.44	0.01	0.04	0.16
hydrocinnamic acid	***	−0.06	−0.38	−0.22	0.01	0.02
3-hydroxyphenylacetic acid	**	−0.15	−0.36	−0.23	−0.10	−0.08
trimethylamine-N-oxide		−0.38	−0.62	−0.43	−0.24	0.17
allantoin		−0.03	−0.36	−0.36	0.02	0.09
1-propanol		−0.11	−0.37	−0.37	0.01	−0.12
D-mannose		−0.27	−0.37	−0.26	−0.05	0.43
isobutyric acid		−0.25	−0.19	−0.32	−0.03	−0.09
D-alanine		0.02	−0.19	−0.28	−0.04	0.01
oxalic acid		0.08	−0.24	−0.11	−0.01	0.14
trimethylamine		0.00	−0.25	−0.26	0.00	−0.13
vanillic acid		0.03	−0.11	−0.24	0.08	0.10
formic acid		−0.04	−0.13	−0.25	0.11	0.07
4-hydroxyphenylacetic acid		−0.01	−0.25	−0.16	0.11	0.04
trans-ferulic acid		0.08	−0.05	−0.12	−0.21	0.25
hippuric acid		0.05	−0.11	−0.17	−0.18	−0.19
3,4-dihydroxyphenylacetic acid		0.03	−0.16	−0.13	−0.05	0.04
D-mannitol		0.02	−0.19	−0.04	−0.05	0.03
L-pipecolic acid		−0.14	−0.14	−0.19	0.08	0.21
D-glutamic acid		−0.04	−0.14	0.03	0.05	0.09
shikimic acid		−0.14	−0.08	−0.02	0.13	0.05
butyric acid		−0.01	−0.06	0.01	0.17	0.14
3-hydroxypropionic acid		−0.10	−0.05	−0.10	−0.07	0.02
1-butanol		−0.12	−0.05	−0.08	0.10	−0.08
propionic acid		0.06	−0.08	0.15	0.19	0.21
4-aminobenzoic acid		−0.07	−0.11	−0.03	0.11	0.05
acetic acid		−0.01	−0.06	0.03	0.13	0.13
ethylene glycol		0.16	−0.05	−0.02	0.38	0.24
glycolic acid		0.02	0.00	−0.08	0.04	0.31

−1.5 1.5

Figure 30: Bacterial metabolites in physiological concentration affect cell morphology

A total of 800 4T1 cells were seeded per well in 96-well high content imaging microplates and treated with the specific metabolites at the concentrations provided in **Table 5** for a duration of 48 hours. The acquired images were processed using the Harmony 4.8 software (PerkinElmer) to identify cells exhibiting either epithelial or mesenchymal morphology. The proportions of mesenchymal cells were normalized based on the total cell count within each sample, as well as inter-sample cell number differences. The normality of the data was assessed, and statistical significance was calculated according to the described methods. Each metabolite was evaluated independently in the statistical analysis. *, **, and *** indicate statistically significant difference between vehicle and treated groups at $p<0.05$ or $p<0.01$, and $p<0.001$ respectively. Abbreviations: CC 1-5 corresponds to the concentrations indicated in **Table 5**, with increasing doses assigned numerical references.

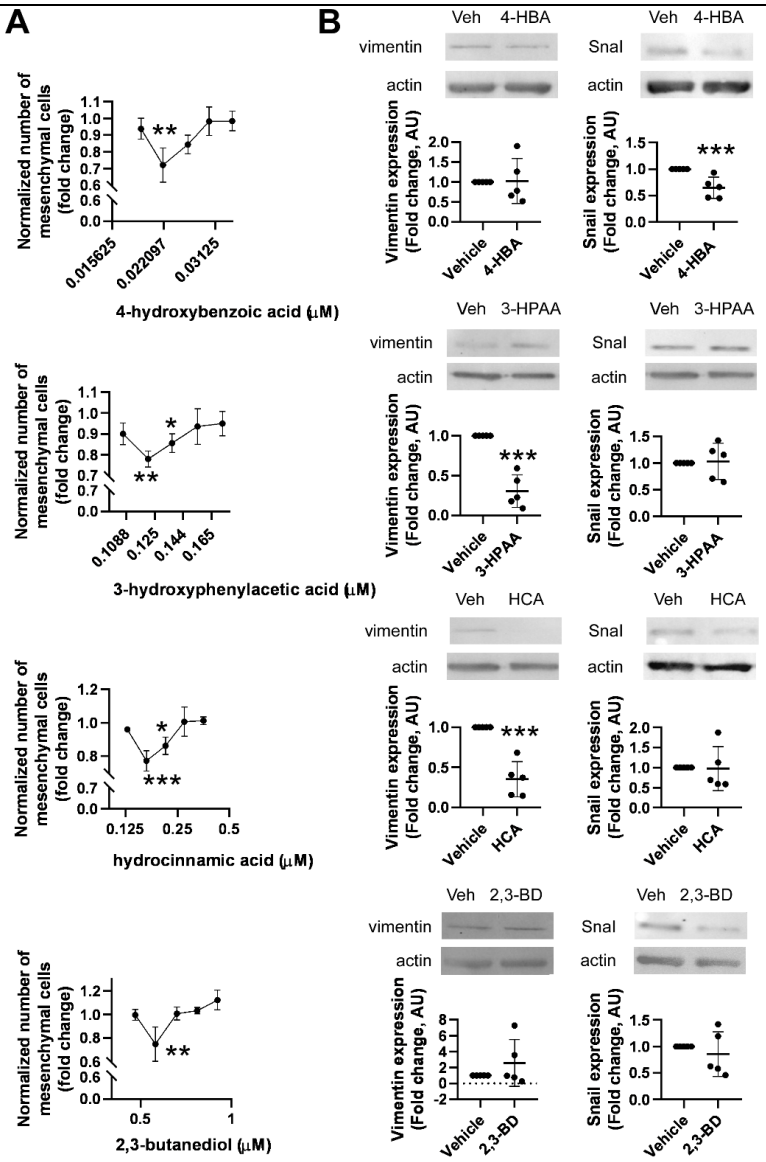

Figure 31: Bacterial metabolites affect cell morphology in physiological concentration

A total of 800 4T1 cells were seeded in 96-well high content imaging microplates and treated with the indicated metabolites at the concentrations specified in **Table 5** for a duration of 48 hours. The acquired images were processed using the Harmony 4.8 software (PerkinElmer) to segment and distinguish cells exhibiting either epithelial or mesenchymal morphology. The proportions of mesenchymal cells were normalized based on the total cell count within each sample, as well as the differences in cell numbers among samples. Normality was assessed and statistical significance was determined following the methods outlined in the study. Each metabolite was analyzed separately during the statistical evaluation (n=3, **A**). A total of $1.5x10^6$ 4T1 cells were seeded in Petri dishes and treated with the specified metabolites at the concentrations listed in **Table 5** for a duration of 48 hours. Cellular proteins were then analyzed using SDS-PAGE followed by Western blotting with the indicated antibodies. The obtained sample blots were subjected to densitometry analysis, and the results are presented as the mean ± SD. The values were normalized to the control cells treated with the vehicle, where a density of 1 was assigned (n=5, **B**). *, **, and *** indicate statistically significant difference between vehicle and treated groups at $p<0.05$ or $p<0.01$, and $p<0.001$ respectively.

6. Discussion

The human body hosts a complex ecosystem of microorganisms, collectively known as the microbiome, which plays a crucial role in various physiological processes. The normal composition of the microbiome varies significantly from person to person, and defining the exact composition of the healthy microbiome is a challenging task. However, imbalance (dysbiosis) in the gut microbiome composition is linked to several intestinal and extra-intestinal diseases, e.g.: irritable bowel syndrome, coeliac disease, allergy, asthma, cardiovascular diseases, and obesity [210]. In the last decade, dysbiosis was also linked to breast cancer. In breast cancer, the microbiome's composition undergoes significant changes, and becomes less diverse in the early stage [10], [211]. The exact cause of dysbiosis, and the pathomechanisms between breast cancer and the microbiome is still unknown. However, microbial metabolites reaching breast tissues affect cancer cells. Among the blood-transported bacterial metabolites, cadaverine, indoxyl sulfate, and indolepropionic acid were identified as antineoplastic agents in in breast cancer, in serum concentration range [5]–[7].

6.1. The effects of LCA in breast cancer

Earlier studies have suggested possible oncogenic properties of secondary bile acids [212]. For instance, LCA demonstrated transforming capacity towards colon epithelial cells [212], while DCA (inactive in our model systems) was found to reprogram the secretome and promote hepatocellular carcinoma [187][188]. Furthermore, DCA induced antineoplastic effects in pancreateic adenocarcinoma cells by inhibiting EMT, reducing cancer stemness [215]. Additionally, bile acids have been implicated in pharyngeal cancer [216].

LCA is synthesized from primary bile acids by the gut microbiome and then reabsorbed at the terminal ileum, entering the enterohepatic circulation. Most of the LCA is then reabsorbed by the liver, but a small portion of it reaches remote parts of the body. In our experiments, LCA reduced the proliferation of MCF7, 4T1 and SKBR3 breast cancer cell lines. DCA and UDCA did not affect cell proliferation. These results were confirmed by SRB and colony forming assays. The effect was specific to breast cancer cell lines, as the primary fibroblast cell proliferation remained unchanged upon LCA treatment.

Changes in the total protein content or the colony size during the proliferation experiments could also be attributed to cell death. Previous studies reported that LCA can induce cell death in neuroblastoma, prostate cancer, and MCF7 cells [217], [218]. However, the concentrations used in those studies were much higher than the serum concentrations we used during the experiments, which may account the absence of acute cytotoxicity. Our experiments showed, that propidium iodide cell number remained unchanged in treatments with physiological LCA concentrations, cell death was not the primary cause of change in the proliferation experiments.

LCA also reduced ratio of mesenchymal cell number in 4T1 breast cancer cell line. ECIS experiments also confirmed this observation in MCF7 and 4T1 cells, where the resistance values showed stronger cell-cell and cell-surface adhesion. Cell going through EMT have increased mobility, and weaker cell-cell connections [70]. In scratch assays, we measured slower gap closure in 4T1 cell lines upon LCA treatment. Together these results show mesenchymal to epithelial transition (MET) upon LCA treatment.

β-catenin, an important transcription factor in the Wnt pathway, regulating cell proliferation in the G1 phase. In colorectal cancers, β-catenin also induces EMT and pro-invasion expression profiles through T-cell and lymphoid enhancer (TCF-LEF) factor activation [219]. Conventionally, β-catenin level assessment requires the evaluation of pGSK-3α/β / GSK-3α/β levels, as phosphorylated GSK-3α/β promotes β-catenin degradation [68]. Our *in vitro* Western blot analysis revealed that β-catenin protein level decreased, while GSK-3α/β goes through dephosphorylation in MCF7 and 4T1 cell lines during LCA treatment. β-catenin levels can give an explanation for the proliferation changes in our experiments. GSK-3α/β signaling on the other hand seems to be disconnected from β-signaling. This can be explained in several ways, e.g.: mutations in growth signaling pathways, or alternative GSK-3α/β activation through PI3K/Akt, protein phosphatase2, or protein kinase B [220], [221], [222]. β-catenin protein level was also decreased in our *in vivo* samples, in LCA treatment.

Our *In vivo* experiments showed, that tumor infiltrating lymphocyte number is increasing upon LCA treatment, while qPCR measurements showed decreased Vegfa mRNA in tumor samples. TIL number is a common prognostic marker in breast cancer, indicating better prognosis, while VEGFA is a vascularization marker.

We also wanted to assess the typical Warburg metabolism markers in the study. Generally, OCR and ECAR, oxidative phosphorylation gene (CytC, ATP5g1, NUDFB5) and energy

metabolism regulator gene expression (FOXO1, PGC1-β, NRF1) and activity was increased upon LCA treatment both *in vitro* and in *in vivo* experiments. Pulse-chase metabolomic measurements showed a higher succinate/lactate and citrate/lactate level in MCF7 and 4T1 cell lines. These collectively indicate increased activity of TCA cycle and oxidative phosphorylation upon LCA treatment. In other words, LCA treatment induced an anti-Warburg response in the breast cancer cells, providing a possible explanation for decreased cell proliferation [48].

LCA most likely affects cell signaling pathways through multiple receptors. In our experiments, part of the observed effects were most likely the result of TGR5 signaling, as specific inhibition of this receptor reverted back LCA-induced cell morphology and proliferation changes.

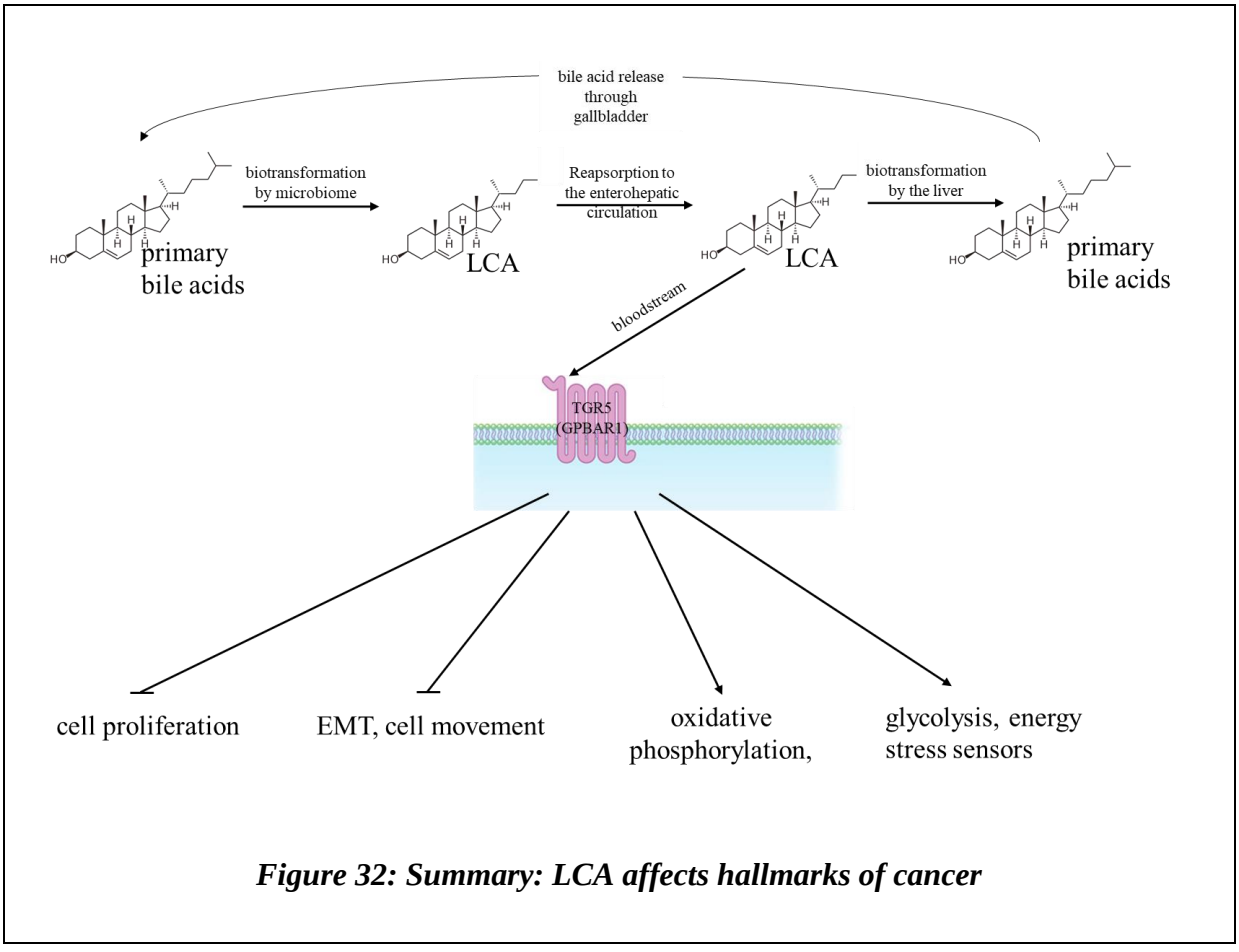

Figure 32: Summary: LCA affects hallmarks of cancer

6.3. Standardization of microscopy image analysis

In this study, one of our aim was to create a standardized high throughput image analysis method, to measure cell proliferation and EMT in varying conditions via fluorescent microscopy. For this purpose, we applied conventional image analysis techniques and deep learning techniques.

The base of the deep learning model was a fine-tuned a VGG16 feature extraction model pretrained on ImageNet, joined with a U-Net segmentation model. VGG16 is broadly used for image classification, and pretrained weights are readily available for this model. U-Net is a general purpose segmentation model, commonly used in biomedical image analysis applications [165]. After training, our fine-tuned nuclei segmentation model performed >98% accuracy on the validation dataset. The deep learning-coupled nuclei counting method analyzed more than 60 000 images without human interference and were comparable to conventional nuclei counting methods, where parameter adjustments were required for each independent dataset. This method outperforms conventional image analysis methods and SRB proliferation assay as well, showing higher accuracy in extreme low and high cell counts (100 – 100 000 cell/well).

The trained neural network is well-generalized for at least 4T1 nuclei segmentation tasks, and potentially well trained to segment other cell lines' nuclei included in the training set as well. Cancer cells however, could show nuclear pleomorphism [223], that may easily disrupt fine-tuned image analysis methods. Another problem is the time- and resource-consuming imaging and image analysis, compared to other well-established chemistry-based proliferation assays (as SRB-assay). An easy solution to these problems would be specifically including images of pleomorphism in the training dataset for the deep learning segmentation models, to train the model for amorphous nuclei segmentation as well. Furthermore, using exclusively brightfield images (no fluorescent labeling) for cell and nuclei segmentation could lead to drastically reduced cost and time of imaging/analysis without losing significant accuracy [224]. These principles can also be applied to develop a stand-alone automatized analytic method to measure breast cancer cell features, such as proliferation and EMT.

6.2. The role of bacterial metabolites in breast cancer

To date, the majority of bioactive bacterial metabolites discovered have shown anti-

neoplastic properties. Additionally, in breast cancer patients, levels of enzymes involved in producing these bacterial metabolites have been found to decrease in the gut microbiome compared to healthy individuals [10].

In our research, we identified 9 bacterial metabolites that impact the proliferation and morphology of the 4T1 breast cancer cell line. Notably, formic acid significantly decreased cell proliferation. However, it's important to acknowledge that the concentration used in our study exceeds the upper limit of the physiological serum concentration range.

A recent study revealed the occurrence of ileopathy in various cancers, including breast cancer [133]. Slower passage through the gastrointestinal tract not only changes the composition of the microbiome but also likely impacts the redox balance of the GI tract contents [204], [225]. Due to this observation, we also explored bacterial metabolites in redox pairs. Several redox pairs were identified within the short-chain fatty acid and polyol group (e.g., D-mannitol – D-mannose, 1-butanol – butyric acid, ethylene glycol – glycolic acid – oxalic acid), where only one partner displayed cytostatic properties (**Figure 33**). This finding suggests that altered redox environment may influence the metabolome/secretome in breast cancer.

The bacterial metabolites identified in our experiments belong to various chemical groups, necessitating separate discussions. D-mannose is a monosaccharide, and D-mannitol is a sugar alcohol or polyol. In our experiments, D-mannitol significantly reduced cell proliferation, whereas its redox pair, D-mannose, did not affect breast cancer cell proliferation. Literature shows, that mannitol is already a therapeutic target in cisplatin treated cancer patients due to its nephroprotective properties [226], although the concentration applied in that study (approximately 16 mM) is significantly higher than that of the highest concentration (128 µM) we used in our current research. Controversially, other studies appropriate mannitol nephrotoxic properties at high concentrations, in patients with renal failure [227], [228]. To date, D-mannitol was not studied in other cancer related research projects.

Another polyol, 2,3-butanediol is unique among the bacterial metabolites investigated in our research, due to its ability to inhibit both proliferation and EMT. It is also worth noting, that the ability to synthesize 2,3-butanediol is widespread among bacteria [229], [230]. According to these findings, 2,3-butanediol could be the most promising candidate as an anti-neoplastic bacterial metabolite.

On the oxalic acid, glycolic acid, and ethylene glycol redox axis, we found that only one of

these bacterial metabolites exhibited an effect on breast cancer cells. Glycolic acid, a short-chain fatty acid, significantly decreased cell proliferation. Similar to D-mannitol, glycolic acid has not been previously investigated in breast cancer. Apart from its physiological serum concentration range, the known information about glycolic acid pertains to its use in chemical peels and anti-acne formulations in dermatology [231], [232].

Butyric acid, another short-chain fatty acid, has demonstrated antiproliferative properties in our experiments. Butyric acid affects breast cancer cells through various mechanisms, serving as an inhibitor of histone deacetylases (an epigenetic modifier), a metabolic substrate, and a ligand to free fatty acid receptors [10]. Notably, butyric acid levels were found to decrease in the feces of breast cancer patients [233].

Trans-ferulic acid, a polyphenol, reduced cell proliferation. Literature indicates, that ferulic acid, a potentially anti-tumor microbial metabolite, inhibits breast cancer cell proliferation, promotes apoptosis, and reduce migration speed *in vitro* within the range of 10-100 μM [234]. Recent studies suggest that it may also inhibit breast cancer formation [235]. It is important to note that the molecule investigated in our experiments is the trans isoform of ferulic acid, and our findings should be interpreted accordingly.

4-hydroxybenzoic acid is synthesized from chorismic acid and can bind to the estrogen receptor [236], peroxisome proliferator activated receptor (PPAR)γ [237] and G-protein-coupled receptor 40 (GPR40) [237]. 4-hydroxybenzoic acid treatment increased cell proliferation, while inhibited EMT.

Vanillic acid belongs to the benzoic acid chemical class. In our experiments, vanillic acid significantly increased cell proliferation. Notably, trans-ferulic acid and vanillic acid are present in the extracts of bacteria or plants tested for their anticancer potential. Furthermore, vanillic acid has been shown to act as pro-oxidant and suppress cell proliferation [238].

Lastly, among the polyphenols, 3-hydroxyphenylacetic acid reduced cell proliferation, furthermore both hydrocinnamic acid and 3-hydroxyphenylacetic acid inhibited EMT. Compounds such as hydrocinnamic acid, 3-hydroxyphenylacetic acid, and 4-hydroxyphenylacetic acid comprise an aromatic ring and a polar carboxylic and moiety. Hydrocinnamic acid has been demonstrated to be a product of lactic acid-producing bacteria [239]. On the other hand, 3-hydroxyphenylacetic acid is a flavonoid compound generated through the degradation of quercetin-derivatives, which are synthesized by the human microbiome [240]–

[242], partly by *Clostridiales* [243]. Notably, 3-hydroxyphenylacetic acid exhibits cytoprotective features [244] and can bind to the γ-hydroxybutirate receptor [245], [246].

Several metabolites identified in this study, such as glycolic acid, hydrocinnamic acid, 2,3-butanediol, 3-hydroxyphenylacetic acid, and 4-hydroxyphenylacetic acid, have been shown to have antibacterial activity or are involved in quorum sensing [232], [236], [243], [247]–[250]. This suggests that these metabolites may not only affect breast tumor cells but also influence the microbiome.

In our experiments, we have seen a V-shaped or inverted V-shaped dose-response curve in several cases (e.g. 2,3-butanediol/EMT, 4-hydroxybenzoic acid/proliferation). This behavior is similar to certain previously identified antineoplastic bacterial metabolites, such as indoxyl-sulfate [6] or indolepropionic acid [7] (in both cases, V-shape was observed). An inverted V-shaped curve suggests a sequence of events where a receptor is initially stimulated, promoting proliferation at low concentrations, and then another receptor becomes activated, inhibiting proliferation at higher concentrations. It's worth noting that although toxicity can sometimes show similar patterns at high concentrations, in this study, the compounds were kept within the recommended range, reducing the likelihood of a toxic effect.

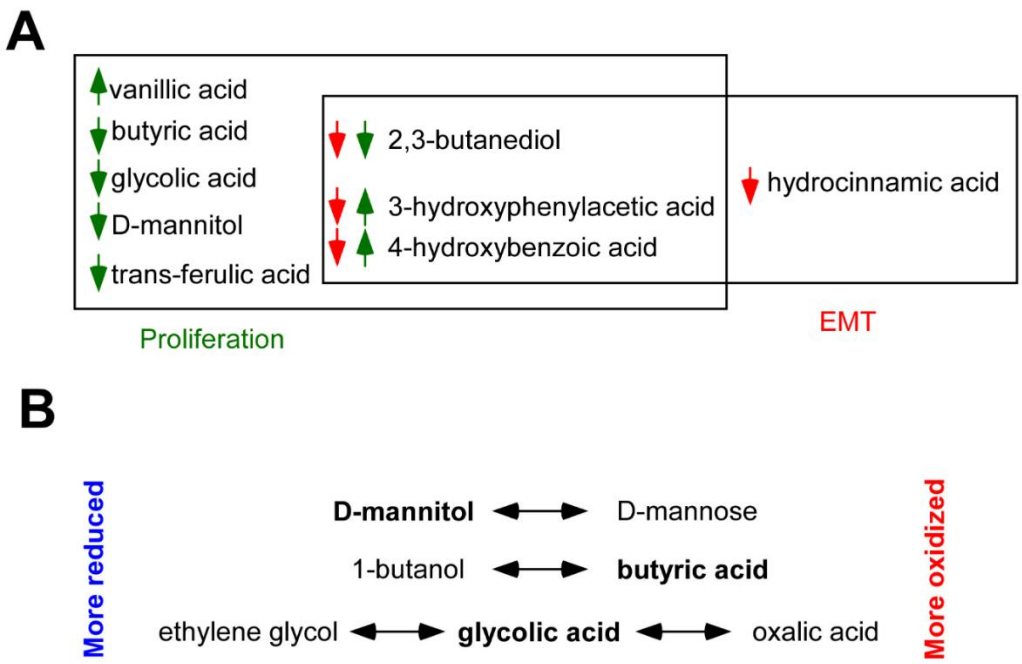

Figure 33: Summary: Bacterial metabolites affect cell proliferation and EMT in 4T1 breast cancer cell line

There are multiple aspects of this work, that could lead to possible future research projects. Firstly, bacterial metabolites are already proven to modify breast cancer cell behavior *in vivo* and *in vitro*. Cellular processes altered by the bacterial metabolites could prove to be a valuable therapeutic target, as well as a diagnostic tool. This work has already started with the description of LCA signaling pathways in this work. As a logical continuation, LCA could be potentially applied as a cytostatic agent to complement the currently available therapeutic approaches in pilot experiments.

Secondly, the identified bacterial metabolites in the metabolite screening experiments show, that next to LCA, other bacterial metabolites could affect the metabolism of breast cancer cells. Considering that dysbiosis is correlated with breast cancer, a small glimpse of a possible diagnostic tool is showing from these results. The next step in this direction would be the identification of the bacterial enzymes responsible for the synthesis of the identified metabolites.

And finally, as the current work also focused on research method development, a fully automatized and cheap research tool in breast cancer can be developed by fine-tuning the imaging and analysis tools. In the current state, two of the cancer hallmarks – namely cell proliferation and EMT – can be monitored with microscopy in 4T1 breast cancer cell model. However, these methods can be generally applied in every *in vitro* experiments, even beyond cancer research with modifications (e.g. only changing input and ground truth images for the neural network in the learning process).

7. Summary

There is a strong connection between the microbiome and the host. Bacteria residing in various parts of the human body generate a multitude of bacterial metabolites, which have the ability to impact the host. Vice versa, the host – through diet, personal hygiene, genetics, and age – can also affect the composition and function of the microbiome. Changes in the microbiome's composition or function are linked to several diseases, including breast cancer.

Lithocholic acid (LCA), a secondary bile acid, which is produced by bacteria coding the baiH ORF. LCA reaches breast cancer cells through the bloodstream located distantly from the gut microbiome. LCA reduced the proliferation and colony formation ability of MCF7, 4T1 and SKBR3 breast cancer cells, inhibited the epithelial-mesenchymal transition (EMT), and shifted energy metabolism toward oxidative phosphorylation, hence, reverting the Warburg effect in cultured cells. LCA also inhibits cell migration while promoting cell-to-cell and cell-to-surface connections. LCA supplementation in mice increases the number of tumor-infiltrating lymphocytes in the primary tumor. LCA elicited its effects through the TGR5 receptor, as inhibiting or silencing this receptor prevents LCA-induced EMT and the expression of LCA-induced genes (pACC, ATP5G1, and NDFUB5).

The study also evaluated a carefully curated library of 30 other bacterial metabolites and applied these in their serum reference concentrations in cellular models. Nine of these metabolites were found to be bioactive. Butyric acid, glycolic acid, D-mannitol, 2,3-butanediol, and trans-ferulic acid were shown to reduce cell proliferation, while 4-hydroxybenzoic acid, vanillic acid, and 3-hydroxyphenylacetic acid increased cell proliferation. Among these metabolites, 4-hydroxybenzoic acid, 2,3-butanediol, hydrocinnamic acid, and 3-hydroxyphenylacetic acid were found to significantly inhibit, while no metabolite increased EMT.

In conclusion, the study suggests that LCA can suppress key features of breast cancer cells, potentially exerting a control over carcinogenesis. Furthermore, the newly discovered bioactive metabolites may also have a similar effect. However, more extensive research is required to firmly establish the role of these metabolites in breast cancer.

8. Összefoglalás

A mikrobiom és a gazdaszervezet között kétirányú kapcsolat áll fenn. A baktériumok – melyek az emberi szervezet különböző testüregeiben élnek – számos metabolitot termelnek, melyek befolyásolhatják a gazdaszervezet metabolizmusát és energia háztartását. Külső és belső tényezők (étrend, személyes higiénia, genetika, életkor) által a gazdaszervezet is befolyásolja a mikrobiom összetételét és működését. Számos betegség, köztük az emlődaganat is összefüggésbe hozható a mikrobiom összetételében és működésében bekövetkező változásokkal.

A litokólsav (LCA), egy másodlagos epesav, melyet a baiH ORF-et kódoló baktériumok állítanak elő. Az LCA a véráram útján a test távoli pontjaiba is eljut, így az emlődaganat szövetekhez is. Kísérleteinkben az LCA gátolta a sejtosztódást és a kolóniaformálási kapacitást MCF7, 4T1 és SKBR3 sejtekben, valamint gátolta az epithelialis-mesenchymalis tranzíciót, a sejt energia-anyagcseréjét az oxidatív foszforiláció irányába változtatta, tehát anti-Warburg hatást mutatott a sejtkultúrákban. Az LCA gátolta a sejt migrációt és elősegítette a sejt-sejt és sejt-felszín kapcsolatokat. Primer tumorokban LCA hatására a tumor-infiltráló limfociták száma megnőtt. A kísérletek azt mutatják, hogy az LCA ezen hatásait a TGR5 receptoron keresztül fejti ki, mivel a receptor gátlásával vagy csendesítésével az LCA-indukált EMT és az EMT-re jellemző gének kifejeződése (pACC, ATP5G1, NDUFB5) gátolt.

A tanulmányban továbbá megvizsgáltuk az általunk válogatott bakteriális metabolit könyvtár tagjainak hatását. Ezeknek a bakteriális metabolitoknak ismert a fiziológiás szérum koncentrációja. A könyvtárból kilenc metabolit bizonyult bioaktívnak. A butirát, glikolát, D-mannitol, 2,3-butándiol és transz-ferulát csökkentette, míg a 4-hidroxibenzoát, vanilinsav, 3-hidroxiphenilacetát elősegítette a sejtproliferációt. A metabolitok közül a 4-hidroxibenzoát, 2,3-butándiol, hidrocinnamonsav és 3-hidroxifenilacetát szignifikánsan gátolta az EMT-t és nem találtunk olyan metabolitot, mely elősegítette volna.

Jelen disszertáció alapján az LCA gátolja az emlőtumoros sejtek főbb jellemzőit, potenciálisan befolyásolja a karcinogenezist. Továbbá, az újonnan felfedezett bioaktív metabolitoknak hasonló tulajdonságaik lehetnek. Azonban ez a terület további kutatásokat igényel, hogy igazoljuk ezeket a hatásokat.

9. Bibliography

[1] J.-T. Huang and Y.-Q. Mao, “The impact of the microbiome in cancer: Targeting metabolism of cancer cells and host,” *Front. Oncol.*, vol. 12, p. 1029033, Nov. 2022, doi: 10.3389/fonc.2022.1029033.

[2] A. Parker, S. Fonseca, and S. R. Carding, “Gut microbes and metabolites as modulators of blood-brain barrier integrity and brain health,” *Gut Microbes*, vol. 11, no. 2, pp. 135–157, Mar. 2020, doi: 10.1080/19490976.2019.1638722.

[3] D. S. Wishart *et al.*, “MiMeDB: the Human Microbial Metabolome Database,” *Nucleic Acids Research*, vol. 51, no. D1, pp. D611–D620, Jan. 2023, doi: 10.1093/nar/gkac868.

[4] J. Liu, Y. Tan, H. Cheng, D. Zhang, W. Feng, and C. Peng, “Functions of Gut Microbiota Metabolites, Current Status and Future Perspectives,” *Aging and disease*, vol. 13, no. 4, p. 1106, 2022, doi: 10.14336/AD.2022.0104.

[5] T. Kovács *et al.*, “Cadaverine, a metabolite of the microbiome, reduces breast cancer aggressiveness through trace amino acid receptors,” *Sci Rep*, vol. 9, no. 1, p. 1300, Feb. 2019, doi: 10.1038/s41598-018-37664-7.

[6] Z. Sári *et al.*, “Indoxylsulfate, a Metabolite of the Microbiome, Has Cytostatic Effects in Breast Cancer via Activation of AHR and PXR Receptors and Induction of Oxidative Stress,” *Cancers*, vol. 12, no. 10, p. 2915, Oct. 2020, doi: 10.3390/cancers12102915.

[7] Z. Sári *et al.*, “Indolepropionic Acid, a Metabolite of the Microbiome, Has Cytostatic Properties in Breast Cancer by Activating AHR and PXR Receptors and Inducing Oxidative Stress,” *Cancers*, vol. 12, no. 9, p. 2411, Aug. 2020, doi: 10.3390/cancers12092411.

[8] M. Thirunavukkarasan *et al.*, “Short-chain fatty acid receptors inhibit invasive phenotypes in breast cancer cells,” *PLoS ONE*, vol. 12, no. 10, p. e0186334, Oct. 2017, doi: 10.1371/journal.pone.0186334.

[9] T. Yonezawa, Y. Kobayashi, and Y. Obara, “Short-chain fatty acids induce acute phosphorylation of the p38 mitogen-activated protein kinase/heat shock protein 27 pathway via GPR43 in the MCF-7 human breast cancer cell line,” *Cellular Signalling*, vol. 19, no. 1, pp. 185–193, Jan. 2007, doi: 10.1016/j.cellsig.2006.06.004.

[10] T. Kovács *et al.*, “The involvement of oncobiosis and bacterial metabolite signaling in metastasis formation in breast cancer,” *Cancer Metastasis Rev*, vol. 40, no. 4, pp. 1223–1249, Dec. 2021, doi: 10.1007/s10555-021-10013-3.

[11] S. Kumari and R. R. Malla, “Recent advances in metabolomics of triple negative breast cancer,” *Breast J*, vol. 26, no. 3, pp. 498–501, Mar. 2020, doi: 10.1111/tbj.13524.

[12] E. Mikó *et al.*, “Microbiome—Microbial Metabolome—Cancer Cell Interactions in Breast Cancer—Familiar, but Unexplored,” *Cells*, vol. 8, no. 4, p. 293, Mar. 2019, doi: 10.3390/cells8040293.

[13] T. Wilmanski *et al.*, “Blood metabolome predicts gut microbiome α-diversity in humans,” *Nat Biotechnol*, vol. 37, no. 10, pp. 1217–1228, Oct. 2019, doi: 10.1038/s41587-019-0233-9.

[14] D. Hanahan and R. A. Weinberg, “Hallmarks of Cancer: The Next Generation,” *Cell*, vol. 144, no. 5, pp. 646–674, Mar. 2011, doi: 10.1016/j.cell.2011.02.013.

[15] “Magyar Nemzeti Rákregiszter.” [Online]. Available: https://onkol.hu/nemzeti-rakregiszter/

[16] C. E. DeSantis *et al.*, “Breast cancer statistics, 2019,” *CA A Cancer J Clin*, vol. 69, no. 6, pp. 438–451, Nov. 2019, doi: 10.3322/caac.21583.
[17] E. Senkus *et al.*, “Primary breast cancer: ESMO Clinical Practice Guidelines for diagnosis, treatment and follow-up,” *Annals of Oncology*, vol. 26, pp. v8–v30, Sep. 2015, doi: 10.1093/annonc/mdv298.
[18] R. Guo *et al.*, “The Function and Mechanism of Lipid Molecules and Their Roles in The Diagnosis and Prognosis of Breast Cancer,” *Molecules*, vol. 25, no. 20, p. 4864, Oct. 2020, doi: 10.3390/molecules25204864.
[19] “Breast Cancer Facts & Statistics 2023.” [Online]. Available: https://www.breastcancer.org/facts-statistics
[20] P. Baade, “Geographical Variation in Breast Cancer Outcomes,” *IJERPH*, vol. 14, no. 5, p. 523, May 2017, doi: 10.3390/ijerph14050523.
[21] “National Cancer Institute: Surveillance, Epidemiology and End Results Program - Cancer Stat Facts: Female Breast Cancer Subtypes.” [Online]. Available: https://seer.cancer.gov/statfacts/html/breast-subtypes.html
[22] “Global Cancer Observatory.” [Online]. Available: https://gco.iarc.fr/
[23] “Breast Cancer Risk - Cancer Research UK.” [Online]. Available: https://www.cancerresearchuk.org/health-professional/cancer-statistics/statistics-by-cancer-type/breast-cancer/risk-factors
[24] Y.-S. Sun *et al.*, “Risk Factors and Preventions of Breast Cancer,” *Int. J. Biol. Sci.*, vol. 13, no. 11, pp. 1387–1397, 2017, doi: 10.7150/ijbs.21635.
[25] P. Minicozzi *et al.*, “Comorbidities, age and period of diagnosis influence treatment and outcomes in early breast cancer: Comorbidities, treatments and outcomes in early breast cancer,” *Int. J. Cancer*, vol. 144, no. 9, pp. 2118–2127, May 2019, doi: 10.1002/ijc.31974.
[26] H. Oh *et al.*, “Breast cancer risk factors in relation to estrogen receptor, progesterone receptor, insulin-like growth factor-1 receptor, and Ki67 expression in normal breast tissue,” *npj Breast Cancer*, vol. 3, no. 1, p. 39, Oct. 2017, doi: 10.1038/s41523-017-0041-7.
[27] P. H. Tan *et al.*, “The 2019 World Health Organization classification of tumours of the breast,” *Histopathology*, vol. 77, no. 2, pp. 181–185, Aug. 2020, doi: 10.1111/his.14091.
[28] C. R. Eheman, K. M. Shaw, A. B. Ryerson, J. W. Miller, U. A. Ajani, and M. C. White, “The Changing Incidence of *In situ* and Invasive Ductal and Lobular Breast Carcinomas: United States, 1999-2004,” *Cancer Epidemiology, Biomarkers & Prevention*, vol. 18, no. 6, pp. 1763–1769, Jun. 2009, doi: 10.1158/1055-9965.EPI-08-1082.
[29] J. C. Trent, R. S. Benjamin, and V. Valero, “Primary soft tissue sarcoma of the breast,” *Curr. Treat. Options in Oncol.*, vol. 2, no. 2, pp. 169–176, Apr. 2001, doi: 10.1007/s11864-001-0059-8.
[30] H. Schatten, Ed., *Cell and Molecular Biology of Breast Cancer*. Totowa, NJ: Humana Press, 2013. doi: 10.1007/978-1-62703-634-4.
[31] B. O’Sullivan *et al.*, “The TNM classification of malignant tumours—towards common understanding and reasonable expectations,” *The Lancet Oncology*, vol. 18, no. 7, pp. 849–851, Jul. 2017, doi: 10.1016/S1470-2045(17)30438-2.
[32] G. Cserni, E. Chmielik, B. Cserni, and T. Tot, “The new TNM-based staging of breast cancer,” *Virchows Arch*, vol. 472, no. 5, pp. 697–703, May 2018, doi: 10.1007/s00428-018-2301-9.

[33] L. Madaras *et al.*, “Clinicopathological Features and Prognosis of Pregnancy Associated Breast Cancer – A Matched Case Control Study,” *Pathol. Oncol. Res.*, vol. 20, no. 3, pp. 581–590, Jul. 2014, doi: 10.1007/s12253-013-9735-9.
[34] C. Sotiriou and L. Pusztai, “Gene-Expression Signatures in Breast Cancer,” *N Engl J Med*, vol. 360, no. 8, pp. 790–800, Feb. 2009, doi: 10.1056/NEJMra0801289.
[35] H.-P. Sinn and H. Kreipe, “A Brief Overview of the WHO Classification of Breast Tumors, 4th Edition, Focusing on Issues and Updates from the 3rd Edition,” *Breast Care*, vol. 8, no. 2, pp. 149–154, 2013, doi: 10.1159/000350774.
[36] D. Hanahan, “Hallmarks of Cancer: New Dimensions,” *Cancer Discovery*, vol. 12, no. 1, pp. 31–46, Jan. 2022, doi: 10.1158/2159-8290.CD-21-1059.
[37] W. Clark, “Tumour progression and the nature of cancer,” *Br J Cancer*, vol. 64, no. 4, pp. 631–644, Oct. 1991, doi: 10.1038/bjc.1991.375.
[38] J. N. Rich, “Cancer stem cells: understanding tumor hierarchy and heterogeneity,” *Medicine*, vol. 95, no. 1S, pp. S2–S7, Sep. 2016, doi: 10.1097/MD.0000000000004764.
[39] M. Al-Hajj, M. S. Wicha, A. Benito-Hernandez, S. J. Morrison, and M. F. Clarke, “Prospective identification of tumorigenic breast cancer cells,” *Proc. Natl. Acad. Sci. U.S.A.*, vol. 100, no. 7, pp. 3983–3988, Apr. 2003, doi: 10.1073/pnas.0530291100.
[40] E. Buck *et al.*, “Loss of homotypic cell adhesion by epithelial-mesenchymal transition or mutation limits sensitivity to epidermal growth factor receptor inhibition,” *Molecular Cancer Therapeutics*, vol. 6, no. 2, pp. 532–541, Feb. 2007, doi: 10.1158/1535-7163.MCT-06-0462.
[41] C. J. Creighton *et al.*, “Residual breast cancers after conventional therapy display mesenchymal as well as tumor-initiating features,” *Proc. Natl. Acad. Sci. U.S.A.*, vol. 106, no. 33, pp. 13820–13825, Aug. 2009, doi: 10.1073/pnas.0905718106.
[42] T. Reya, S. J. Morrison, M. F. Clarke, and I. L. Weissman, “Stem cells, cancer, and cancer stem cells,” *Nature*, vol. 414, no. 6859, pp. 105–111, Nov. 2001, doi: 10.1038/35102167.
[43] A. Singh and J. Settleman, “EMT, cancer stem cells and drug resistance: an emerging axis of evil in the war on cancer,” *Oncogene*, vol. 29, no. 34, pp. 4741–4751, Aug. 2010, doi: 10.1038/onc.2010.215.
[44] R. Sato, T. Semba, H. Saya, and Y. Arima, “Concise Review: Stem Cells and Epithelial-Mesenchymal Transition in Cancer: Biological Implications and Therapeutic Targets,” *Stem Cells*, vol. 34, no. 8, pp. 1997–2007, Aug. 2016, doi: 10.1002/stem.2406.
[45] K. M. Bussard, L. Mutkus, K. Stumpf, C. Gomez-Manzano, and F. C. Marini, “Tumor-associated stromal cells as key contributors to the tumor microenvironment,” *Breast Cancer Res*, vol. 18, no. 1, p. 84, Dec. 2016, doi: 10.1186/s13058-016-0740-2.
[46] R. Baghban *et al.*, “Tumor microenvironment complexity and therapeutic implications at a glance,” *Cell Commun Signal*, vol. 18, no. 1, p. 59, Dec. 2020, doi: 10.1186/s12964-020-0530-4.
[47] A. Orimo *et al.*, “Stromal Fibroblasts Present in Invasive Human Breast Carcinomas Promote Tumor Growth and Angiogenesis through Elevated SDF-1/CXCL12 Secretion,” *Cell*, vol. 121, no. 3, pp. 335–348, May 2005, doi: 10.1016/j.cell.2005.02.034.
[48] Y. Fu *et al.*, “The reverse Warburg effect is likely to be an Achilles’ heel of cancer that can be exploited for cancer therapy,” *Oncotarget*, vol. 8, no. 34, pp. 57813–57825, Aug. 2017, doi: 10.18632/oncotarget.18175.

[49] M. Kloc, J. Z. Kubiak, X. C. Li, and R. M. Ghobrial, "Pericytes, Microvasular Dysfunction, and Chronic Rejection," *Transplantation*, vol. 99, no. 4, pp. 658–667, Apr. 2015, doi: 10.1097/TP.0000000000000648.
[50] P. Baluk, S. Morikawa, A. Haskell, M. Mancuso, and D. M. McDonald, "Abnormalities of Basement Membrane on Blood Vessels and Endothelial Sprouts in Tumors," *The American Journal of Pathology*, vol. 163, no. 5, pp. 1801–1815, Nov. 2003, doi: 10.1016/S0002-9440(10)63540-7.
[51] H. F. Dvorak, "Tumors: Wounds That Do Not Heal—Redux," *Cancer Immunology Research*, vol. 3, no. 1, pp. 1–11, Jan. 2015, doi: 10.1158/2326-6066.CIR-14-0209.
[52] E. Uribe-Querol and C. Rosales, "Neutrophils in Cancer: Two Sides of the Same Coin," *Journal of Immunology Research*, vol. 2015, pp. 1–21, 2015, doi: 10.1155/2015/983698.
[53] G. J. Yuen, E. Demissie, and S. Pillai, "B Lymphocytes and Cancer: A Love–Hate Relationship," *Trends in Cancer*, vol. 2, no. 12, pp. 747–757, Dec. 2016, doi: 10.1016/j.trecan.2016.10.010.
[54] C. Murdoch, M. Muthana, S. B. Coffelt, and C. E. Lewis, "The role of myeloid cells in the promotion of tumour angiogenesis," *Nat Rev Cancer*, vol. 8, no. 8, pp. 618–631, Aug. 2008, doi: 10.1038/nrc2444.
[55] Y. Mao, Q. Qu, X. Chen, O. Huang, J. Wu, and K. Shen, "The Prognostic Value of Tumor-Infiltrating Lymphocytes in Breast Cancer: A Systematic Review and Meta-Analysis," *PLoS ONE*, vol. 11, no. 4, p. e0152500, Apr. 2016, doi: 10.1371/journal.pone.0152500.
[56] Y. Yuan, Y.-C. Jiang, C.-K. Sun, and Q.-M. Chen, "Role of the tumor microenvironment in tumor progression and the clinical applications (Review)," *Oncology Reports*, vol. 35, no. 5, pp. 2499–2515, May 2016, doi: 10.3892/or.2016.4660.
[57] M. L. Uribe, I. Marrocco, and Y. Yarden, "EGFR in Cancer: Signaling Mechanisms, Drugs, and Acquired Resistance," *Cancers*, vol. 13, no. 11, p. 2748, Jun. 2021, doi: 10.3390/cancers13112748.
[58] M. P. Barr *et al.*, "Vascular endothelial growth factor is an autocrine growth factor, signaling through neuropilin-1 in non-small cell lung cancer," *Mol Cancer*, vol. 14, no. 1, p. 45, Dec. 2015, doi: 10.1186/s12943-015-0310-8.
[59] H. K. Matthews, C. Bertoli, and R. A. M. De Bruin, "Cell cycle control in cancer," *Nat Rev Mol Cell Biol*, vol. 23, no. 1, pp. 74–88, Jan. 2022, doi: 10.1038/s41580-021-00404-3.
[60] L. Santarpia, S. M. Lippman, and A. K. El-Naggar, "Targeting the MAPK–RAS–RAF signaling pathway in cancer therapy," *Expert Opinion on Therapeutic Targets*, vol. 16, no. 1, pp. 103–119, Jan. 2012, doi: 10.1517/14728222.2011.645805.
[61] T. L. Yuan and L. C. Cantley, "PI3K pathway alterations in cancer: variations on a theme," *Oncogene*, vol. 27, no. 41, pp. 5497–5510, Sep. 2008, doi: 10.1038/onc.2008.245.
[62] H. Pópulo, J. M. Lopes, and P. Soares, "The mTOR Signalling Pathway in Human Cancer," *IJMS*, vol. 13, no. 2, pp. 1886–1918, Feb. 2012, doi: 10.3390/ijms13021886.
[63] A. Gomez-Pinillos and A. C. Ferrari, "mTOR Signaling Pathway and mTOR Inhibitors in Cancer Therapy," *Hematology/Oncology Clinics of North America*, vol. 26, no. 3, pp. 483–505, Jun. 2012, doi: 10.1016/j.hoc.2012.02.014.
[64] C. Kandoth *et al.*, "Mutational landscape and significance across 12 major cancer types," *Nature*, vol. 502, no. 7471, pp. 333–339, Oct. 2013, doi: 10.1038/nature12634.
[65] A. R. M. R. Amin *et al.*, "Evasion of anti-growth signaling: A key step in tumorigenesis and potential target for treatment and prophylaxis by natural compounds," *Seminars in Cancer Biology*, vol. 35, pp. S55–S77, Dec. 2015, doi: 10.1016/j.semcancer.2015.02.005.

[66] T. Kohno, “How many tumor suppressor genes are involved in human lung carcinogenesis?,” *Carcinogenesis*, vol. 20, no. 8, pp. 1403–1410, Aug. 1999, doi: 10.1093/carcin/20.8.1403.
[67] Y. Lecarpentier, O. Schussler, J.-L. Hébert, and A. Vallée, “Multiple Targets of the Canonical WNT/β-Catenin Signaling in Cancers,” *Front. Oncol.*, vol. 9, p. 1248, Nov. 2019, doi: 10.3389/fonc.2019.01248.
[68] M. A. Feitelson *et al.*, “Sustained proliferation in cancer: Mechanisms and novel therapeutic targets,” *Seminars in Cancer Biology*, vol. 35, pp. S25–S54, Dec. 2015, doi: 10.1016/j.semcancer.2015.02.006.
[69] H. Acloque, J. P. Thiery, and M. A. Nieto, “The physiology and pathology of the EMT: Meeting on the Epithelial–Mesenchymal Transition,” *EMBO Reports*, vol. 9, no. 4, pp. 322–326, Apr. 2008.
[70] X. Lai *et al.*, “Epithelial-Mesenchymal Transition and Metabolic Switching in Cancer: Lessons From Somatic Cell Reprogramming,” *Front. Cell Dev. Biol.*, vol. 8, p. 760, Aug. 2020, doi: 10.3389/fcell.2020.00760.
[71] S. B. Harosh-Davidovich and I. Khalaila, “O -GlcNAcylation affects β-catenin and E-cadherin expression, cell motility and tumorigenicity of colorectal cancer,” *Experimental Cell Research*, vol. 364, no. 1, pp. 42–49, Mar. 2018, doi: 10.1016/j.yexcr.2018.01.024.
[72] H. Yuksel, M. Ocalan, and O. Yilmaz, “E-Cadherin: An Important Functional Molecule at Respiratory Barrier Between Defence and Dysfunction,” *Front. Physiol.*, vol. 12, p. 720227, Oct. 2021, doi: 10.3389/fphys.2021.720227.
[73] B. E. Sundström and T. I. Stigbrand, “Cytokeratins and Tissue Polypeptide Antigen,” *Int J Biol Markers*, vol. 9, no. 2, pp. 102–108, Apr. 1994, doi: 10.1177/172460089400900207.
[74] G. L. Radice, “N-Cadherin-Mediated Adhesion and Signaling from Development to Disease,” in *Progress in Molecular Biology and Translational Science*, vol. 116, Elsevier, 2013, pp. 263–289. doi: 10.1016/B978-0-12-394311-8.00012-1.
[75] D. Paulin, A. Lilienbaum, S. Kardjian, O. Agbulut, and Z. Li, “Vimentin: Regulation and pathogenesis,” *Biochimie*, vol. 197, pp. 96–112, Jun. 2022, doi: 10.1016/j.biochi.2022.02.003.
[76] N. Nishida, H. Yano, T. Nishida, T. Kamura, and M. Kojiro, “Angiogenesis in cancer,” *Vascular Health and Risk Management*, vol. 2, no. 3, pp. 213–219, Aug. 2006, doi: 10.2147/vhrm.2006.2.3.213.
[77] R. Lugano, M. Ramachandran, and A. Dimberg, “Tumor angiogenesis: causes, consequences, challenges and opportunities,” *Cell. Mol. Life Sci.*, vol. 77, no. 9, pp. 1745–1770, May 2020, doi: 10.1007/s00018-019-03351-7.
[78] B. R. Zetter, “Angiogenesis and Tumor Metastasis,” *Annu. Rev. Med.*, vol. 49, no. 1, pp. 407–424, Feb. 1998, doi: 10.1146/annurev.med.49.1.407.
[79] B. L. Krock, N. Skuli, and M. C. Simon, “Hypoxia-Induced Angiogenesis: Good and Evil,” *Genes & Cancer*, vol. 2, no. 12, pp. 1117–1133, Dec. 2011, doi: 10.1177/1947601911423654.
[80] M. V. Liberti and J. W. Locasale, “The Warburg Effect: How Does it Benefit Cancer Cells?,” *Trends in Biochemical Sciences*, vol. 41, no. 3, pp. 211–218, Mar. 2016, doi: 10.1016/j.tibs.2015.12.001.
[81] K. O. Alfarouk *et al.*, “Glycolysis, tumor metabolism, cancer growth and dissemination. A new pH-based etiopathogenic perspective and therapeutic approach to an old cancer

question," *Oncoscience*, vol. 1, no. 12, pp. 777–802, Dec. 2014, doi: 10.18632/oncoscience.109.
[82] J. Chen *et al.*, "Warburg Effect Is a Cancer Immune Evasion Mechanism Against Macrophage Immunosurveillance," *Front. Immunol.*, vol. 11, p. 621757, Feb. 2021, doi: 10.3389/fimmu.2020.621757.
[83] S. Bose, C. Zhang, and A. Le, "Glucose Metabolism in Cancer: The Warburg Effect and Beyond," in *The Heterogeneity of Cancer Metabolism*, vol. 1311, A. Le, Ed., in Advances in Experimental Medicine and Biology, vol. 1311. , Cham: Springer International Publishing, 2021, pp. 3–15. doi: 10.1007/978-3-030-65768-0_1.
[84] C. S. Ahn and C. M. Metallo, "Mitochondria as biosynthetic factories for cancer proliferation," *Cancer Metab*, vol. 3, no. 1, p. 1, Dec. 2015, doi: 10.1186/s40170-015-0128-2.
[85] J. E. Unterlass and N. J. Curtin, "Warburg and Krebs and related effects in cancer," *Expert Rev. Mol. Med.*, vol. 21, p. e4, 2019, doi: 10.1017/erm.2019.4.
[86] P. Gao *et al.*, "c-Myc suppression of miR-23a/b enhances mitochondrial glutaminase expression and glutamine metabolism," *Nature*, vol. 458, no. 7239, pp. 762–765, Apr. 2009, doi: 10.1038/nature07823.
[87] I. Marin-Valencia *et al.*, "Analysis of Tumor Metabolism Reveals Mitochondrial Glucose Oxidation in Genetically Diverse Human Glioblastomas in the Mouse Brain In Vivo," *Cell Metabolism*, vol. 15, no. 6, pp. 827–837, Jun. 2012, doi: 10.1016/j.cmet.2012.05.001.
[88] H.-N. Kung, J. R. Marks, and J.-T. Chi, "Glutamine Synthetase Is a Genetic Determinant of Cell Type–Specific Glutamine Independence in Breast Epithelia," *PLoS Genet*, vol. 7, no. 8, p. e1002229, Aug. 2011, doi: 10.1371/journal.pgen.1002229.
[89] Y. Liu, G. L. Borchert, S. P. Donald, B. A. Diwan, M. Anver, and J. M. Phang, "Proline Oxidase Functions as a Mitochondrial Tumor Suppressor in Human Cancers," *Cancer Research*, vol. 69, no. 16, pp. 6414–6422, Aug. 2009, doi: 10.1158/0008-5472.CAN-09-1223.
[90] J. Son *et al.*, "Glutamine supports pancreatic cancer growth through a KRAS-regulated metabolic pathway," *Nature*, vol. 496, no. 7443, pp. 101–105, Apr. 2013, doi: 10.1038/nature12040.
[91] F. Weinberg *et al.*, "Mitochondrial metabolism and ROS generation are essential for Kras-mediated tumorigenicity," *Proc. Natl. Acad. Sci. U.S.A.*, vol. 107, no. 19, pp. 8788–8793, May 2010, doi: 10.1073/pnas.1003428107.
[92] A. A. Khutornenko, V. V. Roudko, B. V. Chernyak, A. B. Vartapetian, P. M. Chumakov, and A. G. Evstafieva, "Pyrimidine biosynthesis links mitochondrial respiration to the p53 pathway," *Proc. Natl. Acad. Sci. U.S.A.*, vol. 107, no. 29, pp. 12828–12833, Jul. 2010, doi: 10.1073/pnas.0910885107.
[93] R. El Ansari, A. McIntyre, M. L. Craze, I. O. Ellis, E. A. Rakha, and A. R. Green, "Altered glutamine metabolism in breast cancer; subtype dependencies and alternative adaptations," *Histopathology*, vol. 72, no. 2, pp. 183–190, Jan. 2018, doi: 10.1111/his.13334.
[94] C.-C. Chen *et al.*, "FoxOs Inhibit mTORC1 and Activate Akt by Inducing the Expression of Sestrin3 and Rictor," *Developmental Cell*, vol. 18, no. 4, pp. 592–604, Apr. 2010, doi: 10.1016/j.devcel.2010.03.008.
[95] S. M. Hadad *et al.*, "Histological evaluation of AMPK signalling in primary breast cancer," *BMC Cancer*, vol. 9, no. 1, p. 307, Dec. 2009, doi: 10.1186/1471-2407-9-307.

[96] N. Hay, “Interplay between FOXO, TOR, and Akt,” *Biochimica et Biophysica Acta (BBA) - Molecular Cell Research*, vol. 1813, no. 11, pp. 1965–1970, Nov. 2011, doi: 10.1016/j.bbamcr.2011.03.013.
[97] R. K. Yadav, A. S. Chauhan, L. Zhuang, and B. Gan, “FoxO transcription factors in cancer metabolism,” *Seminars in Cancer Biology*, vol. 50, pp. 65–76, Jun. 2018, doi: 10.1016/j.semcancer.2018.01.004.
[98] B. Faubert *et al.*, “AMPK Is a Negative Regulator of the Warburg Effect and Suppresses Tumor Growth In Vivo,” *Cell Metabolism*, vol. 17, no. 1, pp. 113–124, Jan. 2013, doi: 10.1016/j.cmet.2012.12.001.
[99] S. Herzig and R. J. Shaw, “AMPK: guardian of metabolism and mitochondrial homeostasis,” *Nat Rev Mol Cell Biol*, vol. 19, no. 2, pp. 121–135, Feb. 2018, doi: 10.1038/nrm.2017.95.
[100] X. Song, S. Rahimnejad, W. Zhou, L. Cai, and K. Lu, “Molecular Characterization of Peroxisome Proliferator-Activated Receptor-Gamma Coactivator-1α (PGC1α) and Its Role in Mitochondrial Biogenesis in Blunt Snout Bream (Megalobrama amblycephala),” *Front. Physiol.*, vol. 9, p. 1957, Jan. 2019, doi: 10.3389/fphys.2018.01957.
[101] A. P. Gureev, E. A. Shaforostova, and V. N. Popov, “Regulation of Mitochondrial Biogenesis as a Way for Active Longevity: Interaction Between the Nrf2 and PGC-1α Signaling Pathways,” *Front. Genet.*, vol. 10, p. 435, May 2019, doi: 10.3389/fgene.2019.00435.
[102] T. Fodor *et al.*, “Combined Treatment of MCF-7 Cells with AICAR and Methotrexate, Arrests Cell Cycle and Reverses Warburg Metabolism through AMP-Activated Protein Kinase (AMPK) and FOXO1,” *PLoS ONE*, vol. 11, no. 2, p. e0150232, Feb. 2016, doi: 10.1371/journal.pone.0150232.
[103] H. D. Soule, J. Vazquez, A. Long, S. Albert, and M. Brennan, “A Human Cell Line From a Pleural Effusion Derived From a Breast Carcinoma 2,” *JNCI: Journal of the National Cancer Institute*, vol. 51, no. 5, pp. 1409–1416, Nov. 1973, doi: 10.1093/jnci/51.5.1409.
[104] Ş. Comşa, A. M. Cîmpean, and M. Raica, “The Story of MCF-7 Breast Cancer Cell Line: 40 years of Experience in Research,” *Anticancer Res*, vol. 35, no. 6, pp. 3147–3154, Jun. 2015.
[105] E. Orrantia-Borunda, P. Anchondo-Nuñez, L. E. Acuña-Aguilar, F. O. Gómez-Valles, and C. A. Ramírez-Valdespino, “Subtypes of Breast Cancer,” in *Breast Cancer*, Department of Medical Education, Dr. Kiran C. Patel College of Allopathic Medicine, Nova Southeastern University, FL, USA and H. N. Mayrovitz, Eds., Exon Publications, 2022, pp. 31–42. doi: 10.36255/exon-publications-breast-cancer-subtypes.
[106] B. L. Jensen, J. Skouv, B. K. Lundholt, and A. E. Lykkesfeldt, “Differential regulation of specific genes in MCF-7 and the ICI 182780-resistant cell line MCF-7/182R-6,” *Br J Cancer*, vol. 79, no. 3–4, pp. 386–392, Feb. 1999, doi: 10.1038/sj.bjc.6690061.
[107] E. E. Sweeney, R. E. McDaniel, P. Y. Maximov, P. Fan, and V. C. Jordan, “Models and mechanisms of acquired antihormone resistance in breast cancer: significant clinical progress despite limitations,” *Hormone Molecular Biology and Clinical Investigation*, vol. 9, no. 2, pp. 143–163, Apr. 2012, doi: 10.1515/hmbci-2011-0004.
[108] B. A. Pulaski and S. Ostrand-Rosenberg, “Mouse 4T1 Breast Tumor Model,” *CP in Immunology*, vol. 39, no. 1, Oct. 2000, doi: 10.1002/0471142735.im2002s39.
[109] B. Schrörs *et al.*, “Multi-Omics Characterization of the 4T1 Murine Mammary Gland Tumor Model,” *Front. Oncol.*, vol. 10, p. 1195, Jul. 2020, doi: 10.3389/fonc.2020.01195.

[110] School of Health Sciences, Universiti Sains Malaysia, Kelantan, Malaysia *et al.*, "Passage Number of 4T1 Cells Influences the Development of Tumour and the Progression of Metastasis in 4T1 Orthotopic Mice," *MJMS*, vol. 29, no. 3, pp. 30–42, Jun. 2022, doi: 10.21315/mjms2022.29.3.4.
[111] C. Garcia, M. R. Araújo, M. Lopes, M. D. Ferreira, and G. Cassali, "Morphological and Immunophenotipical Characterization of Murine Mammary Carcinoma 4t1".
[112] R. V. Simões *et al.*, "Metabolic Plasticity of Metastatic Breast Cancer Cells: Adaptation to Changes in the Microenvironment," *Neoplasia*, vol. 17, no. 8, pp. 671–684, Aug. 2015, doi: 10.1016/j.neo.2015.08.005.
[113] A. Vida, B. L. Bodrogi, B. Balogh, and P. Bai, "Taxamat: Automated biodiversity data management tool – Implications for microbiome studies," *Physiol. Int.*, vol. 107, no. 1, pp. 12–17, Mar. 2020, doi: 10.1556/2060.2020.00004.
[114] A. B. Hall, A. C. Tolonen, and R. J. Xavier, "Human genetic variation and the gut microbiome in disease," *Nat Rev Genet*, vol. 18, no. 11, pp. 690–699, Nov. 2017, doi: 10.1038/nrg.2017.63.
[115] T. Hrncir, "Gut Microbiota Dysbiosis: Triggers, Consequences, Diagnostic and Therapeutic Options," *Microorganisms*, vol. 10, no. 3, p. 578, Mar. 2022, doi: 10.3390/microorganisms10030578.
[116] S. W. Ruo *et al.*, "Role of Gut Microbiota Dysbiosis in Breast Cancer and Novel Approaches in Prevention, Diagnosis, and Treatment," *Cureus*, Aug. 2021, doi: 10.7759/cureus.17472.
[117] R. M. Thomas and C. Jobin, "The Microbiome and Cancer: Is the 'Oncobiome' Mirage Real?," *Trends in Cancer*, vol. 1, no. 1, pp. 24–35, Sep. 2015, doi: 10.1016/j.trecan.2015.07.005.
[118] A. A. Chan *et al.*, "Characterization of the microbiome of nipple aspirate fluid of breast cancer survivors," *Sci Rep*, vol. 6, no. 1, p. 28061, Jun. 2016, doi: 10.1038/srep28061.
[119] G. Hogan *et al.*, "Biopsy bacterial signature can predict patient tissue malignancy," *Sci Rep*, vol. 11, no. 1, p. 18535, Sep. 2021, doi: 10.1038/s41598-021-98089-3.
[120] S. Banerjee *et al.*, "Prognostic correlations with the microbiome of breast cancer subtypes," *Cell Death Dis*, vol. 12, no. 9, p. 831, Sep. 2021, doi: 10.1038/s41419-021-04092-x.
[121] R. Rao Malla, R. Marni, S. Kumari, A. Chakraborty, and P. Lalitha, "Microbiome Assisted Tumor Microenvironment: Emerging Target of Breast Cancer," *Clinical Breast Cancer*, vol. 22, no. 3, pp. 200–211, Apr. 2022, doi: 10.1016/j.clbc.2021.09.002.
[122] G. S. Jones *et al.*, "Mammographic breast density and its association with urinary estrogens and the fecal microbiota in postmenopausal women," *PLoS ONE*, vol. 14, no. 5, p. e0216114, May 2019, doi: 10.1371/journal.pone.0216114.
[123] A. H. Wu *et al.*, "Gut microbiome associations with breast cancer risk factors and tumor characteristics: a pilot study," *Breast Cancer Res Treat*, vol. 182, no. 2, pp. 451–463, Jul. 2020, doi: 10.1007/s10549-020-05702-6.
[124] A. D. Frugé, W. Van Der Pol, L. Q. Rogers, C. D. Morrow, Y. Tsuruta, and W. Demark-Wahnefried, "Fecal Akkermansia muciniphila Is Associated with Body Composition and Microbiota Diversity in Overweight and Obese Women with Breast Cancer Participating in a Presurgical Weight Loss Trial," *Journal of the Academy of Nutrition and Dietetics*, vol. 120, no. 4, pp. 650–659, Apr. 2020, doi: 10.1016/j.jand.2018.08.164.
[125] M. Dabek, S. I. McCrae, V. J. Stevens, S. H. Duncan, and P. Louis, "Distribution of Î²-glucosidase and Î²-glucuronidase activity and of Î²-glucuronidase gene gus in human

colonic bacteria: Î²-Glycosidase activity in human gut bacteria," *FEMS Microbiology Ecology*, vol. 66, no. 3, pp. 487–495, Dec. 2008, doi: 10.1111/j.1574-6941.2008.00520.x.
[126] K. Gloux, O. Berteau, H. El Oumami, F. Béguet, M. Leclerc, and J. Doré, "A metagenomic β-glucuronidase uncovers a core adaptive function of the human intestinal microbiome," *Proc. Natl. Acad. Sci. U.S.A.*, vol. 108, no. supplement_1, pp. 4539–4546, Mar. 2011, doi: 10.1073/pnas.1000066107.
[127] F. M. McIntosh *et al.*, "Phylogenetic distribution of genes encoding β-glucuronidase activity in human colonic bacteria and the impact of diet on faecal glycosidase activities: β-glucuronidase genes in human colonic bacteria," *Environmental Microbiology*, vol. 14, no. 8, pp. 1876–1887, Aug. 2012, doi: 10.1111/j.1462-2920.2012.02711.x.
[128] "The Intestinal Microbiome and Estrogen Receptor–Positive Female Breast Cancer," *JNCI: Journal of the National Cancer Institute*, Apr. 2016, doi: 10.1093/jnci/djw029.
[129] T. Režen *et al.*, "The role of bile acids in carcinogenesis," *Cell. Mol. Life Sci.*, vol. 79, no. 5, p. 243, May 2022, doi: 10.1007/s00018-022-04278-2.
[130] D. Kesavelu and P. Jog, "Current understanding of antibiotic-associated dysbiosis and approaches for its management," *Therapeutic Advances in Infection*, vol. 10, p. 204993612311544, Jan. 2023, doi: 10.1177/20499361231154443.
[131] L. Chen *et al.*, "Influence of the microbiome, diet and genetics on inter-individual variation in the human plasma metabolome," *Nat Med*, vol. 28, no. 11, pp. 2333–2343, Nov. 2022, doi: 10.1038/s41591-022-02014-8.
[132] M. Million and D. Raoult, "Linking gut redox to human microbiome," *Human Microbiome Journal*, vol. 10, pp. 27–32, Dec. 2018, doi: 10.1016/j.humic.2018.07.002.
[133] S. Yonekura *et al.*, "Cancer Induces a Stress Ileopathy Depending on β-Adrenergic Receptors and Promoting Dysbiosis that Contributes to Carcinogenesis," *Cancer Discovery*, vol. 12, no. 4, pp. 1128–1151, Apr. 2022, doi: 10.1158/2159-8290.CD-21-0999.
[134] J. Y. L. Chiang, "Bile Acid Metabolism and Signaling," in *Comprehensive Physiology*, 1st ed., R. Terjung, Ed., Wiley, 2013, pp. 1191–1212. doi: 10.1002/cphy.c120023.
[135] K. L. Mertens, A. Kalsbeek, M. R. Soeters, and H. M. Eggink, "Bile Acid Signaling Pathways from the Enterohepatic Circulation to the Central Nervous System," *Front. Neurosci.*, vol. 11, p. 617, Nov. 2017, doi: 10.3389/fnins.2017.00617.
[136] H. Zeng, S. Umar, B. Rust, D. Lazarova, and M. Bordonaro, "Secondary Bile Acids and Short Chain Fatty Acids in the Colon: A Focus on Colonic Microbiome, Cell Proliferation, Inflammation, and Cancer," *IJMS*, vol. 20, no. 5, p. 1214, Mar. 2019, doi: 10.3390/ijms20051214.
[137] H. Liu, "Ursodeoxycholic acid induces apoptosis in hepatocellular carcinoma xenografts in mice," *WJG*, vol. 21, no. 36, p. 10367, 2015, doi: 10.3748/wjg.v21.i36.10367.
[138] A. B. Larabi, H. L. P. Masson, and A. J. Bäumler, "Bile acids as modulators of gut microbiota composition and function," *Gut Microbes*, vol. 15, no. 1, p. 2172671, Dec. 2023, doi: 10.1080/19490976.2023.2172671.
[139] M. B. Miller and B. L. Bassler, "Quorum Sensing in Bacteria," *Annu. Rev. Microbiol.*, vol. 55, no. 1, pp. 165–199, Oct. 2001, doi: 10.1146/annurev.micro.55.1.165.
[140] J. M. Ridlon, D.-J. Kang, and P. B. Hylemon, "Bile salt biotransformations by human intestinal bacteria," *Journal of Lipid Research*, vol. 47, no. 2, pp. 241–259, Feb. 2006, doi: 10.1194/jlr.R500013-JLR200.

[141] U. Raju, M. Levitz, and N. B. Javitt, “Bile Acids in Human Breast Cyst Fluid: The Identification of Lithocholic Acid*,” *The Journal of Clinical Endocrinology & Metabolism*, vol. 70, no. 4, pp. 1030–1034, Apr. 1990, doi: 10.1210/jcem-70-4-1030.
[142] J. L. Smith *et al.*, “Endogenous ursodeoxycholic acid and cholic acid in liver disease due to cystic fibrosis,” *Hepatology*, vol. 39, no. 6, pp. 1673–1682, Jun. 2004, doi: 10.1002/hep.20238.
[143] K. Fukushima, “Neocognitron: A self-organizing neural network model for a mechanism of pattern recognition unaffected by shift in position,” *Biol. Cybernetics*, vol. 36, no. 4, pp. 193–202, Apr. 1980, doi: 10.1007/BF00344251.
[144] Y. Lecun, L. Bottou, Y. Bengio, and P. Haffner, “Gradient-based learning applied to document recognition,” *Proc. IEEE*, vol. 86, no. 11, pp. 2278–2324, Nov. 1998, doi: 10.1109/5.726791.
[145] Y. LeCun, Y. Bengio, and G. Hinton, “Deep learning,” *Nature*, vol. 521, no. 7553, pp. 436–444, May 2015, doi: 10.1038/nature14539.
[146] D. Eigen, J. Rolfe, R. Fergus, and Y. LeCun, “Understanding Deep Architectures using a Recursive Convolutional Network,” 2013, doi: 10.48550/ARXIV.1312.1847.
[147] K. Simonyan and A. Zisserman, “Very Deep Convolutional Networks for Large-Scale Image Recognition,” 2014, doi: 10.48550/ARXIV.1409.1556.
[148] C. Szegedy *et al.*, “Going Deeper with Convolutions,” 2014, doi: 10.48550/ARXIV.1409.4842.
[149] M. D. Zeiler and R. Fergus, “Visualizing and Understanding Convolutional Networks,” 2013, doi: 10.48550/ARXIV.1311.2901.
[150] D. Erhan, P.-A. Manzagol, Y. Bengio, S. Bengio, and P. Vincent, “The Difficulty of Training Deep Architectures and the Effect of Unsupervised Pre-Training,” *Twelfth International Conference on Artificial Intelligence and Statistics (AISTATS)*, vol. MLR Workshop and Conference Procedings (2009), pp. 153–160.
[151] H. Azizpour, A. S. Razavian, J. Sullivan, A. Maki, and S. Carlsson, “From generic to specific deep representations for visual recognition,” in *2015 IEEE Conference on Computer Vision and Pattern Recognition Workshops (CVPRW)*, Boston, MA, USA: IEEE, Jun. 2015, pp. 36–45. doi: 10.1109/CVPRW.2015.7301270.
[152] O. A. B. Penatti, K. Nogueira, and J. A. Dos Santos, “Do deep features generalize from everyday objects to remote sensing and aerial scenes domains?,” in *2015 IEEE Conference on Computer Vision and Pattern Recognition Workshops (CVPRW)*, Boston, MA, USA: IEEE, Jun. 2015, pp. 44–51. doi: 10.1109/CVPRW.2015.7301382.
[153] A. S. Razavian, H. Azizpour, J. Sullivan, and S. Carlsson, “CNN Features off-the-shelf: an Astounding Baseline for Recognition,” 2014, doi: 10.48550/ARXIV.1403.6382.
[154] J. Arevalo, F. A. Gonzalez, R. Ramos-Pollan, J. L. Oliveira, and M. A. Guevara Lopez, “Convolutional neural networks for mammography mass lesion classification,” in *2015 37th Annual International Conference of the IEEE Engineering in Medicine and Biology Society (EMBC)*, Milan: IEEE, Aug. 2015, pp. 797–800. doi: 10.1109/EMBC.2015.7318482.
[155] Y. Bar, I. Diamant, L. Wolf, and H. Greenspan, “Deep learning with non-medical training used for chest pathology identification,” presented at the SPIE Medical Imaging, L. M. Hadjiiski and G. D. Tourassi, Eds., Orlando, Florida, United States, Mar. 2015, p. 94140V. doi: 10.1117/12.2083124.

[156] B. Van Ginneken, A. A. A. Setio, C. Jacobs, and F. Ciompi, “Off-the-shelf convolutional neural network features for pulmonary nodule detection in computed tomography scans,” in *2015 IEEE 12th International Symposium on Biomedical Imaging (ISBI)*, Brooklyn, NY, USA: IEEE, Apr. 2015, pp. 286–289. doi: 10.1109/ISBI.2015.7163869.
[157] D. Ciresan, A. Giusti, L. Gambardella, and J. Schmidhuber, “Deep neural networks segment neuronal membranes in electron microscopy images,” *Advances in Neural Information Processing Systems 25 (NIPS 2012)*, pp. 2852–2860, 2012.
[158] B. Hariharan, P. Arbeláez, R. Girshick, and J. Malik, “Hypercolumns for Object Segmentation and Fine-grained Localization,” 2014, doi: 10.48550/ARXIV.1411.5752.
[159] M. Seyedhosseini, M. Sajjadi, and T. Tasdizen, “Image Segmentation with Cascaded Hierarchical Models and Logistic Disjunctive Normal Networks,” in *2013 IEEE International Conference on Computer Vision*, Sydney, Australia: IEEE, Dec. 2013, pp. 2168–2175. doi: 10.1109/ICCV.2013.269.
[160] J. Y. Shin, N. Tajbakhsh, R. T. Hurst, C. B. Kendall, and J. Liang, “Automating Carotid Intima-Media Thickness Video Interpretation with Convolutional Neural Networks,” in *2016 IEEE Conference on Computer Vision and Pattern Recognition (CVPR)*, Las Vegas, NV, USA: IEEE, Jun. 2016, pp. 2526–2535. doi: 10.1109/CVPR.2016.277.
[161] H. R. Roth, A. Farag, L. Lu, E. B. Turkbey, and R. M. Summers, “Deep convolutional networks for pancreas segmentation in CT imaging,” 2015, doi: 10.48550/ARXIV.1504.03967.
[162] M. Havaei *et al.*, “Brain Tumor Segmentation with Deep Neural Networks,” 2015, doi: 10.48550/ARXIV.1505.03540.
[163] W. Zhang *et al.*, “Deep convolutional neural networks for multi-modality isointense infant brain image segmentation,” *NeuroImage*, vol. 108, pp. 214–224, Mar. 2015, doi: 10.1016/j.neuroimage.2014.12.061.
[164] A. Prasoon, K. Petersen, C. Igel, F. Lauze, E. Dam, and M. Nielsen, “Deep Feature Learning for Knee Cartilage Segmentation Using a Triplanar Convolutional Neural Network,” in *Advanced Information Systems Engineering*, vol. 7908, C. Salinesi, M. C. Norrie, and Ó. Pastor, Eds., in Lecture Notes in Computer Science, vol. 7908. , Berlin, Heidelberg: Springer Berlin Heidelberg, 2013, pp. 246–253. doi: 10.1007/978-3-642-40763-5_31.
[165] O. Ronneberger, P. Fischer, and T. Brox, “U-Net: Convolutional Networks for Biomedical Image Segmentation,” 2015, doi: 10.48550/ARXIV.1505.04597.
[166] L.-C. Chen, G. Papandreou, I. Kokkinos, K. Murphy, and A. L. Yuille, “DeepLab: Semantic Image Segmentation with Deep Convolutional Nets, Atrous Convolution, and Fully Connected CRFs,” *IEEE Trans. Pattern Anal. Mach. Intell.*, vol. 40, no. 4, pp. 834–848, Apr. 2018, doi: 10.1109/TPAMI.2017.2699184.
[167] R. Anantharaman, M. Velazquez, and Y. Lee, “Utilizing Mask R-CNN for Detection and Segmentation of Oral Diseases,” in *2018 IEEE International Conference on Bioinformatics and Biomedicine (BIBM)*, Madrid, Spain: IEEE, Dec. 2018, pp. 2197–2204. doi: 10.1109/BIBM.2018.8621112.
[168] H. Zhao, J. Shi, X. Qi, X. Wang, and J. Jia, “Pyramid Scene Parsing Network,” 2016, doi: 10.48550/ARXIV.1612.01105.
[169] M. Drozdzal, E. Vorontsov, G. Chartrand, S. Kadoury, and C. Pal, “The Importance of Skip Connections in Biomedical Image Segmentation,” 2016, doi: 10.48550/ARXIV.1608.04117.

[170] T. M. Geethanjali, Minavathi, and M. S. Dinesh, “Semantic Segmentation of Kidney and Tumors Using LinkNet Models,” in *Cognition and Recognition*, vol. 1697, D. S. Guru, S. K. Y. H., B. K., R. K. Agrawal, and M. Ichino, Eds., in Communications in Computer and Information Science, vol. 1697. , Cham: Springer Nature Switzerland, 2022, pp. 380–389. doi: 10.1007/978-3-031-22405-8_30.
[171] H. M. Liebich, H. J. Buelow, and R. Kallmayer, “Quantification of endogenous aliphatic alcohols in serum and urine,” *Journal of Chromatography A*, vol. 239, pp. 343–349, Apr. 1982, doi: 10.1016/S0021-9673(00)81993-7.
[172] J. A. Montgomery, M. Jetté, and H. Brunengraber, “Assay of physiological levels of 2,3-butanediol diastereomers in blood and urine by gas chromatography-mass spectrometry,” *Analytical Biochemistry*, vol. 185, no. 1, pp. 71–76, Feb. 1990, doi: 10.1016/0003-2697(90)90256-9.
[173] R. Feliciano, G. Istas, C. Heiss, and A. Rodriguez-Mateos, “Plasma and Urinary Phenolic Profiles after Acute and Repetitive Intake of Wild Blueberry,” *Molecules*, vol. 21, no. 9, p. 1120, Aug. 2016, doi: 10.3390/molecules21091120.
[174] J. L. Izzo and D. Greulich, “Radioenzymatic assay for plasma dihydroxyphenylglycol (DHPG), dihydroxymandelic acid (DOMA) and dihydroxyphenylacetic acid (DOPAC),” *Life Sciences*, vol. 33, no. 5, pp. 483–488, Aug. 1983, doi: 10.1016/0024-3205(83)90798-1.
[175] G. Novarino *et al.*, “Mutations in *BCKD-kinase* Lead to a Potentially Treatable Form of Autism with Epilepsy,” *Science*, vol. 338, no. 6105, pp. 394–397, Oct. 2012, doi: 10.1126/science.1224631.
[176] E. S. Lianidou and P. C. Ioannou, “Simple spectrofluorometric determination of p-aminobenzoic and p-aminosalicylic acids in biological fluids by use of terbium-sensitized luminescence,” *Clin Chem*, vol. 42, no. 10, pp. 1659–1665, Oct. 1996.
[177] G. Jakobsdottir, J. H. Bjerregaard, H. Skovbjerg, and M. Nyman, “Fasting serum concentration of short-chain fatty acids in subjects with microscopic colitis and celiac disease: no difference compared with controls, but between genders,” *Scandinavian Journal of Gastroenterology*, vol. 48, no. 6, pp. 696–701, Jun. 2013, doi: 10.3109/00365521.2013.786128.
[178] A. Koh, F. De Vadder, P. Kovatcheva-Datchary, and F. Bäckhed, “From Dietary Fiber to Host Physiology: Short-Chain Fatty Acids as Key Bacterial Metabolites,” *Cell*, vol. 165, no. 6, pp. 1332–1345, Jun. 2016, doi: 10.1016/j.cell.2016.05.041.
[179] R. H. Richards, J. A. Dowling, H. J. Vreman, C. Feldman, and M. W. Weiner, “Acetate levels in human plasma,” *Proc Clin Dial Transplant Forum*, vol. 6, pp. 73–79, Nov. 1976.
[180] A. Shafaei, V. Vamathevan, J. Pandohee, N. G. Lawler, D. Broadhurst, and M. C. Boyce, “Sensitive and quantitative determination of short-chain fatty acids in human serum using liquid chromatography mass spectrometry,” *Anal Bioanal Chem*, vol. 413, no. 25, pp. 6333–6342, Oct. 2021, doi: 10.1007/s00216-021-03589-w.
[181] J. Gruber *et al.*, “Allantoin in Human Plasma, Serum, and Nasal-Lining Fluids as a Biomarker of Oxidative Stress: Avoiding Artifacts and Establishing Real *in vivo* Concentrations,” *Antioxidants & Redox Signaling*, vol. 11, no. 8, pp. 1767–1776, Aug. 2009, doi: 10.1089/ars.2008.2364.
[182] R. Kand’ár and P. Žáková, “Allantoin as a marker of oxidative stress in human erythrocytes,” *Clinical Chemistry and Laboratory Medicine*, vol. 46, no. 9, Jan. 2008, doi: 10.1515/CCLM.2008.244.

[183] D. V. Pavitt, S. De Fonseka, N. Al-Khalaf, J. M. Cam, and D. A. Reaveley, "Assay of serum allantoin in humans by gas chromatography–mass spectrometry," *Clinica Chimica Acta*, vol. 318, no. 1–2, pp. 63–70, Apr. 2002, doi: 10.1016/S0009-8981(01)00805-1.
[184] C.-H. Lin, H.-T. Yang, C.-C. Chiu, and H.-Y. Lane, "Blood levels of D-amino acid oxidase vs. D-amino acids in reflecting cognitive aging," *Sci Rep*, vol. 7, no. 1, p. 14849, Nov. 2017, doi: 10.1038/s41598-017-13951-7.
[185] B. Campi *et al.*, "Quantification of d-mannose in plasma: Development and validation of a reliable and accurate HPLC-MS-MS method," *Clinica Chimica Acta*, vol. 493, pp. 31–35, Jun. 2019, doi: 10.1016/j.cca.2019.02.024.
[186] E. Pitkänen, O. Pitkänen, and L. Uotila, "Enzymatic Determination of Unbound *D* - Mannose in Serum," *cclm*, vol. 35, no. 10, pp. 761–766, 1997, doi: 10.1515/cclm.1997.35.10.761.
[187] T. Taguchi *et al.*, "Determination of d-Mannose in Plasma by HPLC," *Clinical Chemistry*, vol. 49, no. 1, pp. 181–183, Jan. 2003, doi: 10.1373/49.1.181.
[188] K. Baumann and J. Angerer, "Occupational chronic exposure to organic solvents: VI. Formic acid concentration in blood and urine as an indicator of methanol exposure," *Int. Arch Occup Environ Heath*, vol. 42, no. 3–4, pp. 241–249, 1979, doi: 10.1007/BF00377778.
[189] M. Marangella, M. Petrarulo, O. Bianco, C. Vitale, P. Finocchiaro, and F. Linari, "Glycolate determination detects type I primary hyperoxaluria in dialysis patients," *Kidney International*, vol. 39, no. 1, pp. 149–154, Jan. 1991, doi: 10.1038/ki.1991.19.
[190] P. J. Nowak *et al.*, "Hemodialysis Decreases the Concentration of Accumulated Plant Phenols in the Plasma of Patients on Maintenance Dialysis: Influence of Residual Renal Function: Hemodialysis and Plant Phenols in Plasma," *Ther Apher Dial*, vol. 21, no. 6, pp. 572–585, Dec. 2017, doi: 10.1111/1744-9987.12586.
[191] B. Afessa, J. Mullon, A. Badley, and O. Gajic, "The impact of protocolized sepsis order set on the process of care in patients with severe sepsis/septic shock," *Crit Care*, vol. 11, no. Suppl 4, p. P6, 2007, doi: 10.1186/cc5985.
[192] J. C. M. Baas *et al.*, "Short Report: Plasma pipecolic acid is frequently elevated in non-peroxisomal disease," *J Inherit Metab Dis*, vol. 25, no. 8, pp. 699–701, Feb. 2003, doi: 10.1023/A:1022889400302.
[193] N. Psychogios *et al.*, "The Human Serum Metabolome," *PLoS ONE*, vol. 6, no. 2, p. e16957, Feb. 2011, doi: 10.1371/journal.pone.0016957.
[194] P. Zarembski and A. Hodgkinson, "The fluorimetric determination of oxalic acid in blood and other biological materials," *Biochemical Journal*, vol. 96, no. 3, pp. 717–721, Sep. 1965, doi: 10.1042/bj0960717.
[195] A. Sreekumar *et al.*, "Metabolomic profiles delineate potential role for sarcosine in prostate cancer progression," *Nature*, vol. 457, no. 7231, pp. 910–914, Feb. 2009, doi: 10.1038/nature07762.
[196] R. O. Bahado-Singh *et al.*, "Metabolomics and first-trimester prediction of early-onset preeclampsia," *The Journal of Maternal-Fetal & Neonatal Medicine*, vol. 25, no. 10, pp. 1840–1847, Oct. 2012, doi: 10.3109/14767058.2012.680254.
[197] M. A. Bain, R. Faull, G. Fornasini, R. W. Milne, and A. M. Evans, "Accumulation of trimethylamine and trimethylamine-N-oxide in end-stage renal disease patients undergoing haemodialysis," *Nephrology Dialysis Transplantation*, vol. 21, no. 5, pp. 1300–1304, May 2006, doi: 10.1093/ndt/gfk056.

[198] E. Garcia *et al.*, "NMR quantification of trimethylamine- N -oxide in human serum and plasma in the clinical laboratory setting," *Clinical Biochemistry*, vol. 50, no. 16–17, pp. 947–955, Nov. 2017, doi: 10.1016/j.clinbiochem.2017.06.003.
[199] J. Nie *et al.*, "Serum Trimethylamine N-Oxide Concentration Is Positively Associated With First Stroke in Hypertensive Patients," *Stroke*, vol. 49, no. 9, pp. 2021–2028, Sep. 2018, doi: 10.1161/STROKEAHA.118.021997.
[200] E. Randrianarisoa *et al.*, "Relationship of Serum Trimethylamine N-Oxide (TMAO) Levels with early Atherosclerosis in Humans," *Sci Rep*, vol. 6, no. 1, p. 26745, May 2016, doi: 10.1038/srep26745.
[201] E. Shin and J. S. Koo, "Glucose Metabolism and Glucose Transporters in Breast Cancer," *Front. Cell Dev. Biol.*, vol. 9, p. 728759, Sep. 2021, doi: 10.3389/fcell.2021.728759.
[202] J. Cheng, X. Shuai, J. Gao, M. Cai, G. Wang, and K. Tao, "Prognostic significance of AMPK in human malignancies: A meta-analysis," *Oncotarget*, vol. 7, no. 46, pp. 75739–75748, Nov. 2016, doi: 10.18632/oncotarget.12405.
[203] D. G. Hardie, "Molecular Pathways: Is AMPK a Friend or a Foe in Cancer?," *Clinical Cancer Research*, vol. 21, no. 17, pp. 3836–3840, Sep. 2015, doi: 10.1158/1078-0432.CCR-14-3300.
[204] A. Malik, R. K. Morya, S. K. Bhadada, and S. Rana, "Type 1 diabetes mellitus: Complex interplay of oxidative stress, cytokines, gastrointestinal motility and small intestinal bacterial overgrowth," *Eur J Clin Invest*, vol. 48, no. 11, p. e13021, Nov. 2018, doi: 10.1111/eci.13021.
[205] S. González-Martínez, B. Pérez-Mies, D. Pizarro, T. Caniego-Casas, J. Cortés, and J. Palacios, "Epithelial Mesenchymal Transition and Immune Response in Metaplastic Breast Carcinoma," *IJMS*, vol. 22, no. 14, p. 7398, Jul. 2021, doi: 10.3390/ijms22147398.
[206] R. Kalluri and R. A. Weinberg, "The basics of epithelial-mesenchymal transition," *J. Clin. Invest.*, vol. 119, no. 6, pp. 1420–1428, Jun. 2009, doi: 10.1172/JCI39104.
[207] S. Lamouille, J. Xu, and R. Derynck, "Molecular mechanisms of epithelial–mesenchymal transition," *Nat Rev Mol Cell Biol*, vol. 15, no. 3, pp. 178–196, Mar. 2014, doi: 10.1038/nrm3758.
[208] C. B. Trelford, L. Dagnino, and G. M. Di Guglielmo, "Transforming growth factor-β in tumour development," *Front. Mol. Biosci.*, vol. 9, p. 991612, Oct. 2022, doi: 10.3389/fmolb.2022.991612.
[209] G. J. Inman *et al.*, "SB-431542 Is a Potent and Specific Inhibitor of Transforming Growth Factor-β Superfamily Type I Activin Receptor-Like Kinase (ALK) Receptors ALK4, ALK5, and ALK7," *Mol Pharmacol*, vol. 62, no. 1, pp. 65–74, Jul. 2002, doi: 10.1124/mol.62.1.65.
[210] S. Carding, K. Verbeke, D. T. Vipond, B. M. Corfe, and L. J. Owen, "Dysbiosis of the gut microbiota in disease," *Microbial Ecology in Health & Disease*, vol. 26, no. 0, Feb. 2015, doi: 10.3402/mehd.v26.26191.
[211] J. J. Goedert *et al.*, "Investigation of the Association Between the Fecal Microbiota and Breast Cancer in Postmenopausal Women: a Population-Based Case-Control Pilot Study," *JNCI: Journal of the National Cancer Institute*, vol. 107, no. 8, Aug. 2015, doi: 10.1093/jnci/djv147.
[212] I. R. Rowland, Ed., *Role of the gut flora in toxicity and cancer*. London ; San Diego: Academic Press, 1988.

[213] G. Xie *et al.*, "Dysregulated hepatic bile acids collaboratively promote liver carcinogenesis: Bile acids in liver carcinogenesis," *Int. J. Cancer*, vol. 139, no. 8, pp. 1764–1775, Oct. 2016, doi: 10.1002/ijc.30219.
[214] S. Yoshimoto *et al.*, "Obesity-induced gut microbial metabolite promotes liver cancer through senescence secretome," *Nature*, vol. 499, no. 7456, pp. 97–101, Jul. 2013, doi: 10.1038/nature12347.
[215] S. Schwarcz *et al.*, "The pro- and antineoplastic effects of deoxycholic acid in pancreatic adenocarcinoma cell models," *Mol Biol Rep*, vol. 50, no. 6, pp. 5273–5282, Jun. 2023, doi: 10.1007/s11033-023-08453-x.
[216] Z. Shellman *et al.*, "Bile acids: a potential role in the pathogenesis of pharyngeal malignancy," *Clin Otolaryngol*, vol. 42, no. 5, pp. 969–973, Oct. 2017, doi: 10.1111/coa.12822.
[217] A. A. Goldberg, A. Beach, G. F. Davies, T. A. A. Harkness, A. LeBlanc, and V. I. Titorenko, "Lithocholic bile acid selectively kills neuroblastoma cells, while sparing normal neuronal cells," *Oncotarget*, vol. 2, no. 10, pp. 761–782, Oct. 2011, doi: 10.18632/oncotarget.338.
[218] A. A. Goldberg, V. I. Titorenko, A. Beach, and J. T. Sanderson, "Bile acids induce apoptosis selectively in androgen-dependent and -independent prostate cancer cells," *PeerJ*, vol. 1, p. e122, Aug. 2013, doi: 10.7717/peerj.122.
[219] E. Sánchez-Tilló, O. De Barrios, L. Siles, M. Cuatrecasas, A. Castells, and A. Postigo, "β-catenin/TCF4 complex induces the epithelial-to-mesenchymal transition (EMT)-activator ZEB1 to regulate tumor invasiveness," *Proc. Natl. Acad. Sci. U.S.A.*, vol. 108, no. 48, pp. 19204–19209, Nov. 2011, doi: 10.1073/pnas.1108977108.
[220] D. Kapfhamer *et al.*, "Protein Phosphatase 2A and Glycogen Synthase Kinase 3 Signaling Modulate Prepulse Inhibition of the Acoustic Startle Response by Altering Cortical M-Type Potassium Channel Activity," *Journal of Neuroscience*, vol. 30, no. 26, pp. 8830–8840, Jun. 2010, doi: 10.1523/JNEUROSCI.1292-10.2010.
[221] X. Fang, S. X. Yu, Y. Lu, R. C. Bast, J. R. Woodgett, and G. B. Mills, "Phosphorylation and inactivation of glycogen synthase kinase 3 by protein kinase A," *Proc. Natl. Acad. Sci. U.S.A.*, vol. 97, no. 22, pp. 11960–11965, Oct. 2000, doi: 10.1073/pnas.220413597.
[222] M. A. Hermida, J. Dinesh Kumar, and N. R. Leslie, "GSK3 and its interactions with the PI3K/AKT/mTOR signalling network," *Advances in Biological Regulation*, vol. 65, pp. 5–15, Aug. 2017, doi: 10.1016/j.jbior.2017.06.003.
[223] C. Mercan *et al.*, "Automated Scoring of Nuclear Pleomorphism Spectrum with Pathologist-level Performance in Breast Cancer," 2020, doi: 10.48550/ARXIV.2012.04974.
[224] D. Fishman *et al.*, "Practical segmentation of nuclei in brightfield cell images with neural networks trained on fluorescently labelled samples," *Journal of Microscopy*, vol. 284, no. 1, pp. 12–24, Oct. 2021, doi: 10.1111/jmi.13038.
[225] M. Million *et al.*, "Increased Gut Redox and Depletion of Anaerobic and Methanogenic Prokaryotes in Severe Acute Malnutrition," *Sci Rep*, vol. 6, no. 1, p. 26051, May 2016, doi: 10.1038/srep26051.
[226] P. Sainamthip, S. Saichaemchan, B. Satirapoj, and N. Prasongsook, "The Effect of Intravenous Mannitol Combined With Normal Saline in Preventing Cisplatin-Induced Nephrotoxicity: A Randomized, Double-Blind, Placebo-Controlled Trial," *JCO Global Oncology*, no. 8, p. e2100275, May 2022, doi: 10.1200/GO.21.00275.

[227] P. Visweswaran, E. K. Massin, and T. D. Dubose, “Mannitol-induced acute renal failure.,” *Journal of the American Society of Nephrology*, vol. 8, no. 6, pp. 1028–1033, Jun. 1997, doi: 10.1681/ASN.V861028.
[228] M. F. Gadallah, M. Lynn, and J. Work, “Case Report: Mannitol Nephrotoxicity Syndrome: Role of Hemodialysis and Postulate of Mechanisms,” *The American Journal of the Medical Sciences*, vol. 309, no. 4, pp. 219–222, Apr. 1995, doi: 10.1097/00000441-199504000-00006.
[229] S. K. Garg and A. Jain, “Fermentative production of 2,3-butanediol: A review,” *Bioresource Technology*, vol. 51, no. 2–3, pp. 103–109, Jan. 1995, doi: 10.1016/0960-8524(94)00136-O.
[230] C. Ng, M. Jung, J. Lee, and M.-K. Oh, “Production of 2,3-butanediol in Saccharomyces cerevisiae by in silico aided metabolic engineering,” *Microb Cell Fact*, vol. 11, no. 1, p. 68, Dec. 2012, doi: 10.1186/1475-2859-11-68.
[231] J. Sharad, “Glycolic acid peel therapy – a current review,” *CCID*, p. 281, Nov. 2013, doi: 10.2147/CCID.S34029.
[232] E. R. Valle-González, J. A. Jackman, B. K. Yoon, N. Mokrzecka, and N.-J. Cho, “pH-Dependent Antibacterial Activity of Glycolic Acid: Implications for Anti-Acne Formulations,” *Sci Rep*, vol. 10, no. 1, p. 7491, May 2020, doi: 10.1038/s41598-020-64545-9.
[233] Q. Zhu *et al.*, “L-norvaline affects the proliferation of breast cancer cells based on the microbiome and metabolome analysis,” *Journal of Applied Microbiology*, vol. 133, no. 2, pp. 1014–1026, Aug. 2022, doi: 10.1111/jam.15620.
[234] X. Zhang, D. Lin, R. Jiang, H. Li, J. Wan, and H. Li, “Ferulic acid exerts antitumor activity and inhibits metastasis in breast cancer cells by regulating epithelial to mesenchymal transition,” *Oncology Reports*, vol. 36, no. 1, pp. 271–278, Jul. 2016, doi: 10.3892/or.2016.4804.
[235] X. Bao, W. Li, R. Jia, D. Meng, H. Zhang, and L. Xia, “Molecular mechanism of ferulic acid and its derivatives in tumor progression,” *Pharmacol. Rep*, vol. 75, no. 4, pp. 891–906, Aug. 2023, doi: 10.1007/s43440-023-00494-0.
[236] D. Pugazhendhi, G. S. Pope, and P. D. Darbre, “Oestrogenic activity ofp-hydroxybenzoic acid (common metabolite of paraben esters) and methylparaben in human breast cancer cell lines,” *J. Appl. Toxicol.*, vol. 25, no. 4, pp. 301–309, Jul. 2005, doi: 10.1002/jat.1066.
[237] W. Rosiles-Alanis *et al.*, “4-Hydroxybenzoic Acid and β -Sitosterol from *Cucurbita ficifolia* Act as Insulin Secretagogues, Peroxisome Proliferator-Activated Receptor-Gamma Agonists, and Liver Glycogen Storage Promoters: *In Vivo* , *In Vitro* , and *In Silico* Studies,” *Journal of Medicinal Food*, vol. 25, no. 6, pp. 588–596, Jun. 2022, doi: 10.1089/jmf.2021.0071.
[238] A. D. S. Pessoa *et al.*, “The dimerization of methyl vanillate improves its effect against breast cancer cells via pro-oxidant effect,” *Chemico-Biological Interactions*, vol. 361, p. 109962, Jul. 2022, doi: 10.1016/j.cbi.2022.109962.
[239] M. Rouxel *et al.*, “Characterization of antifungal compounds produced by lactobacilli in cheese-mimicking matrix: Comparison between active and inactive strains,” *International Journal of Food Microbiology*, vol. 333, p. 108798, Nov. 2020, doi: 10.1016/j.ijfoodmicro.2020.108798.

[240] A.-M. Aura *et al.*, "Quercetin Derivatives Are Deconjugated and Converted to Hydroxyphenylacetic Acids but Not Methylated by Human Fecal Flora in Vitro," *J. Agric. Food Chem.*, vol. 50, no. 6, pp. 1725–1730, Mar. 2002, doi: 10.1021/jf0108056.
[241] A. Rechner, "Colonic metabolism of dietary polyphenols: influence of structure on microbial fermentation products," *Free Radical Biology and Medicine*, vol. 36, no. 2, pp. 212–225, Jan. 2004, doi: 10.1016/j.freeradbiomed.2003.09.022.
[242] G. Williamson and M. N. Clifford, "Role of the small intestine, colon and microbiota in determining the metabolic fate of polyphenols," *Biochemical Pharmacology*, vol. 139, pp. 24–39, Sep. 2017, doi: 10.1016/j.bcp.2017.03.012.
[243] O. O. Ozdemir and F. Soyer, "*Pseudomonas aeruginosa* Presents Multiple Vital Changes in Its Proteome in the Presence of 3-Hydroxyphenylacetic Acid, a Promising Antimicrobial Agent," *ACS Omega*, vol. 5, no. 32, pp. 19938–19951, Aug. 2020, doi: 10.1021/acsomega.0c00703.
[244] Y. Liu *et al.*, "A Major Intestinal Catabolite of Quercetin Glycosides, 3-Hydroxyphenylacetic Acid, Protects the Hepatocytes from the Acetaldehyde-Induced Cytotoxicity through the Enhancement of the Total Aldehyde Dehydrogenase Activity," *IJMS*, vol. 23, no. 3, p. 1762, Feb. 2022, doi: 10.3390/ijms23031762.
[245] W. Chen *et al.*, "Ethers of 3-hydroxyphenylacetic acid as selective gamma-hydroxybutyric acid receptor ligands," *Bioorganic & Medicinal Chemistry Letters*, vol. 15, no. 13, pp. 3201–3202, Jul. 2005, doi: 10.1016/j.bmcl.2005.05.011.
[246] M. K. Ticku and A. K. Mehta, "Characterization and Pharmacology of the GHB Receptor," *Annals of the New York Academy of Sciences*, vol. 1139, no. 1, pp. 374–385, Oct. 2008, doi: 10.1196/annals.1432.048.
[247] C. A. Batt and M. L. Tortorello, Eds., *Encyclopedia of food microbiology*, 2. ed. Amsterdam: AP, Academic Press/Elsevier, 2014.
[248] Y. Chen, Y. Chen, L. Liu, Y. Zhang, and J. Yuan, "Microbial synthesis of 4-hydroxybenzoic acid from renewable feedstocks," *Food Chemistry: Molecular Sciences*, vol. 3, p. 100059, Dec. 2021, doi: 10.1016/j.fochms.2021.100059.
[249] S. Sharma, V. Gopu, C. Sivasankar, and P. H. Shetty, "Hydrocinnamic acid produced by *Enterobacter xiangfangensis* impairs AHL-based quorum sensing and biofilm formation in *Pseudomonas aeruginosa*," *RSC Adv.*, vol. 9, no. 49, pp. 28678–28687, 2019, doi: 10.1039/C9RA05725K.
[250] M. Sousa *et al.*, "Hydrocinnamic Acid and Perillyl Alcohol Potentiate the Action of Antibiotics against Escherichia coli," *Antibiotics*, vol. 12, no. 2, p. 360, Feb. 2023, doi: 10.3390/antibiotics12020360.

Keywords

Lithocholic acid, breast cancer, bacterial metabolites, EMT, semantic segmentation

Acknowledgements

I would like to thank my supervisor, Prof. Dr. Péter Bay for the patient guidance, encouragement, continuous support and motivation during my PhD study. I am grateful that he gave me the opportunity to learn and work in his research group.

I would also like to thank to Prof. Dr. László Virág, head of Department of Medical Chemistry, for giving me the opportunity to work at the department and Dr. Endre Kókai for enabling me the use of the advanced microscopic equipment during this work.

Many thanks to my colleagues, Dr. Edit Mikó and Dr. Adrienn Sipos for the valuable discussions and helpful advices, and - besides them – to Boglárka Rauch, Szandra Schwarz, and Dr. Tünde Kovács for their help in carrying out the experiments.

I am also thankful to László Finta and Kitti Bartha for their excellent technical assistance, and at last but not least, I would like to thank to my loving family and to all my dear friends for their continuous encouragement during my PhD studies.

UNIVERSITY AND NATIONAL LIBRARY
UNIVERSITY OF DEBRECEN
H-4002 Egyetem tér 1, Debrecen
Phone: +3652/410-443, email: publikaciok@lib.unideb.hu

Registry number: DEENK/448/2023.PL
Subject: PhD Publication List

Candidate: Gyula Ujlaki
Doctoral School: Doctoral School of Molecular Medicine

List of publications related to the dissertation

1. **Ujlaki, G.**, Kovács, T., Vida, A., Kókai, E., Rauch, B., Schwarcz, S., Mikó, E., Janka, E. A., Sipos, A., Hegedűs, C., Uray, K., Nagy, P., Bai, P.: Identification of bacterial metabolites modulating breast cancer cell proliferation and epithelial-mesenchymal transition.
Molecules. 28 (15), 1-18, 2023.
DOI: http://dx.doi.org/10.3390/molecules28155898
IF: 4.6 (2022)

2. Mikó, E., Vida, A., Kovács, T., **Ujlaki, G.**, Trencsényi, G., Márton, J., Sári, Z., Kovács, P., Boratkó, A., Hujber, Z., Csonka, T., Antal-Szalmás, P., Watanabe, M., Gombos, I., Csóka, B., Kiss, B. K., Vígh, L., Szabó, J., Méhes, G., Sebestyén, A., Goedert, J. J., Bai, P.: Lithocholic acid, a bacterial metabolite reduces breast cancer cell proliferation and aggressiveness.
Biochim. Biophys. Acta Bioenerg. 1859 (9), 958-974, 2018.
DOI: http://dx.doi.org/10.1016/j.bbabio.2018.04.002
IF: 4.441

List of other publications

3. Skopál, A., **Ujlaki, G.**, Gerencsér, A., Bankó, C., Bacsó, Z., Ciruela, F., Virág, L., Haskó, G., Kókai, E.: Adenosine A2A Receptor Activation Regulates Niemann-Pick C1 Expression and Localization in Macrophages.
Curr. Issues Mol. Biol. 45 (6), 4948-4969, 2023.
DOI: http://dx.doi.org/10.3390/cimb45060315
IF: 3.1 (2022)

4. Antal, D., Pór, Á., Kovács, I., Dull, K., Póliska, S., **Ujlaki, G.**, Demény, M. Á., Szöllősi, A. G., Kiss, B. K., Szegedi, A., Bai, P., Szántó, M.: PARP2 promotes inflammation in psoriasis by modulating estradiol biosynthesis in keratinocytes.
J. Mol. Med. (Berl). 101 (8), 987-999, 2023.
DOI: http://dx.doi.org/10.1007/s00109-023-02338-z
IF: 4.7 (2022)

5. Schwarcz, S., Kovács, P., Kovács, T., **Ujlaki, G.**, Nyerges, P., Uray, K., Bai, P., Mikó, E.: The pro- and antineoplastic effects of deoxycholic acid in pancreatic adenocarcinoma cell models.
Mol. Biol. Rep. 50 (6), 5273-5282, 2023.
DOI: http://dx.doi.org/10.1007/s11033-023-08453-x
IF: 2.8 (2022)

6. Lénárt, K., Bankó, C., **Ujlaki, G.**, Póliska, S., Kis, G., Csősz, É., Antal, M., Bacsó, Z., Bai, P., Fésüs, L., Mádi, A.: Tissue Transglutaminase Knock-Out Preadipocytes and Beige Cells of Epididymal Fat Origin Possess Decreased Mitochondrial Functions Required for Thermogenesis.
Int. J. Mol. Sci. 23 (9), 5175, 2022.
DOI: http://dx.doi.org/10.3390/ijms23095175
IF: 5.6

7. Kiss, B. K., Mikó, E., Sebő, É., Tóth, J., **Ujlaki, G.**, Szabó, J., Uray, K., Bai, P., Árkosy, P.: Onkobiózis és mikrobiális metabolikus jelátvitel pancreas-adenocarcinomában.
Cent. Eur. J. Gastro. Hepatol. 7 (2), 57-65, 2021.
DOI: http://dx.doi.org/10.33570/CEUJGH.7.2.57

8. Kacsir, I., Sipos, A., **Ujlaki, G.**, Buglyó, P., Somsák, L., Bai, P., Bokor, É.: Ruthenium half-sandwich type complexes with bidentate monosaccharide ligands show antineoplastic activity in ovarian cancer cell models through reactive oxygen species production.
Int. J. Mol. Sci. 221, 1-41, 2021.
DOI: http://dx.doi.org/10.3390/ijms221910454
IF: 6.208

9. Jankó, L., Kovács, T., Laczik, M., Sári, Z., **Ujlaki, G.**, Kis, G., Horváth, I., Antal, M., Vígh, L., Bálint, B. L., Uray, K., Bai, P.: Silencing of Poly(ADP-Ribose) Polymerase-2 Induces Mitochondrial Reactive Species Production and Mitochondrial Fragmentation.
Cells. 10 (6), 1387, 2021.
DOI: http://dx.doi.org/10.3390/cells10061387
IF: 7.666

10. Kovács, T., Mikó, E., **Ujlaki, G.**, Mustafa, H. Y. H., Csontos, V., Uray, K., Bai, P.: The involvement of oncobiosis and bacterial metabolite signaling in metastasis formation in breast cancer.
Cancer Metastasis Rev. 40, 1223-1249, 2021.
DOI: http://dx.doi.org/10.1007/s10555-021-10013-3
IF: 9.237

11. Sipos, A., **Ujlaki, G.**, Mikó, E., Maka, E., Szabó, J., Uray, K., Krasznai, Z. T., Bai, P.: The role of the microbiome in ovarian cancer: mechanistic insights into oncobiosis and to bacterial metabolite signaling.
Mol. Med. 27 (1), 1-20, 2021.
DOI: http://dx.doi.org/10.1186/s10020-021-00295-2
IF: 6.376

UNIVERSITY of DEBRECEN

UNIVERSITY AND NATIONAL LIBRARY
UNIVERSITY OF DEBRECEN
H-4002 Egyetem tér 1, Debrecen
Phone: +3652/410-443, email: publikaciok@lib.unideb.hu

12. Sári, Z., Mikó, E., Kovács, T., Jankó, L., Csonka, T., Lente, G., Sebő, É., Tóth, J., Tóth, D., Árkosy, P., Boratkó, A., **Ujlaki, G.**, Török, M., Kovács, I., Szabó, J., Kiss, B. K., Méhes, G., Goedert, J. J., Bai, P.: Indolepropionic Acid, a Metabolite of the Microbiome, Has Cytostatic Properties in Breast Cancer by Activating AHR and PXR Receptors and Inducing Oxidative Stress.
Cancers (Basel). 12 (9), 1-27, 2020.
DOI: http://dx.doi.org/10.3390/cancers12092411
IF: 6.639

13. Sári, Z., Mikó, E., Kovács, T., Boratkó, A., **Ujlaki, G.**, Jankó, L., Kiss, B. K., Uray, K., Bai, P.: Indoxylsulfate, a Metabolite of the Microbiome, Has Cytostatic Effects in Breast Cancer via Activation of AHR and PXR Receptors and Induction of Oxidative Stress.
Cancers (Basel). 12 (10), 1-23, 2020.
DOI: http://dx.doi.org/10.3390/cancers12102915
IF: 6.639

14. Kiss, B. K., Mikó, E., Sebő, É., Tóth, J., **Ujlaki, G.**, Szabó, J., Uray, K., Bai, P., Árkosy, P.: Oncobiosis and microbial metabolite signaling in pancreatic adenocarcinoma.
Cancers (Basel). 12 (5), 1-34, 2020.
DOI: http://dx.doi.org/10.3390/cancers12051068
IF: 6.639

15. Kovács, T., Mikó, E., **Ujlaki, G.**, Sári, Z., Bai, P.: The Microbiome as a Component of the Tumor Microenvironment.
In: Tumor Microenvironment / Alexander Birbrair, Springer Nature - Springer Cham, Switzerland, 137-153, 2020, (dvances in Experimental Medicine and Biology, 0065-2598 ; 1225)

16. Kovács, T., Mikó, E., Vida, A., Sebő, É., Tóth, J., Csonka, T., Boratkó, A., **Ujlaki, G.**, Lente, G., Kovács, P., Tóth, D., Árkosy, P., Kiss, B. K., Méhes, G., Goedert, J. J., Bai, P.: Cadaverine, a metabolite of the microbiome, reduces breast cancer aggressiveness through trace amino acid receptors.
Sci Rep. 9 (1), 1-14, 2019.
DOI: http://dx.doi.org/10.1038/s41598-018-37664-7
IF: 3.998

17. Kovács, P., Csonka, T., Kovács, T., Sári, Z., **Ujlaki, G.**, Sipos, A., Karányi, Z., Szeőcs, D., Hegedűs, C., Uray, K., Jankó, L., Kiss, M., Kiss, B. K., Laoui, D., Virág, L., Méhes, G., Bai, P., Mikó, E.: Lithocholic acid, a metabolite of the microbiome, increases oxidative stress in breast cancer.
Cancers (Basel). 11, 1-31, 2019.
DOI: http://dx.doi.org/10.3390/cancers11091255
IF: 6.126

UNIVERSITY AND NATIONAL LIBRARY
UNIVERSITY OF DEBRECEN
H-4002 Egyetem tér 1, Debrecen
Phone: +3652/410-443, email: publikaciok@lib.unideb.hu

18. Mikó, E., Kovács, T., Sebő, É., Tóth, J., Csonka, T., **Ujlaki, G.**, Sipos, A., Szabó, J., Méhes, G., Bai, P.: Microbiome-Microbial Metabolome-Cancer Cell Interactions in Breast Cancer-Familiar, but Unexplored.
Cells. 8 (4), 1-33, 2019.
DOI: http://dx.doi.org/10.3390/cells8040293
IF: 4.366

19. Nagy, L., Rauch, B., Balla, N., **Ujlaki, G.**, Kis, G., Omar, A. R., Kristóf, E., Sipos, A., Antal, M., Tóth, A., Debreceni, T., Horváth, A., Maros, T. M., Csizmadia, P., Szerafin, T., Bai, P.: Olaparib induces browning of in vitro cultures of human primary white adipocytes.
Biochem. Pharmacol. 167, 76-85, 2019.
DOI: http://dx.doi.org/10.1016/j.bcp.2019.06.022
IF: 4.96

Total IF of journals (all publications): 94,095
Total IF of journals (publications related to the dissertation): 9,041

The Candidate's publication data submitted to the iDEa Tudóstér have been validated by DEENK on the basis of the Journal Citation Report (Impact Factor) database.

02 October, 2023

DEBRECENI EGYETEM
Egyetemi és Nemzeti Könyvtár